Fullerene isomers for Organic Photovoltaics

Wenda Shi

School of Physics and Astronomy
Queen Mary, University of London

Supervisors-Dr John Dennis, Dr Theo Kreouzis

Thesis submitted to the University of London for the Degree of Doctor of Philosophy
2016

Declaration

All the work contained within this thesis is my own and has not previously been submitted to satisfy any of other degree requirements at this or any other university. This thesis contains no material published or written by another person except where due reference is made in this thesis itself.

Wenda Shi

Nine out of ten of my experiments fail, and that is considered a pretty good record amongst scientist.

Harry Kroto

Contents

Acknowledgement

Foremost, I would like to express my sincere gratitude to my supervisor Dr John Dennis for his patience, passion and immense knowledge. He always taught me everything by himself in details. He offers me great help during my difficult time in experiment and also writing thesis. He is the guider for me to enter the wonderful fullerene world. I want to express my appreciation to my colleagues Miss Xueyan Hou, Mr Xiaoming Zhao, and Miss Tong Liu in our group for their great help for my PhD research. Thank China scholarship Council for providing me fund for my research and living in London.

Also Thank Prof. J. C. Hummelen of the Department of Chemistry, University of Groningen, NL, for the raw materials studies for my whole research; Dr I.Pokes (University of Warwick) and Dr H. Toms (QMUL) for technical help in recording NMR spectra; and Dr G.E. Moss (QMUL and IUPAC) for his help with nomenclature; Mr Kaipei Qiu and Miss Mo Qiao for a strong support in cyclic voltammetry tests.

Besides, I would like to thank all the staffs in CCMMP. Dr Ken Scott always helped me for daily experiment. Terry helped me to solve out my computer problems. Sarah supported me to go for conference of solar cell. I also would like to thank other staffs who helped me during my PhD study.

Last but not the last, I would like to thank my parents, my wife Mengmeng Wu and my friends. They gave me a great spiritual support during my research.

Abstract

The as-produced isomer mixture of the organic photovoltaic device acceptor material bis$PC_{62}BM$ has been purified into its constituents by peak-recycling HPLC, and those individual isomers were characterised by UV-Vis absorption spectroscopy and cyclic voltammetry. A total of 18 isomers were purified from the mixture to a standard exceeding 99.5% with respect to other isomers. The HOMOs, LUMOs, and HOMO-LUMO gaps of the purified isomers vary from (-5.673 to -5.402 eV), (-3.901 to -3.729 eV), and (1.664 to 1.883 eV), respectively. We also find a correlation between HPLC retention time and the relative positions of the addends; in that generally the closer the addends are to each other the longer the retention time of the isomer, and vice versa.

The OPV acceptor molecule $PC_{71}BM$ was also purified into its constituent isomers to a standard of at least 99%. The total three purified isomers were each characterized by ^{13}C NMR and UV-vis spectroscopy, and cyclic voltammetry. These characterizations were supported by HF/DFT ab-initio calculations. All three isomers are methano-fullerenes. The most abundant isomer (85% of the mixture) exists as a racemate involving the 8-25 bond of C_{70}. The other two isomers both involved the 9-10 bond of C_{70}, but are distinguished by opposing orientations of the addend with r and s pseudo-asymmetry about carbon atom 71. The r and s isomers comprised 9% and 6% of the as-produced of the mixture, respectively. In order of decreasing abundance, the LUMO levels of the isomers were –3.9316, –3.9194 and –3.9197 eV and the HOMO-LUMO gaps were 1,772, 1.754 and 1.748 eV.

Introduction and Objectives

Organic photovoltaic devices (OPVs) have attracted strong interest from both the academic and industrial fields in the last 15 years, for their low cost (less than 1$/Wp), easy processing, low weight and the continuous increasing power conversion efficiency (PCE) that has reached 13.2% (the world record) [1] [2]. The bulk-heterojunction OPV is the most promising structure comprising a blend of a conjugated polymer donor and a fullerene-based acceptor. Fullerene derivatives have many properties that makes them ideal acceptors; polyhedral shape, excellent miscibility with the acceptor polymer, a tendency to aggregate, and favourable electron affinity that is the key for electron and hole dissociation from the conjugated polymer [3] [4]. Although there have been considerable advances in OPV performance with significant improvements in the donor polymer, the acceptor material remains primarily the fullerene derivative methyl 4-[61-phenyl,3H-cyclopropa(C_{60}-Ih)[5,6]fulleren-61-yl]butanoate, which is more commonly known as phenyl-C_{61}-butyric acid methyl ester ($PC_{61}BM$).

Empirically, the energy difference between the highest occupied molecular orbital (HOMO) of the donor and the lowest unoccupied molecular orbital (LUMO) of the acceptor scales linearly with OPV open circuit voltage (Voc) under standard conditions [5] [6] [7] [8] [9] [10] [11] [12]. Increasing the LUMO of the fullerene acceptor in principle leads to a higher Voc. This can be achieved by adding electron-pushing functional groups to the fullerene cage [11]. A bis-adduct of $PC_{61}BM$, bis$PC_{62}BM$ (dimethyl 4,4'-[61,62-diphenyl,3H,3H'dicyclopropa(C_{60}-Ih)[5,6]fulleren-61,62-

diyl]dibutanoate), has proved successful in this respect [13] [14]. The additional addend results in an increase in the LUMO of the acceptor by about 100 meV compared to that of $PC_{61}BM$ [15]. However, the increase in PCE is not as high as expected from the increase in Voc. This is because, unlike $PC_{61}BM$, bis$PC_{62}BM$ exists as a mixture of a large number of isomers, which leads to a morphological and energetic disorder in the active layer of photovoltaic devices with a degrading effect on the photocurrent [15]. The disorder induced by the isomer mixture may be removed through fabricating devices from isomer-pure samples. In addition, isomer-pure samples would facilitate the fabrication of devices with LUMOs substantially above that of the ensemble average, resulting in substantially higher Vocs. Hence, using isomer-pure samples may lead to both a higher voltage and current, compared to the isomer mixture. However, this has been known for more than a decade and there is no progress in the literature on isomer-pure PCBM OPVs.

$PC_{71}BM$ is a variant of the OPV acceptor material PCBM, [16] which has the advantage of lower molecular symmetry – yielding far less optically-forbidden electronic transitions giving a wide range of wider light absorption; and it also has the highest recorded charge carrier mobility in OFETs of 0.1 cm^2/Vs, [17] but it has the disadvantage of slightly greater scarcity in the existing fulllerene family. [18] However, the advantage seems to outweigh the disadvantage in that $PC_{71}BM$ from OFET is used as the acceptor material in the current world record-holding OPV device. [19] $PC_{71}BM$ may exist as up to 14 structural isomers, although only three of these isomers are actually formed in the addition synthesis. [16] A range of isomers may yield a range of molecular properties related to OPV performance, with some

being considerably better than others. As with bis$PC_{62}BM$, a substantial energetic disorder in the $PC_{71}BM$ isomer mixture in bulk heterojunction devices may also exist. It is therefore worth fabricating $PC_{71}BM$ isomer-pure materials and devices based on these for both academic interest and potential applications.

OBJECTIVES

1. Building a nomenclature system of bis$PC_{62}BM$ and $PC_{71}BM$ isomers.
2. Purification of the bis$PC_{62}BM$ isomer mixture and $PC_{71}BM$ isomer mixture into all constituent isomers with 99% purity by preparative peak recycling high performance liquid chromatography (HPLC).
3. Identification of the molecular structures of all $PC_{71}BM$ isomers via ab-initio calculations and ^{13}C NMR spectroscopy.
4. Electronic characterisation by UV-Vis spectroscopy and cyclic voltammetry of all bis$PC_{62}BM$ and $PC_{71}BM$ isomers. The study of the electronic structure of all the isomers can guide us towards potential applications and even the synthesis of promising isomers with a particular structures in future work.

Chapter 1

LITERATURE REVIEW

In this review, a brief history, basic mechanism, material development, device structure and the production process of OPV devices are introduced, followed by discussion about fullerene-based acceptors and purifying techniques. This chapter also includes the key experimental methods and the target isomers in this project.

1.1 Background

With the destruction of the global environment and the decrease of non-renewable energy sources on the planet, humanity is increasingly concerned about the sustainability of energy. The development of new and renewable energy sources has become a popular topic of current research. At present, the main clean energy sources are wind, hydrogen, bio-energy, water, nuclear and solar energy. Among them, only nuclear power and water are mature enough to produce a significant contribution to satisfying demand. However, the anti-nuclear voice became prominent after the Fukushima crisis in March 2011 and people set their sights on solar energy. [20] Solar energy is one of the cleanest and most plentiful energy sources. The earth can receive about 3.85×10^{29} J energy from the Sun per year, which is almost nine orders of magnitude more than global energy consumption (4.9×10^{20} J in 2005). [21] Solar cells, which can convert solar energy into electricity, are expected to become the most popular clean energy products in the future.

In 1954, Bell Labs pioneered the invention of the first silicon solar cell which led to rapid development of photovoltaic (PV) cells. [22] The initial solar cell was mainly focused on single crystal silicon as the active material. In the 1990s, monocrystalline, polycrystalline or amorphous film devices were developed based on inorganic GaAs, CdTe and stacked GaInP/GaAs/Ge layers. [23] However, the global application of solar photovoltaic power has been limited because it is difficult and costly to manufacture commercial PV cells based on silicon crystals. A novel approach to generate electricity from solar energy is by using organic polymer materials. The main advantages of organic photovoltaic (OPV) devices compared to classic solid

state photovoltaic devices is that they are cheaper, lightweight, flexible and semi-transparent. The organic materials can be dissolved into a solution at room temperature, which enables large-area production of solar cells based on spin coating, spray coating and ink-jet printing methods. These advantages can lead to large-scale production of low-cost photovoltaic devices that can either be portable or used in building-integrated photovoltaic systems. The worldwide market for OPVs will grow from $25 million in 2013 to nearly $100 million by 2020, according to Transparency Market Research. [24] This represents an annual growth rate of just over 21%. Building-integrated PV (BIPV) applications from OPVs are predicted to grow by over 24% per year from 2017 to 2020 in volume terms [25] [26].

1.2 Brief introductions to OPVs

1.2.1 The Organic Photovoltaic Mechanism

An organic solar cell is defined as a thin film solar cell based on organic materials. OPVs are mainly made up of four parts, which are the anode, cathode, donor (D) and acceptor (A). The fundamental photovoltaic mechanism in an organic solar cell is shown in Figure 1.1. As solar photons are absorbed by the donor (polymers), excitons are created and diffuse to D/A interface. When excitons reach the interface, they are dissociated into free holes and electrons, which are transported to the anode and cathode, respectively. The efficiency of this 'photon to electron process' is called the power conversion efficiency (PCE) of the solar cell (Equation 1)

$$\eta = \frac{V_{oc} J_{sc} FF}{P_{in}} \quad \textbf{Equation 1 [27]}$$

Where η is The PCE, J_{sc} is short circuit current, FF is the fill factor, Voc is the open circuit voltage under illumination state and P_{in} is the power of illumination on the surface area of the solar cell.

and is affected by the whole process, including absorption efficiency, exciton diffusion, charge dissociation, charge transport and material types. According to the mechanism, the efficiency can be improved by enhancing Voc, Jsc and FF. Jsc is determined by how much the photons absorbed by the OPV can be converted into current, and this is highly influenced by the morphology and materials of the OPV. Favourable morphology can help the electron diffusion from donor to acceptor, finally reaching the electrode without much loss. Low band gap materials with matched electronic structures between donor and acceptor can improve the absorbance of photons from a wider range of energies and reduces energy loss. The way to improve the Voc is by tuning the electronic structures of the key materials based on the existing relationship [8] [7] [11] , that is, Voc is proportional to the gap between the LUMO of the acceptor and the HOMO of the donor, which will be fully introduced in the following chapter. The material innovation plays a key role in directly improving the efficiency.

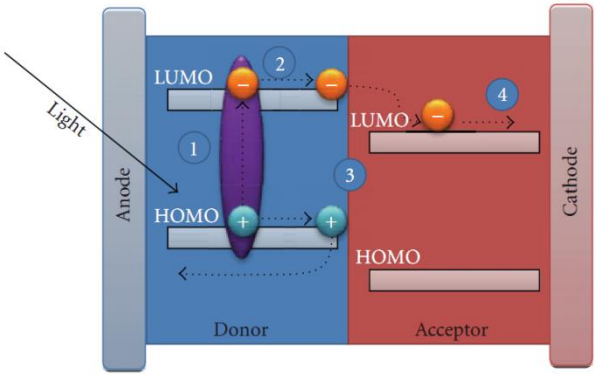

Figure 1.1: Photovoltaic mechanism chart in an organic solar cell [13]

1.2.2 Brief history of OPVs

In 1979, Tang at the Kodak Company invented the first OPV device using a perylenetetracarboxylic acid diimide derivative and copper phthalocyanine. [28] [29] The bilayer device showed an efficiency of about 1%. Its important feature was the introduction of a charge separation mechanism, that is, the donor material generates excitons (electron-hole pairs) and transports electrons to the acceptor material, after which the hole and electrons are separated and transferred to the opposite electrodes. Normally, the lifetime of excitons is about 10 nm diffusion length and most of them recombine before they reach the corresponding electrode. [30] By introducing an organic heterojunction layer, electrons can easily be injected from the LUMO energy level of the excited molecules to the LUMO level of the electron acceptor, and it is much more difficult to reverse the process, improving the separation efficiency of excitons significantly. In 1992, Sariciftci et al. [31] found that the photo-induced electrons can transfer from the conjugated polymer to fullerene and this process happened very fast (45 fs). This is 100 times quicker than that of a poly[2-methoxy-5-(2-ethylhexyloxy)-1,4-phenylenevinylene](MEH-PPV) single layer. The reverse process has to be much slower, which implies a longer-life electron with fewer recombinations with the hole. In 1993, Sariciftci et al. made a polyparaphenylene vinylene (PPV)/C_{60} bilayer heterojunction solar cell (Figure 1.2). [32] In the PPV and C_{60} interface area, the exciton achieved a high charge separation rate, and contributed to the generated photocurrent. After that, C_{60} and its derivatives became widely used as the electron donor materials. In 1995, the single polymer/C_{60} solar cell with bulk-heterojunction architecture was invented. The PCE of the devices is highly improved because this structure decreases the diffusion

length of excitons and increases the D/A interface area, which achieves a high charge dissociation and a low charge recombination. [33] Until now, the bulk-heterojunction is still the most widely-used structure in OPVs. After those milestones, the improvement in OPVs over the last 20 years mainly focused on their efficiency and durability. The lifespan of OPVs was improved up to two years, [32] and better encapsulation techniques are still in progress to achieve better durability by prohibiting the active layer and the electrode contact with oxygen and moisture, which are the main reasons for degradation. [34] [35] The world record efficiency of 13.2% is held by Heliatek, Germany in March 2016[2].

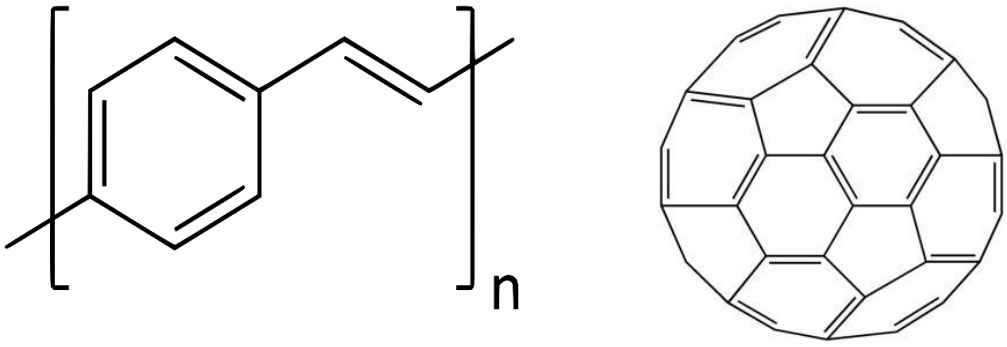

Figure 1.2: Structures of PPV and C_{60}

1.3 Device structure

Organic solar cell devices can be divided into three categories based on their structures: homojunction, heterojunction and dye-sensitised organic solar cells. Heterojunction solar cells also include p-n heterojunction, mixed heterojunction and bulk-heterojunction cascade structures, Figure 1.3. Dye-sensitised solar cells usually use a liquid electrolyte with a difficulty in encapsulation of the liquid. The organic solar cells mainly refer to those based on polymers, as does this thesis. [36]

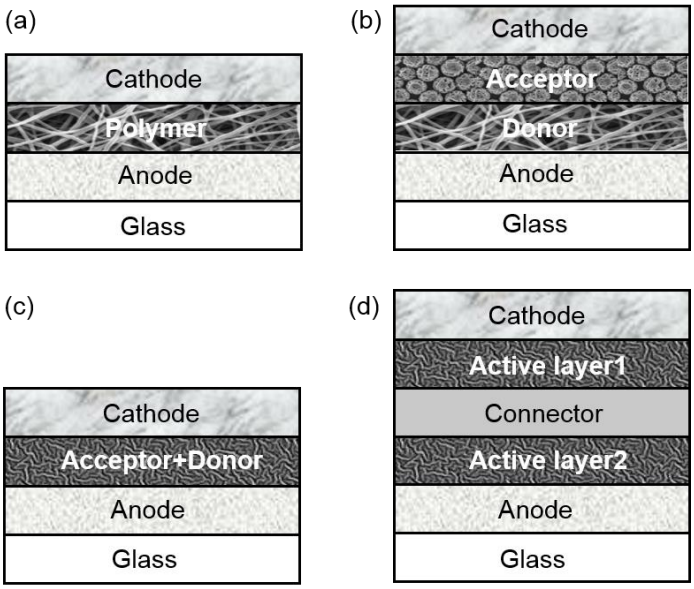

Figure 1.3: Schematics showing construction of (a) a homojunction solar cell; (b) a p-n hereojunction solar cell, (c) a bulk-heterojunction solar cell, and (d) a multijunction concentrator.

The homojuction solar cell is the earliest type with a single active layer sandwiched between two electrodes (Fig. 1-3). Common electrodes are indium tin oxide (ITO) as the anode and a low-work function metal, such as Al, Ca, Ag or Mg as the cathode. The work function difference between the two electrodes or the contacted Schottky barrier between the metal and polymer is the driving force for carrier movement in the active layer. [37] However, since the electron and the hole move in the same material, the recombination probability is very high, so such solar cells usually exhibit a very low light conversion efficiency of less than 1% [38] [39] .

The structure of a p-n heterojunction solar cell is also shown in Figure 1-3. The active layer is composed of donor and acceptor materials for the dissociation of excitons, which contributes to a higher PCE compared to the homojunction cells, due to the high electron affinity and low-lying LUMO of C_{60} which separates the

light generated excitons and allows efficient transport of the electrons. However, the effective dissociation of the excitons only occurs at the acceptor interface. The dissociation length of excitons before the charge combination is of the order of 10 nm [30]. The layer thickness is normally by 100-200 nm hence only the excitons close to the D/A interface can be successfully dissociated. [40] This means the bilayer junction still results in low efficiency due to the highly possibility of recombination of electrons and holes far from the D/A interface.

To increase the interface area between the donor and acceptor and thereby obtain more photocurrent, bulk-heterojunction solar cells have been developed where donor and accepter are mixed in the solution and then cast into a thin film (Figure 1.3). Scharber and Sariciftci reported a glass/anode/MEH-PPV+C_{60}/CATHODE/metal structure, in which the interface increases the contact area greatly and improves the PCE to 4%. [41] The important factors, such as the layer thickness, the domain size, the interface area and the crystallinity of polymer, determine the PCEs quality of the bulk heterojunction. Dennler et al. mixed the poly[2-methoxy-5-(3',7'-dimethyloctyloxy)-1,4-phenylenevinylene] (MDMO-PPV) with PCBM at different ratios as the active layer and found that the layer with more PCBM gave better battery properties. [42] Fan et al. deposited C_{60} and thiophene solution on ITO and poly(3,4-ethylenedioxythiophene) (PEDOT) was used as the modified layer to build the bulk-heterojunction solar cells. [43] They found that decreasing the amount of C_{60} can enhance the photovoltaic effect. Ideally, in the mixed heterojunction, the separation and collection of the charge are equivalent. However, the morphology of

the blend is disordered and there are many defects in the active layer. These defects act as barriers during the dissociation and the transfer of charge carriers. Eckert et al. found that connecting the donor and acceptor through a covalent bond leads to a mutual permeable bicontinuous grid structure with a micro phase separation; this can basically overcome most of the defects. [44] Using a non-conjugated flexible chain as a bridge to connect the donor and acceptor together can also optimise the microstructure and energy level of the system and reduce the loss of photons, excitons and carriers. [45]

The multijunction concentrator, also called the tandem OPV is a series of laminated batteries. It connects two or more device units together in order to absorb as much sunlight as possible and enhance the Voc and PCE. This kind of solar cell is applied with different materials to absorb the photons in the different sunlight spectral ranges, with the aim of decreasing the photon losses due to the conversion of the unused photons into heat. For example, You et al. designed a tandem solar cell with two polymers, Poly(3-hexylthiophene-2,5-diyl) (P3HT) and Poly[2,7-(5,5-bis-(3,7-dimethyloctyl)-5H-dithieno[3,2-b:20,30-d]pyran)-alt-4,7-(5,6-difluoro-2,1,3benzothiadiazole)] (PDTP-DFBT)/$PC_{71}BM$, the PCE of which first achieved over 10% in 2013, [46] the highest efficiency at that time. P3HT has a good absorption from 400-700 nm, while PDTP-DFBT with a lower band gap 1.38 eV, can absorb more light from 500-900 nm, that is the uncovered absorption range of P3HT, Figure 1-4. Therefore, the total absorption of the two polymers covers a large region of the solar spectrum, hence more photo-induced current is produced with

much higher efficiency. In theory, the total Voc is the sum of the Voc of every unit, but it is not easy to achieve. This is because we should consider several factors when designing such solar cells, for example, suitable band gap, layer thickness and transparent connecting layers. The contact between the unit cells should be Ohmic to reach a lower resistance for the system and a higher PCE. [47]

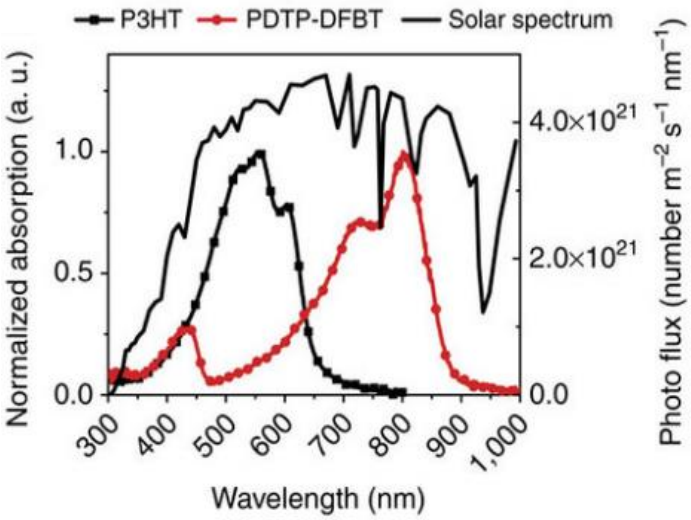

Figure 1.4: UV-Vis absorption of PCPDT-DFBT and P3HT[35]

1.4 Fullerene-based acceptor materials for OPVs

1.4.1 Introduction

In 1985, C_{60} was firstly discovered by Kroto, Smalley and Curl. [48] The name fullerene is from the architect Buckminster Fuller who successfully designed huge geodesic domes that have an analogous structure to C_{60}. Fullerene containing soot can be prepared by the arc method and combustion method. [49] C_{60} and C_{70} are the most abundant forms in fullerene soot. Besides this, soot is composed of higher fullerenes such as C_{76}, C_{82} and up to 100 carbon molecules. Research into the photo-physical, photo-chemical and induced charge transfer properties of fullerene established that fullerene-based materials are among the

best n-type materials for bulk heterojunction (BHJ) OPVs [50]-[51]. Some small organic molecules and polymers were designed and synthesised as acceptor materials [52]. However, the performance of these fullerene free acceptors is normally below expectations, and they perform poorly compared to the fullerene derivatives. Until now, C_{60} and C_{70} based fullerene derivatives are the two most common n-type materials for BHJ OPVs, [12] due to their good solubility, electron mobility and favourable miscibility with polymers.

1.4.2 Ideal properties of fullerenes for OPVs application

The fullerenes have three main properties that make them ideal for organic solar cells. Firstly, the polyhedral shape of fullerenes results in their isotropic or relatively isotropic electron accepting property. Secondly, fullerenes prefer extra electrons, which expand the cage, achieving lower energy and stabilising the fullerene. Ultrafast forward photo-induced electron transfer between fullerene shells hurtle towards the recombination. Thirdly, the fullerene has a large van der Waals surface beneficial for crystal packing, which is good for uniform film formation. Also other properties, such as high electron mobility, a long exciton diffusion length and a high dielectric constant of fullerenes are preferable for high PCEs in OPVs [53]-[54]. Although other candidate acceptor materials have some of these properties, fullerenes are almost ideal acceptors with all their properties.

Electron accepting and transport

Fullerenes tend to accept extra electrons, expanding in size resulting in the lower energy of fullerenes. Fullerenes are not ‘superaromatic’, because they avoid the

double bonds in the pentagonal rings resulting in poor electron delocalisation, therefore fullerenes behave as electron deficient alkenes and prefer reacting with electron rich species. [55] This electron affinity property of fullerene makes exciton dissociation more efficient, while recombination is inhibited.

Ultrafast forward electron transfer in fullerenes exhibit has been studied by femtosecond laser spectroscopy. A 30 fs forward process was found, the forward speed nine orders of magnitude faster than the back transfers [56], which is favourable for charge transfer in a BHJ structure.

Isotropic properties

Fullerene shells with 3D symmetry (polyhedral shape) have isotropic (C_{60}) or relatively isotropic (C_{70}) electron accepting properties. This has a positive impact on exciton diffusion, charge transfer and charge carrier mobility. In BHJ structures, the electron acceptance and transportation are required in all three dimensions. As fullerenes fulfil this requirement, achieving a higher efficiency for charge separation and charge transport, acting as excellent electron transport media between the donor material and the electrode.

Self-Packing

Fullerenes have a large van der Waals surface. The aggregation of fullerene cages arises from the van der Waals force between the cages, e.g. 1.6 eV for each C_{60} shell. [57] The high ordered packing of the shell gives a uniform layer morphology, which

results in high electron mobility of the active layer. Clusters of fullerenes can form favourable crystal structures after moderate annealing.

High dielectric constant

The major difference between inorganic and organic solar cells is in dielectric constant. For inorganic solar cells, the dielectric constant is high, while for OPVs it is much lower. A low dielectric constant of a polymer leads to tightly bonded excitons and high recombination. The high dielectric constant of fullerenes (ε=4.4) can stabilise the holes and electrons from dissociation, inhibiting recombination. [58] The high polarisability of fullerenes results in their high dielectric constant. [59] Therefore, improving the fullerene/polymer ratio in the blend could increase the dielectric constant of the active layer, resulting in better charge generation efficiency.

Other good electrical properties

The fullerenes have an adequate LUMO level for efficient exciton separation and charge transfer. The LUMO of fullerenes can also be tuned to avoid the loss of Voc, which will be discussed later. The electron mobility of fullerenes can reach a value of up to 6 $cm^2V^{-1}s^{-1}$. [60] Additionally, the exciton diffusion length in pure C_{60} was measured as around 40 nm. [61] This long length is beneficial for excitons diffusing to the D/A interface and completing the charge separation there.

1.5 The development of different fullerene derivatives for OPVs

C_{60} is the most common fullerene, accounting for about 70% of all fullerenes. [62] C_{70} is the second most abundant fullerene, accounting for the vast majority of the

remaining fullerenes. So-called higher fullerenes (those larger than C_{70}) are the remaining fullerenes, which comprise about 2% of the fullerenes. [18] Hence, any commercial exploitation of fullerenes is mainly limited to C_{60} and C_{70} based species.

In 1991, the first C_{60} solvent cast film was formed and showed a photovoltaic response as an n-type semiconductor.[63] Shortly after, C_{60} was blended with PPV, and it showed a good quantum efficiency for charge separation, and long lived charges in the microsecond regime with a low charge recombination (Brabec et al. and Sariciftci 1991-1992). [64] The first C_{60}/PPV OPVs with a bilayer structure were made in 1993 with a relatively high FF of 0.48 and a PCE of 0.04%, instead of only single layer OPVs. [65] The characterisation of solar cells shows a strong assistance of charge separation due to the fullerene layer.

Pristine C_{60} has extremely low solubility. This causes problems with the processability of C_{60} with polymer blends for film casting. Chemical modification of the fullerene was needed to increase solubility and thereby processability, while maintaining the good intrinsic properties of C_{60}. $PC_{61}BM$ was first synthesised by Wudl et al. [66] The synthesis route is summarised in Figure 1.5. The first two steps are for the formation of the PCBM addends, and the last step is the addition reaction by adding the PCBM group onto the cage, using sodium light for rebuilding the bond between the two bridge head carbons on the cage, which finally forms two sp^3 hybridised carbons.

Compared to C_{60}, $PC_{61}BM$ shows higher solubility in most aromatic solvents (table 1.1). Since the solvent selection for the active layer will influence its morphology

which will affect the PCE of OPVs, replacing toluene with chlorobenzene was attempted in order to change the morphology of the PPV/PCBM blend and achieve higher PCEs of about 20%. [67] Furthermore, good miscibility of $PC_{61}BM$ with the polymer allows for diffusion into the polymer film to achieve a donor-acceptor network. As $PC_{61}BM$ can self-assemble into acceptor materials, the bulk heterojunction formed has a higher efficiency than that of the bilayer structures. The electronic properties of $PC_{61}BM$ and its derivatives relevant to the PCE of OPVs is described below.

Fullerene	C_{60}	C_{70}	[60]PCBM	[70]PCBM	Bis-[60]PCBM	C60[Ind]	C60[Ind]$_2$
Solubility in Toluene	3	1.5	10	20	>100	5	75

Table 1.1: Solubility (mg/ml) of PCBM and C_{60} in different solvent [67]-[68]

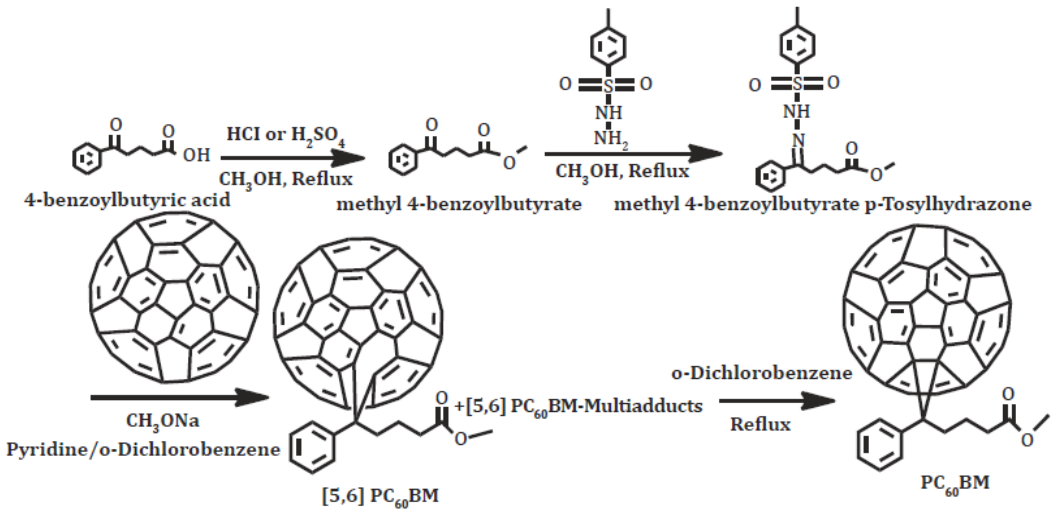

Figure 1.5: Synthesis of PCBM [59]

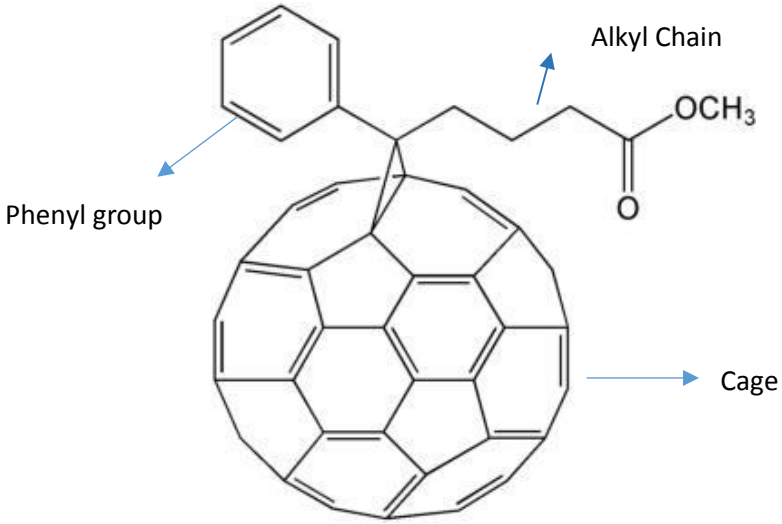

Figure 1.6: Molecular structure of $PC_{61}BM$

Fullerene derivatives

Depending on the molecular structure, the fullerene acceptors can be divided into two types: PCBM derivative acceptors and non-PCBM based acceptors. As a $PC_{61}BM$ acceptor is widely applied in OPVs, many researchers have tried to modify the cages, alkyl chain and phenyl group of $PC_{61}BM$ as shown in Figure 1.6, in order to further improve the PCE and the miscibility with polymers. Additionally, new molecules based on C_{60} with the other functional groups on the cage have been designed with different electronic structures, higher mobility and other properties.

1.5.1 PCBM Derivatives

C_{70} is the second most abundant type of fullerene. Due to the asymmetry of C_{70}, it can absorb more light in the visible region than C_{60}. Hummelen et al. invented $PC_{71}BM$, and found that OPVs based on $PC_{71}BM$ have similar Voc and FF values to ones based on $PC_{61}BM$. However, the Jsc values were up to 1.5 times higher, thereby the PCEs were highly improved. [16] To date $PC_{71}BM$ represents one of the best acceptors for application for in high efficiency OPVs. Hummelen et al. [69] used C_{84} to

replace C_{60} and created $PC_{85}BM$. Light absorption from C_{84} approaches the infrared region. However the LUMO of $PC_{85}BM$ is 0.35 eV lower than that of $PC_{61}BM$, and also due to the lower solubility, the PCE of OPVs based on $PC_{85}BM$ is only 0.25%. The linear relationship between Voc and the LUMO of the acceptor determines the unfavourable properties of $PC_{85}BM$, with a lower LUMO. The details of the relationship between the Voc and LUMO of the acceptor are discussed in section 1.6. In addition, Ross et al. designed Lu3N@C_{80}-PCXM, as the atoms in the cage of endohedral fullerenes improve the LUMO level, which is 0.28 eV higher than $PC_{61}BM$, hence achieving a larger Voc. [70] The PCE was improved to 4.2%, however the cost of endohedral fullerenes is far higher and it is commercially non-viable. They also found that the annealing treatment for the cell after the deposition of the LiF/Al layer can improve the efficiency from 2% to 4%.

Modifying the phenyl group

Addition reaction of the electron donating groups on to the fullerene cage can lower the reduction potential of the fullerene and hence improve the energy of the LUMOs. Substitution reaction to replace an H from the phenyl group by electron donating groups also can improve the LUMO level of PCBM. Substitution of 2,3,4-OMe for H on the phenyl group of $PC_{61}BM$ achieves a 34 meV improvement of the LUMO level of $PC_{61}BM$.[71] Jen's group synthesised TPA-PCBM and MF-PCBM with triphenylamine and fluorine replacing the phenyl group (Figure 1-7). [72] The Voc was improved by 20 mV. Additionally, they have amorphous structures resulting in better stability under heat. Choi made [6, 6]-thienyl-C61-butyric acid methyl ester (TCBM) with thiophene replacing the phenyl group of the PCBM. The efficiency was

not improved much, as TCBM has a similar energy to that of PCBM, while its solubility was significantly increased to 180 mg/ml.

Modifying the alkyl chain and the ester group

The alkyl chain length does not have a significant effect on light absorption and electronic structure much. However, a longer chain can to some extent improve the solubility and miscibility with polymers, but also lowers the mobility of the fullerene as the inter-cage distance is increased. [73] The promising solubility of the fullerene derivatives for achieving the designed properties of the OPVs of 30-80 mg/ml in chloride benzene matching the solubility of P3HT of around 50-70 mg/ml. These matched solubilities can improve the morphology of the active layer with a better fullerene-polymer miscibility. [74] Li et al. synthesised [6,6]-phenyl C_{61}-butylsaure butyl amide (PCB-n-BA) by replacing the ester group with acylamide. [75] The hydrogen bonding effect from acylamide accelerates the agglomeration of fullerenes for a better charge transport hence it slightly improves the PCE. A better modification of the ester group is suggested by Mikroyannidis et al. who replaced the methyl group of the ester group with *N*-heterocyclic carbenes (NHCS): this new molecule is called F-NHCS. [76] Not only can F-NHCS absorb a wider range of light from 250-900 nm, but the LUMO level is improved by around 0.25 eV compared to that of PCBM.

According to the above review, most mono-addictions on the fullerene do not largely improve the PCE of the OPV. In contrast, multi-addition reactions can

efficiently improve the LUMOs of the fullerene derivatives, leading to higher PCEs. BisPC$_{62}$BM is a good example and will be fully introduced in section 1.6.

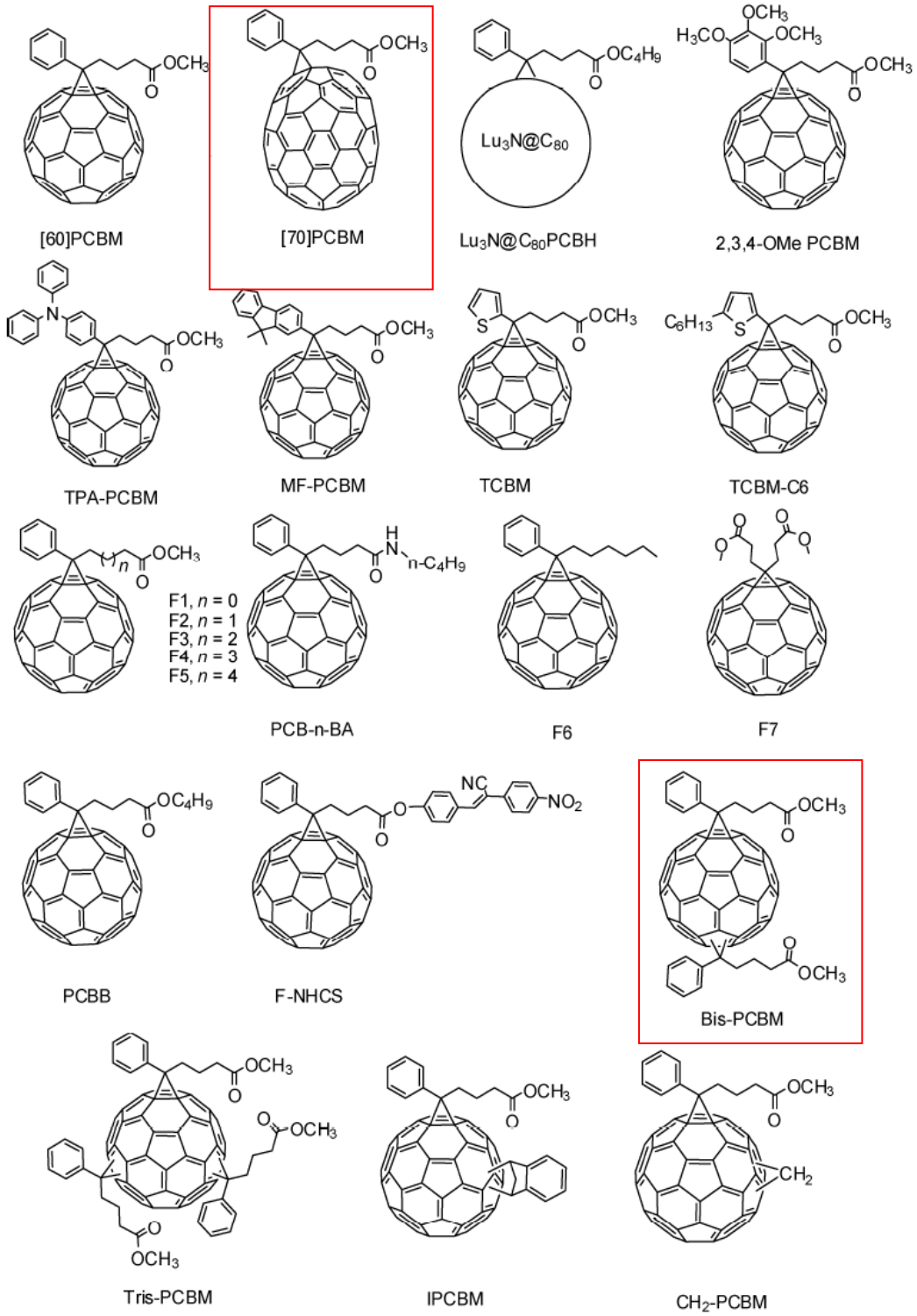

Figure 1.7: Acceptors based on PC$_{61}$BM.

1.5.2 Non-PCBM fullerene acceptors

Some new molecules based on the C_{60} cage were invented to compete with the efficiency of the PCBM based OPVs. Some show performances were below that of PCBM, such as 1,1-bis(4,40-do- decyloxyphenyl)-(5,6)C61 diphenylmethanofullerene (DPM-12) and 4,40 -dihexyloxydiphenylmethano-[60]fullerene (DPM-6) in the double alkoxy group, and Fulleropyrrolidines (FPs) which was synthesised by halogens substituted on the phenyl group. However the PCEs of OPVs based on these are >1% lower than OPVs based on PCBM, although better solubility was achieved. [77] [78] However, it is worth to introduce two compounds silylmethylfullerenes (SIMEF) and 1',1'',4',4''-tetrahydro-di[1,4]methanonaphthaleno[5,6]fullerene-C60 (ICBA). SIMEF is composed of the Si element and thereby it has a good crystal structure for electron transfer. [79] Also it has a LUMO 0.1 eV higher than that of $PC_{61}BM$. The devices based on this material have an improved performance with 5.2% PCE and 0.75 V Voc, compared to PCBM based OPVs.

More recently, a novel indene-C_{60} ($IC_{60}BA$) was reported by Zhao, the LUMO of which is 1.17 eV higher than that of PCBM, and is also higher than that of bisPCBM. P3HT:ICBA has high PCEs of about 6.46% with an impressive Voc = 0.84 V. [80] [81] As for $IC_{70}BA$, it has a higher LUMO of 0.19 eV and Voc 0.84 eV higher than $PC_{71}BM$ in the blend system with P3HT. [82] The typical fullerene acceptors are listed with their LUMO and HOMO energies and mobility in Table 1-2**.** All the molecular structures of the above discussed fullerene derivatives are given in Figure 1.7.

Materials	HOMO (ev)	LUMO(eV)	Mobility (cm^2/eV)
PTCBI	6.1	4.4	2.4×10^{-6}
PTCDA	6.8n	4.6	-
C_{60}	6.2	4.0	5.1×10^{-2}
C_{70}	6.4	4.3	1.3×10^{-3}
$PC_{61}BM$	6.1	4.3	2×10^{-7}
$PC_{71}BM$	6	4.3	$1x\ 10^{-3}$
$BisPC_{62}BM$	-	4.2	$7x\ 10^{-8}$
ICBM	-	4.1	-
$IC_{70}BM$	5.8	4.1	-
$Lu_3N@C_{80}PCBM$	-	4.0	4×10^{-4}

Table 1.2: Summary of electric properties of typical acceptors [83]-[94]

1.6 Improving the LUMO energy of fullerene based derivatives

According to experimental results, the LUMO of $PC_{61}BM$ is around 100 meV higher than that of C_{60}, and OPVs based on $PC_{61}BM$ achieved a larger Voc, so had higher PCEs. [84] In order to demonstrate this clearly, we have to introduce the relationship between the LUMO energy of the acceptor and Voc here.

It is generally believed that the value of Voc is proportional to the energy level offset between the HOMO of the donor and the LUMO of the acceptor (E^D_{HOMO}-E^A_{LUMO}). [85] The LUMO offset is the downhill driving force for exciton splitting and charge dissociation at the interface, but according to previous research, it is much higher than the binding energy for charge dissociation resulting in energy loss and low Voc. Theoretically, two methods can be applied to improve Voc, raising the LUMO energy of the acceptors or lowering the HOMO energy of donors with an according decrease of its LUMO (Figure 1.8). Since the HOMO and LUMO of the

donor and the accepter are completely determined by their structures, modification and synthesis of new materials can efficiently tune the HOMO and LUMO of the donor and the acceptor to obtain promising Voc values. Since the LUMO of C_{60} is too low, the LUMO-LUMO offset between donor and acceptor is obviously larger than the 0.3-0.5 eV necessary for D/A electron transfer and it causes a high loss of Voc. [84]

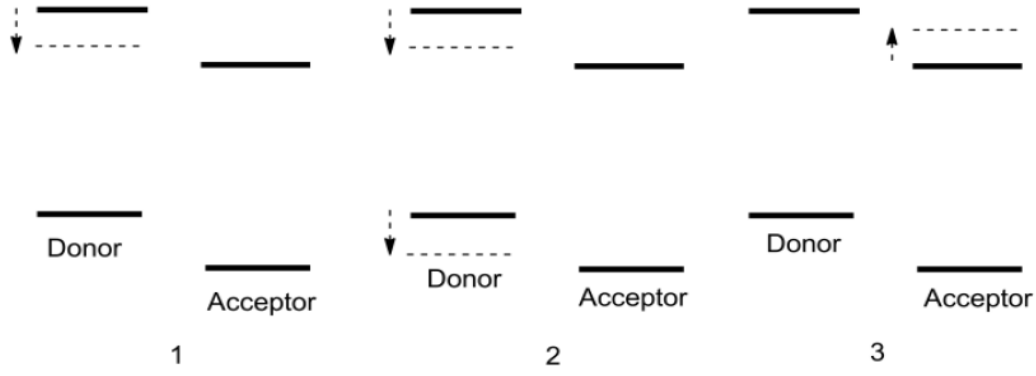

Figure 1.8: Tuning energy level of donor and acceptor for improving V_{oc} [84]

To improve the LUMO level of the fullerenes, the double bonds can be saturated by making multiple additions directly to the cage. The improvement from addends is about 100 meV per double bond, e.g. from C_{60} to $PC_{61}BM$, from bis$PC_{62}BM$ to tris$PC_{63}BM$. [84] A higher LUMO of the $PC_{61}BM$ results in a reduction of the LUMO-LUMO offset between the donor and the acceptor, leading to a higher Voc of OPVs. The major breakthrough is the C_{60} bis-adducts with two electron donating addends, called bis$PC_{62}BM$ that show around a 100 mv higher LUMO than that of $PC_{61}BM$, with a PCE of 20% higher than that of $PC_{61}BM$ based OPVs.[87] Unfortunately the increase in the number of addends leads to a decrease in the mobility of the

electron carriers. The low electron mobility of trisPC$_{63}$BM results in a trapping of the electrons in the active layer. In fact the decrease in mobility for trisPC$_{63}$BM cancels the benefits from the increase in Voc, so that the PCE of trisPC$_{63}$BM is actually lower than that of PC$_{61}$BM. According to the research of Lenes et al., the electron current for trisPC$_{63}$BM was decreased by three orders of magnitude, compared to bisPC$_{62}$BM. [13] However for bisPC$_{62}$BM, the decrease in mobility is small and hence it has a better PCE than PC$_{61}$BM.

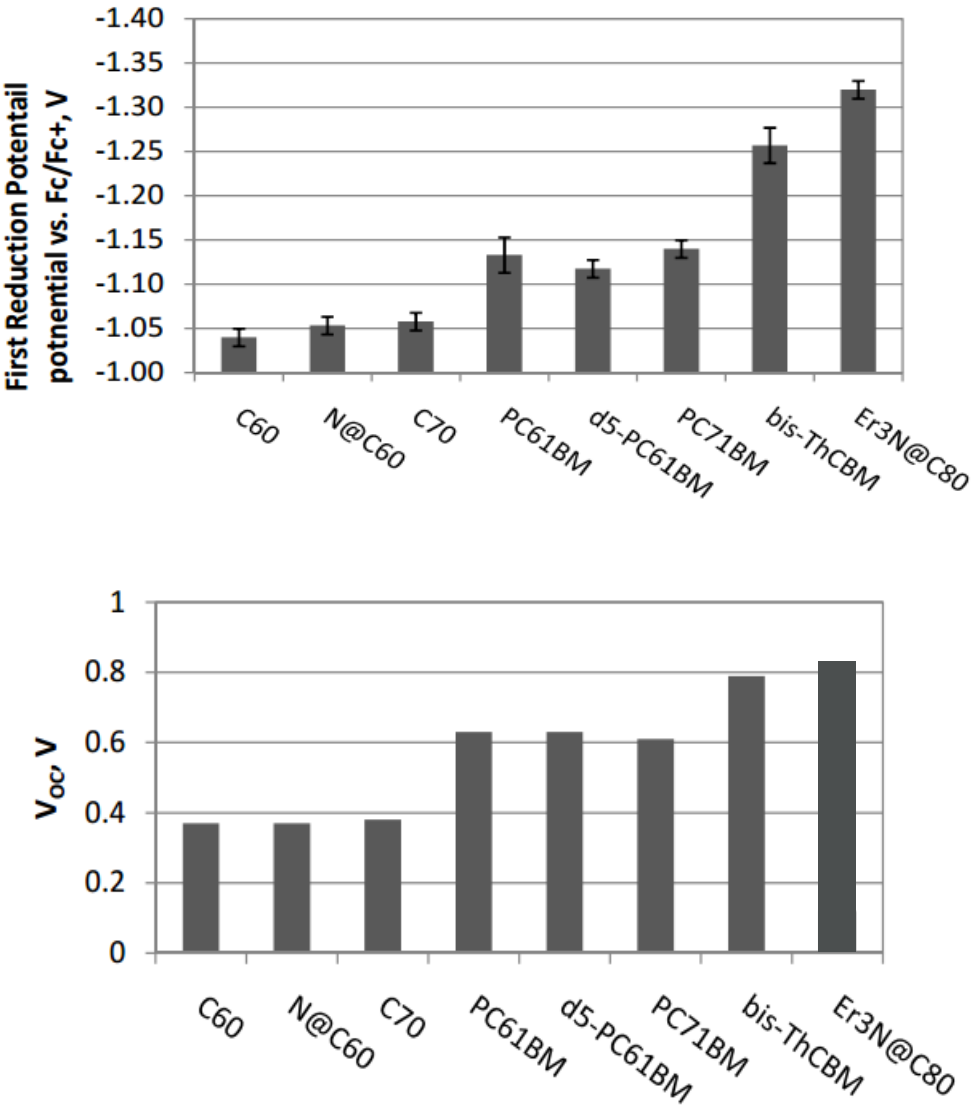

Figure 1.10: The relationship between the first reduction potentials of the fullerene derivatives and the Voc of OPVs based on these materials. [86]

More convincing examples for proving the principles are shown in Figure 1.10. It demonstrates the LUMOs of eight different fullerene-based acceptors from original fullerenes to fullerene derivatives and endohedral fullerenes, and the corresponding Voc of the OPVs with acceptor/P3HT are also listed in ascending order. The lowest LUMO is from C_{60}, higher than that from the mono-adduct fullerenes, and obviously the bis-adducts generally have 100 meV to 200 meV higher LUMOs than both of them. On the other hand, the Voc of OPVs fabricated based on those materials is proportional to the LUMOs of the acceptors. Therefore, electron donating groups added to the cages help to increase the LUMO and the Voc, while the endohedral fullerene exhibits quite high LUMOs but are expensive.

BisPCBM

As mentioned, bisPCBM has a higher LUMO than that of PCBM and achieves a high PCE (higher than 6%) solar cell. Two addends on the fullerene cage make it more soluble, and it was also treated as an effective phase separation inhibitor in PCBM-P3HT with high morphological stability and stable PCEs by Liu et al. [87] However, the different possible bridging points of two addends on the C_{60} derivative theoretically produce more than 20 isomers of bis$PC_{62}BM$, and the number and type of isomers will be fully discussed in chapter 2. The presence of multiple isomers decreases the electron mobility in OPVs, because they interfere in the π-π interactions between the fullerene cages. Also, due to the different reduction potentials of isomers, the isomers with less negative reduction potentials act as electron traps. Moreover, the overall morphology of solar cells is negatively impacted by the mixture of isomers.

Clearly, isomer-pure bis$PC_{62}BM$ can achieve better electron mobility and morphology, which directly improves the PCE of the OPVs. Although, this idea has been known for several years, no isomer-pure device has been fabricated. Recently, Bouwer et al. used an ethylene tether in the synthesis process of bis$PC_{62}BM$ and successfully decreased the isomer number in the mixture from 22 down to seven. [88] This is still far from ideal. My PhD research is to isolate these isomers by the techniques introduced below and characterise them.

1.7 Fullerenes purifying techniques

Normally, fullerenes can be produced by two methods, the vapourisation of carbon fragments and chemical vapour deposition from various carbonaceous or hydrocarbon materials. [89] [90] However due to the thermal reactions, the direct products are typically insoluble soot, together with soluble fullerenes and some potentially soluble impurity molecules. Two more stages are required to isolate pure fullerenes from the soot. The first stage is extraction. This process forms a fullerene-enriched extract and leaves the solid soot and other insoluble remainders behind. The second stage is purification, the isolation of the target fullerene or its isomers from the extract of the first step.

1.7.1 Fullerene extraction

Extraction is normally undertaken by sublimation or solvent extraction. In the sublimation method, in order to avoid oxidation, the soot is heated under helium gas or under vacuum atmosphere, and then condensed in a cooler collector. [91] This

method is rarely used in real production due to the partial decomposition from the thermal stress from condensation (quenching) although it is environmentally friendly. For the solvent extraction, it is very important to choose several solvents (usually based on the solubility of C_{60} fullerene) to increase the extraction of one fullerene over others. The research shows that C_{60} is poorly soluble in polar and H-bonding solvents and has high solubility in halogenated alkane derivatives and aromatics. [92] Orthodichlorobenzene (ODCB) may be the best solvent for extracting fullerenes considering the price and solubility. [93] [94] Both of the extraction methods cannot reach the pure individual fullerene, and end up with a mixture of different fullerene molecules, which tend to bring some impurity molecules along with the fullerene. Further purification is required.

1.7.2 Fullerene purification

There are several methods to purify the extract, such as liquid chromatography, crystallisation and complexation. [95] Liquid chromatography is the main technique of purification and is capable of yielding high purity batches of C_{60}, C_{70} or mixtures of higher fullerenes, fullerene isomers including liquid chromatography and gel permeation chromatography.

1.7.3 High performance liquid chromatography

One of the common separation techniques for fullerene isomers is high performance liquid chromatography (HPLC). Liquid chromatography is a separation technique, where a liquid sample (mixture) is injected into a column packed with a

porous phase. After that, the individual components of the sample are transported along the column by gravity or pressure and come out of column with different retention times, as shown in Figure 1.11. When the liquid phase (the mobile phase) is transported by high pressure from a pump, it is called HPLC which is more efficient and sensitive.

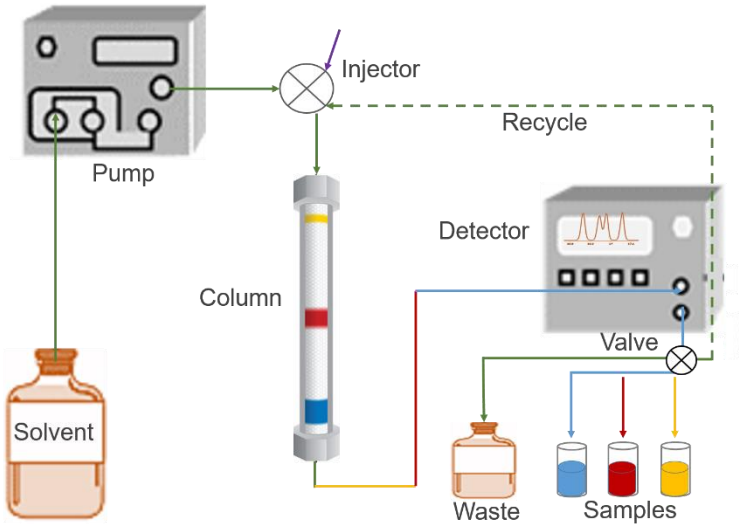

Figure 1.11: Mechanism of liquid chromatography.

The mechanism of HPLC is based on the affinity of samples for the mobile phase or the stationary phase (the particle in the column). The affinity shows in different ways, such as absorption, partition and ion exchange, etc. If the affinity of the sample on the mobile phase is higher than that on the stationary phase, the sample comes out rapidly, whereas if the sample has a strong interaction with the stationary phase, then it is retained in the column and is eluted from the column later.

For the fullerene isomers, the difference in the retention time of isomers from HPLC with a modified silica-based column shows a high possibility of isolating isomers by this technique, because of different polarity and symmetry properties of the isomers, resulting in distinct interaction between the isomers and the stationary phase. However, the overlapping of the peaks representing different isomers is a problem, as shown in Figure 1.12. It is known that a longer length of column can achieve better separation. In practical terms, the length is limited, but a longer length can be achieved by using a recycling technique, which lets the sample pass through the column several times until the baseline resolved separation is obtained. The particle materials in the column highly affect the efficiency of the separation. Three columns for the fullerene isomers separation were introduced here. All the columns are packed with porous particles with sizes from three to 15 micros. The basic silica column is filled with simple Si bonded to hydroxyl. COSMOSIL 5PBB is filled with the five micro particles of the pentabromobenzyl group bonded silica, commonly used for the preparative-scale separation of fullerenes, [96] and it can separate the structure of different isomers even by a double bond difference. COSMOSIL PYE is a pyrenylethyl group bonded silica column for the structural isomer separation based on the π-π interaction, charge transfer and hydrophobic effect. For the separation of chiral isomers, some chiral stationary phases can be used, which are usually used in food and drug purification. Daniel et al. gave a detailed explanation on how to choose the right chiral columns. [97]

HPLC can also be applied for some analysis, mainly for component identification and quantitative analysis. [98] Through comparing the shape and the peak position of two

chromatographs, it is possible to assign an unknown peak to a corresponding peak of a standard chromatograph, due to the quite similar interaction between the solute and the stationary phase. For example, the elution time for C_{60} through a 5PBB column is 380 s at room temperature, as the fluctuation of the temperature would cause a slight shift of the elution time. [99] If we found another fullerene peak from a fullerene mixture with this retention time, we may confidently assign this to C_{60}. For quantitative analysis, integration of the peaks can be applied since the amount of compound eluted is proportional to the area of the peak. Calibration should be carried out to establish the relationship between the peak area and compound concentration.

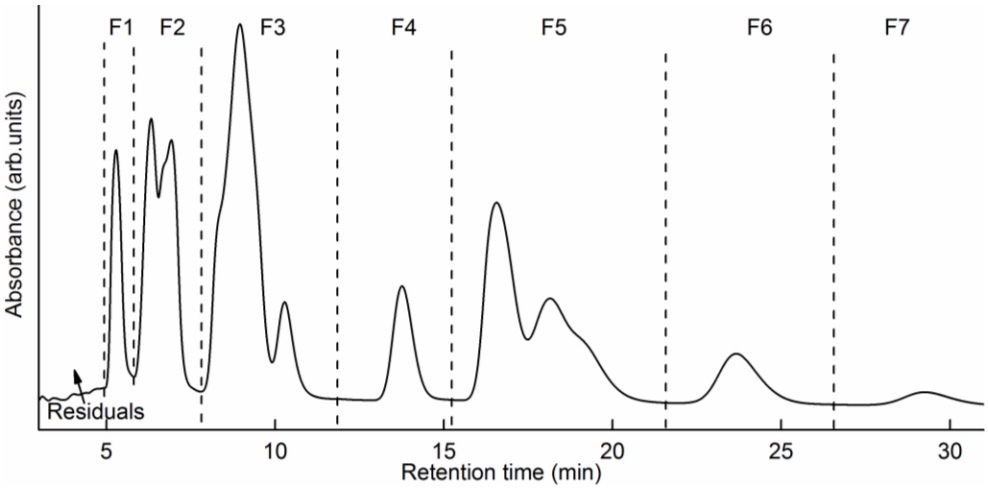

Figure1.12: the HPLC chromatogram of an isomer mixture of bis$PC_{62}BM$

Chapter 2

NOMENCLATURE OF FULLERENE DERIVATIVES

In this chapter, a nomenclature scheme for fullerene derivatives and the isomers is developed. Through full analysis, the distinguished isomers of bis$PC_{62}BM$ are counted and named by the cis and trans methods, while the R-S nomenclature is applied for the isomers of $PC_{71}BM$.

2.1 Nomenclature of PCBM

Applying IUPAC rules, the systematic name of PCBM is 'methyl 4-[phenyl-1a*H*1(9)-C_{60}-I_h[5,6]methanofullerene-yl]butanoate', but PCBM as an abbreviation is easier for pronunciation in common use. It was originally reported that 'phenyl-C_{61}-butyric acid methyl ester' is another name for PCBM. This name represents and properly refers to the whole molecular structure well. From the left to the right of the name, it can be explained as (a phenyl ring bonded to a C_{61} methanofullerene at the 1a carbon of the methanofullerene, which is in turn bonded to a butyric acid methyl ester group) via the 1a carbon. $PC_{61}BM$ accurately clarifies 61 carbons being left, and also implies that the PCBM is based on the C_{60} fullerene cage only. However, with the emergence of new fullerene derivatives, e.g., one based on C_{70}, the number of carbon atoms on the fullerene has to be explicitly stated. There are two main methods: one consists of naming the original fullerene – e.g., C_{70} in C_{70}PCBM, [70]PCBM, etc. The other consists of naming the methanofullerene – e.g., $PC_{71}BM$, bis$PC_{72}BM$, etc. In this work, the latter method in the form of $PC_{71}BM$ was applied. We prefer this method for two reasons. Firstly, it is more faithful to the original systematic naming method; and secondly, it removes the ambiguity of the fullerene used. An example of bis$PC_{84}BM$, the C_{84} moiety is a dimethanofullerene; and it is based on the fullerene C_{82} (*i.e.*, $[2C_1]C_{82}$) – not on the fullerene C_{84}. Next, someone would think that the bridging point on the C_{60} of PCBM should be contained in the name, but in fact, the position of the bridgehead carbon is not necessary noticed. In $PC_{61}BM$, the carbon bridges of any one of the 30 double bonds of the C_{60} molecule can become the 1a carbon of the resulting methanofullerene, and because all 30 double bonds are symmetrically equivalent, there is no difference between the

bridge head carbon attached to [5,6], [7,8], [1,9], etc., as the double bond of C_{60}. Therefore, for $PC_{61}BM$ (Figure 2.1) the bridgehead carbon atoms need not be especially named. The [1,9] double bond is by default.

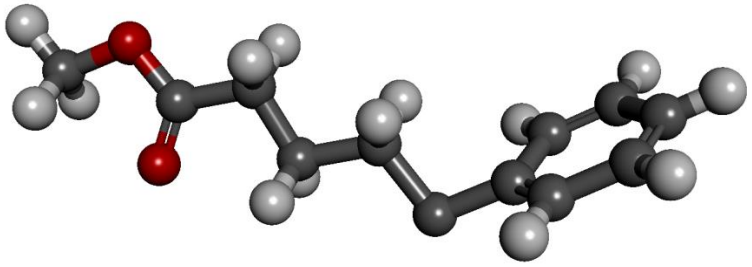

Figure 2.1 A diagram of the PCBM addend, which adds across a former double bond of the fullerene at the carbon before the phenyl ring (becoming the 1a carbon on the methanofullerene). The red atoms are oxygen, the grey atoms are carbon and the white atoms are hydrogen.

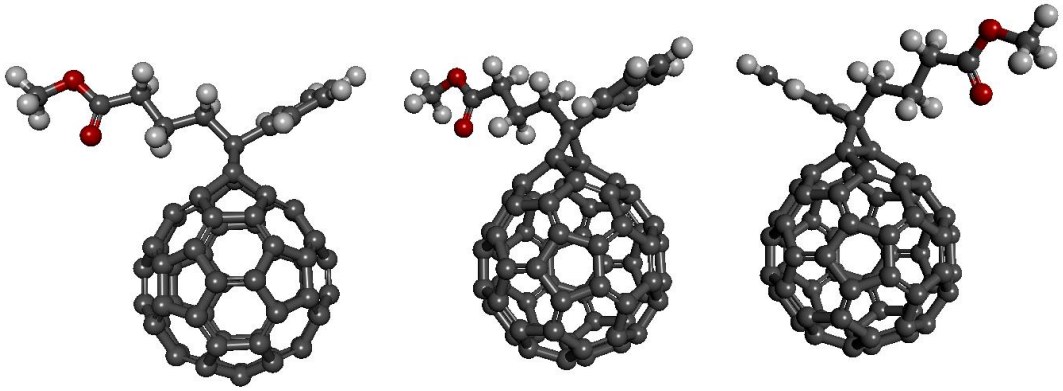

Figure 2.2 The methanofullerene $PC_{61}BM$ shown in three different orientations. The bridgehead carbons have become sp^3 hybridised and the (1,9) double has become a single bond. The figure also shows the attachment occurs at the bridgehead carbon (1a carbon) before the phenyl ring of the PCBM addend.

2.2 Nomenclature on $BisPC_{62}BM$

The IUPAC name for $bisPC_{62}BM$ isomers is too long to fit onto a single line of 12 pt text. One isomer of $bisPC_{62}BM$ with a *cis* arrangement, where the two bridging PCBM groups are diametrically opposite to each other, is named by the IUPAC method showed below. The text is reduced to 10 pt.

"*cis*-dimethyl,4,4'-[phenyl-1a*H*1(9)-phenyl-2a*H*52(60)-C_{60}-I_h[5,6]dimethanofullerene-diyl]dibutanoate,"

Obviously a suitable abbreviation for the name is necessary. BisPC_{62}BM is a good name pattern to represent that there are two PCBM groups attached to C_{60}; the 1a carbon bridging carbons 1 and 9 (by default) and the 2a carbon bridging any one of the rest of the 29 double bonds on the C_{60} molecule. Since there are the two addition points to C_{60}, these bonds names or two bridgehead carbon positions need to be explicitly included in the abbreviated name. An example of the randomly selected isomer given above with the full IUPAC can be shortened to 1, 9-52, 60-bisPC_{62}BM. However, this may be further shortened, because the bridging of the 1 and 9 carbons is common to all bisPC_{62}BM isomers, which could be left implied. Therefore, 52, 60-bisPC_{62}BM represents a bis-adduct where two PCBM groups bridge carbons 52, 60 and carbons 1,9 on the carbon cage.

One final complication is about the trans or cis structure of the two PCBM groups. The asymmetry of the PCBM groups on the 1a and 2a carbons means that 52,60-bisPC_{62}BM has two possible orientations of the two PCBM groups relative to each other, and Figure 2.3 clearly demonstrates the structure of cis- and trans-52,60-bisPC_{62}MB.

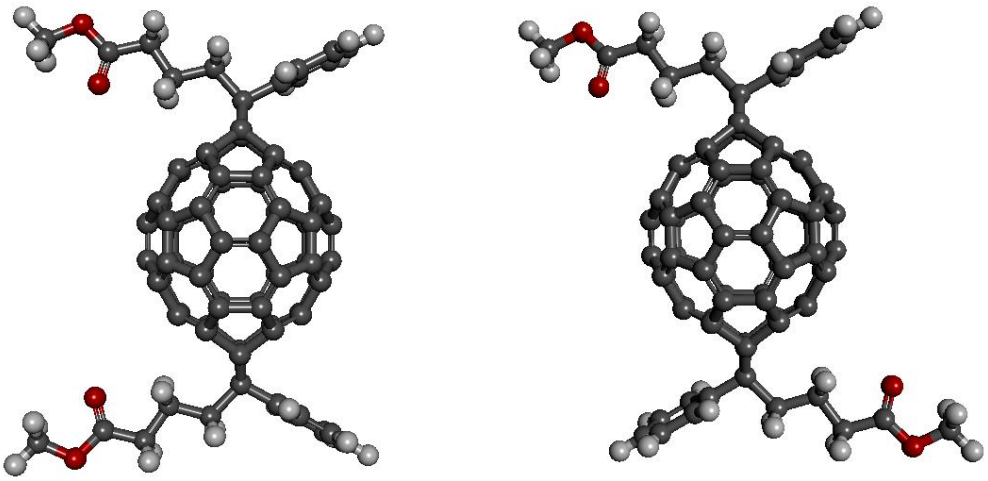

Figure 2.3 The cis (left) and trans (right) isomers of 52,60-Bis$PC_{62}BM$, where cis and trans refer to the orientation of the two addends relative to each other. In the cis arrangement both phenyl groups (for example) are on the same side of a vertical plane perpendicular to the page going through the 1a and 2a carbons, whereas in the trans arrangement the two phenyl groups (for example) are on opposite sides of that plane.

2.2.1 How many isomers are there of bis$PC_{62}BM$?

Literally, there are hundreds of possible isomers of bis$PC_{62}BM$ because there are two major kinds of bis-adducts: methanofullerenes and homofullerenes. They could all be methanofullerenes – where the two bridged carbon-carbon double bonds are converted to single bonds with an associated change in hybridisation from sp^2 to sp^3 for these bridgehead carbons. Similarly, they could all be homofullerenes – where the bridged double bonds are completely broken and the bridgehead carbons retain their sp^2 hybridisation. Furthermore, they could be combinations of both where one PCBM group adds to give a methanofullerene and the second PCBM adds to give a homo-fullerene – or vice versa. These possibilities alone give rise to 232 bis$PC_{62}BM$ isomers. They could also be homofullerenes involving only single bonds, combinations of double bond-based methanofullerenes and single bond-based homofullerenes, and/or double bond-based homofullerenes and single bond-based homofullerenes. However, $PC_{61}BM$ has been clearly proved to be a

methanofullerene. This was demonstrated by ^{13}C NMR spectroscopy, which shows that the two bridgehead carbons are symmetrically equivalent and have a chemical shift that is consistent with sp^3 hybridisation. This means no existence of both single bond-based and double bond-based homofullerenes, since neither of these contain any sp^3 hybridised carbon on the fullerene.

At the beginning of my PhD, three isomers of bis$PC_{62}BM$ were isolated in our lab, and the ^{13}C NMR characterisation was undertaken to prove that all three isomers are methanofullerenes. The ^{13}C NMR spectra are shown in Figure 2.4. The peaks in the regions from 70-90 ppm are for the sp^3 hybridised carbons, which indicate the cage is closed. Two peaks at 78.88, 78.67 ppm for symmetric isomer 1 (two addends have a mirror plane between), four peaks 78.75, 78.72, 78.35, 78.17 ppm, for non-symmetric isomer 2 and 80.48, 80.45, 80.20, 78.82 ppm for the non-symmetric isomer 3 are located in this region, respectively. The next group of lines, ranging from 125 to about 135 are assigned to the 12 carbons of the two phenyl groups, as these lines are close to the 128.0 ppm value for the carbons in the phenyl-related compound, benzene. The forest of 56 lines between 135 and 155 ppm are assigned to the 56 remaining sp^2 hybridised carbons of the fullerene. Finally the two very close lines near 175 ppm in each spectrum are readily assigned to the sp^2-hybridised carbonyl carbon of the butyric acid methyl ester groups (one from each of the two groups). Although this does not prove that all isomers of bis$PC_{62}BM$ are methanofullerenes, it is a strong indicator that this is likely to be true. If this

assumption is true, the next step is to determine the number of methanofullerene isomers of bis$PC_{62}BM$.

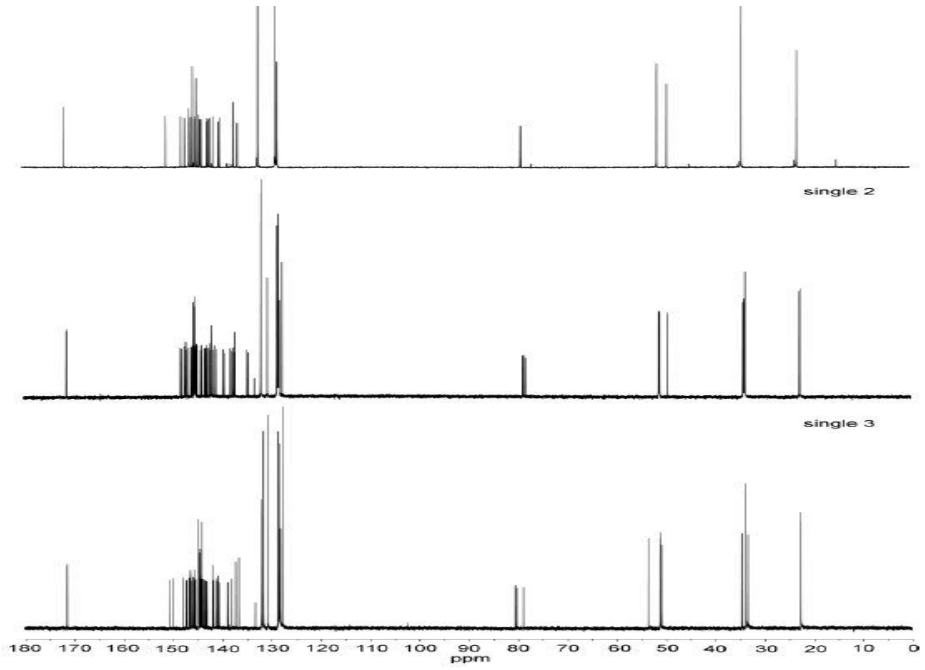

Figure 2.4: The ^{13}C NMR spectra of the three purified isomers; isomer 1, isomer 2 and isomer 3. Peaks below 60 ppm originate from the 'BM' group, and those between around 80 ppm come from the four now sp^3 'bridgehead' carbons of the fullerene – confirming their methanofullerene nature. The lines above 170 ppm correspond to the carbonyl carbon of the BM group. Those in the 125 – 135 ppm region belong to the phenyl group whereas the forest of lines between 135 and 155 ppm correspond to the 56 remaining sp^2-hybrisided carbons of the fullerene.

C_{60} consists of 60 single bonds and 30 double bonds. As all double bonds are symmetrically equivalent, the first PCBM group adds across carbon atoms 1 and 9 of C_{60} by default. That leaves 29 other double bonds, to which the second PCBM group may add. These double bonds are given in Table 2.1 below.

2,12	3,15	4,18	5,6	7,8	10,11	13,14	*16,17*	19,20	*21,40*
22,23	24,25	26,27	28,29	*30,31*	32,33	34,35	36,37	38,39	41,42
43,57	*44,45*	46, 58	47,48	49,59	50,51	52,60	53,54	55,56	

Table 2.1 The 29 remaining double bonds on C_{60} to which the second PCBM group may add to form a C_{60}-bisPCBM methanofullerene isomer.

29 regio-isomers of bis$PC_{62}BM$ are constructed by different bridging points of the second PCBM group to the rest of the 29 double bonds. Moreover, according to the asymmetrical structure about the 1a and about the 2a carbons, each of the 29 regio-isomers may exit two stereo-isomers depending on the relative orientations of the two PCBM groups. Therefore, this gives a nominal total of 58 methanofullerene isomers of bis$PC_{62}BM$.

However, several of these isomers will be symmetrically equivalent because of the very high symmetry of the C_{60} molecule. Additionally, the vast majority of the isomers of bis$PC_{62}BM$ are chiral, which will further reduce the number of isomers. The structures of all 58 nominal isomers can be optimised by semi-empirical methods using the Gaussian 09 software package, and they were compared in order to find symmetrically equivalent isomers and non-equivalent mirror isomers.

2.2.2 Cis and trans of bis$PC_{62}BM$ isomers

However, in this analysis process, it was realised that the division of stereo-isomers into cis and trans groups is much easier, compared to the above method. There are two kinds of definitions of cis and trans definitions for fullerenes. One is from Hirsch, stating that bis-isomers are defined as trans if the two PCBM groups occur in different hemispheres of C_{60}, and are cis if they occur in the same hemisphere [92]. This is pictorially helpful, but is ultimately redundant, because the hemisphere the addends add on is encoded in the carbon atom numbering system. Instead, as

mentioned above, the cis and trans definitions applied in our work refer to the orientation of the two addends relative to each other. An example of cis and trans was given in Figure 2.3 above. This is an extreme example as the bond bridging carbons 1 and 9 are diametrically opposite to the bridging carbons 52 and 60 in the fullerene cage, but it perfectly illustrates the definition of cis and trans in terms of the relative orientations of the two addends.

The number of isomers was determined by comparing a cis and a trans isomer with those based on each of the double bonds. For example, Figure 2-5 below shows trans-2,12-bis$PC_{62}BM$ on the left. Carbons 1 and 9 are at the top and the phenyl group on the corresponding PCBM group is on the right. The second PCBM group (bridging carbons 2 and 12) is located on the near side of the C_{60} molecule, which is at approximately the one o'clock position with the phenyl group pointing roughly towards the viewer. The molecule in the middle of Figure 2-5 also shows trans-2,12-bis$PC_{62}BM$, but this time with the positions of the two PCBM groups exchanged, with the 2,12 carbons at the top with the phenyl group on the right. Again, another PCBM group can be seen on the near side of the C_{60} molecule, however, now it is approximately at the 11 o'clock position with the phenyl group pointing away from the viewer. The molecule on the right of Figure 2.5 shows trans-5,6-bis$PC_{62}BM$, which also has the other PCBM group at approximately the 11 o'clock position with the phenyl group pointing away from the viewer. It is clear that the molecules in the middle and the right of the figure are indistinguishable. Hence, there is no doubt that trans-2,12-bis$PC_{62}BM$ and trans-5,6-bis$PC_{62}BM$ are, in fact, the same isomer.

This also means that trans-2,12 and trans-5,6 are different ways of representing the same isomer. In these cases, the rule of counting the isomer is keeping the isomer with the smaller starting number in the counting system, i.e., as trans-2,12-bis$PC_{62}BM$ (so, trans-5,6-bis$PC_{62}BM$ is not taken into account).

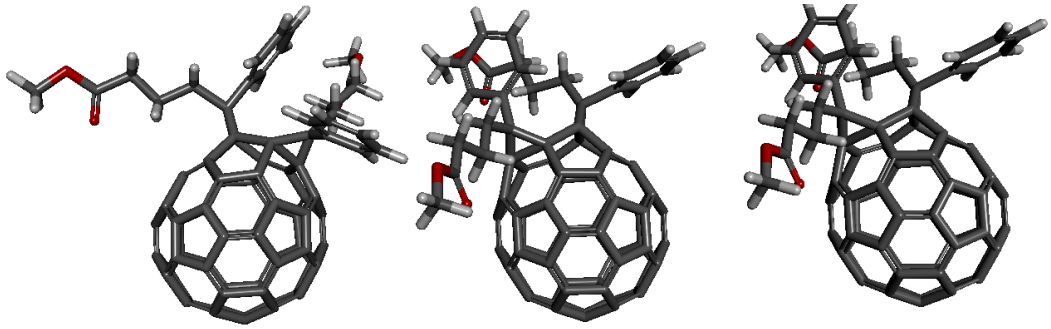

Figure 2.5 Left, trans-2,12-bisPC62BM; centre, trans-2,12-bisPC62BM with the two PCBM groups interchanged; right, trans-5,6-bisPC62BM. As trans-2,12-bisPC62BM and trans-5,6-bisPC62BM are superimposable, they are actually the same isomer.

However, it is not always the case that there are two ways of representing the same isomer. To illustrate this point, Figure 2.6 below shows the trans-13,14-bis$PC_{62}BM$ on the left. The molecule is again orientated so that carbons 1 and 9 are at the top and the phenyl group on the associated PCBM group is on the right. The molecule on the right in Figure 2.5 also shows trans-13,14-bis$PC_{62}BM$, applying the same method as in the previous example, with the positions of the PCBM groups exchanged (i.e., now with the 13,14 carbons at the top with the phenyl group on the right). This time, figures 1.6(a) and (b) are indistinguishable so it is concluded that trans-13,14-bis$PC_{62}BM$ is a uniquely numbered isomer.

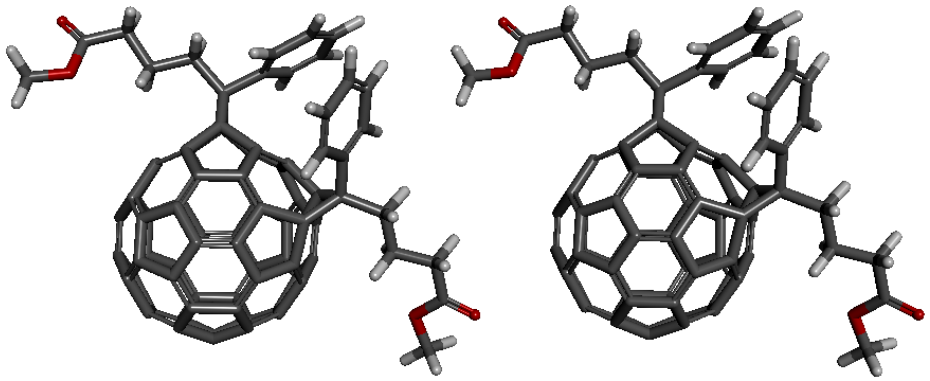

Figure 2.6 Left; trans-13,14-bis$PC_{62}BM$, and right, trans-13,14-bis$PC_{62}BM$ with the two PCBM groups interchanged. The two molecules are indistinguishable indicating that trans-13,14-bis$PC_{62}BM$ is a uniquely numbered isomer (i.e., it has no alternative, but redundant nomenclature).

Every isomer was examined by this method. Through exchanging the carbon atom, it can be determined whether it has a symmetrically-identical partner, or whether it is uniquely numbered, for all trans, cis and equatorial isomers. It was determined that there are 36 distinguishable methanofullerene isomers of bis$PC_{62}BM$. These are listed below in Tables 2.2 (trans), 2.3 (cis) and 2.4 (equatorial).

Trans	2,12 (5,6)	3,15(4,18)	7,8(10,11)	13,14 (u)	19,20 (u)
22,23 (u)	24,25(26,27)	28,29 (u)	32,33 (38,39)	34,35 (u)	36,37 (u)
41,42(47,48)	43,57 (u)	46, 58 (u)	49,59 (53,54)	50,51(55,56)	52,60 (1,9)

Table 2.2 All 25 possible trans isomers of bis$PC_{62}BM$. *x,y* Represents the position of the second PCBM addend. The position of the first PCBM addend, 1,9 in all cases, is left implied. (*a,b*) represents a symmetrically equivalent isomer to *x,y*. (u) represents a unique isomer. This shows that there are in fact only 17 distinguishable trans isomers of bis$PC_{62}BM$.

Cis	2,12 (10,11)	3,15 (26,27)	4,18 (24,25)	5,6 (7,8)	13,14 (22,23)
19,20 (28,29)	32,33 (47,48)	34,35 (43,57)	36,37 (46,58)	38,39 (41,42)	49,59 (u)
51,52 (u)	52,60 (1,9)	53,54 (u)	55, 56 (u)		

Table 2.3 All 25 possible cis isomers of C_{60}-bisPCBM. As for Table 1.2, *x,y* represents the position of the second PCBM, (*a,b*) represents the symmetrically equivalent isomer to *x,y*, and (u) represents a unique isomer. This shows that there are in fact only 15 distinguishable cis isomers of bis$PC_{62}BM$.

Equatorial	21,40 r,f (44,45 r,d)	21,40 r,b (16,17 r,d)
	30,31 r,f (16,17 r,u)	30,31 r,b (44,45 r,u)

Table 2.4 All eight possible equatorial isomers of bis$PC_{62}BM$. These isomers cannot be designated cis or trans as the two PCBM groups are aligned at right angles to each other either way. 21,40 r,f means that is the fullerene is orientated such that the bond between carbons 1 and 9 is at the north pole with the phenyl part of the first PCBM group pointing to the right then the second PCBM group is at the far-left position on the equator with the phenyl group pointing forwards (towards the observer). Whereas for 21,40 r,b, the second PCBM group is in the same position but it has the phenyl group pointing backwards (away from the observer).

2.2.3 Enantiomer of isomers

The final part of the question was to determine which of the 36 isomers have non-superimposable mirror images. Pristine C_{60} has three mirror planes. These go through the three orthogonal C_2 axes of the molecule. However, after adding one PCBM group to form $PC_{61}BM$, this reduces the number of mirror planes to just one; as demonstrated in Figure 2.7 below.

Hence, in order to determine whether an isomer was chiral or not, the comparison between an isomer with the second PCBM group on one side of the mirror plane and its mirror image on the other side was involved. Inspection showed in that two polar isomers cis-52, 60-bis$PC_{62}BM$ and trans-52, 60-bis$PC_{62}BM$, there were in effect not mirror images, because both of the addends lie on the plane and are both aligned along the plane. However, all other trans isomers had mirror images that were not superimposable; so that all other trans isomers were chiral. All equatorial isomers were also chiral. This is because for these isomers, although they lie on the

mirror plane, the second addend (asymmetrical about the bridge) lies orthogonal to the plane. For example, 16,17pf is a non-superimposable reflection of 16,17pb.

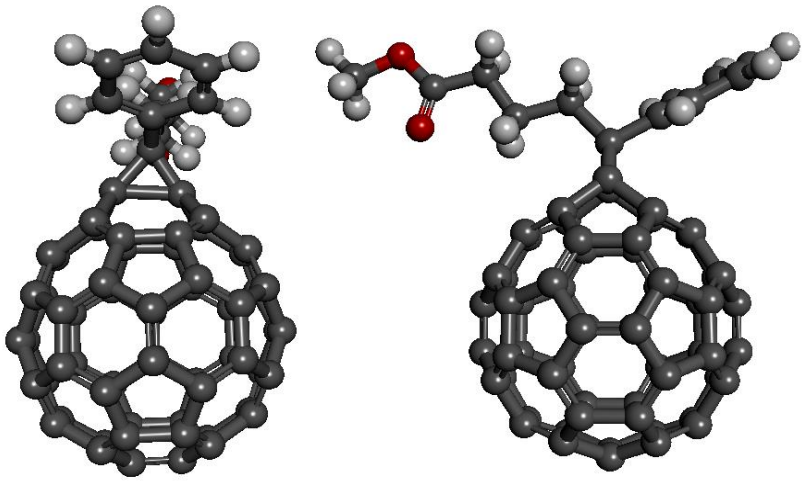

Figure 2.7: The sole remaining mirror plane in C_{60} with a PCBM group can be envisaged in the representation on the left, as the vertical plane perpendicular to the plane of the paper that cuts the molecule into two equal halves. The representation on the right shows the molecule on the left rotated through 90^{O} about the bridging carbon. It shows that the other two mirror planes in C_{60} are removed by the addition of the PCBM group.

The situation for the non-polar cis isomers was not as simple as it was for the equivalent trans isomers. This is because, although all these cis isomers had mirror images, several of them were nevertheless superimposable. Superimposition was achieved by interchanging the two PCBM groups, because in some cases this gave the original isomer. This means that the mirror images of the isomer is exactly same as the structure of itself. For example, Figure 2.7 shows cis-2,12-bis$PC_{62}BM$ (left), its mirror image cis-10,11-bis$PC_{62}BM$ (centre), and finally cis-10,11-bis$PC_{62}BM$ by interchanging the two PCBM groups of the original cis-2,12-bis$PC_{62}BM$ (right). It can be seen that the right and left images are superimposable, hence demonstrating that is not chiral.

Another way of understanding this can be achieved by finding that its mirror image cis-10,11-bis$PC_{62}BM$ has already been shown in our previous analysis (see Table 1.3) to be the symmetrically equivalent isomer of cis-2,12-$PC_{62}BM$, so that it is superimposable. The non-chiral cis isomers were 2,12 ; 3,15; 4,18; and 5,6, because their respective symmetrical equivalents 10,11; 26,27; 24,25 and 7,8 are the same as their mirror images. Interestingly, all achiral isomers are those where the second PCBM group bridges the double bond radiating from the two pentagonal rings that are joined by the 1,9 bridge. These are shown in Figure 2.9.

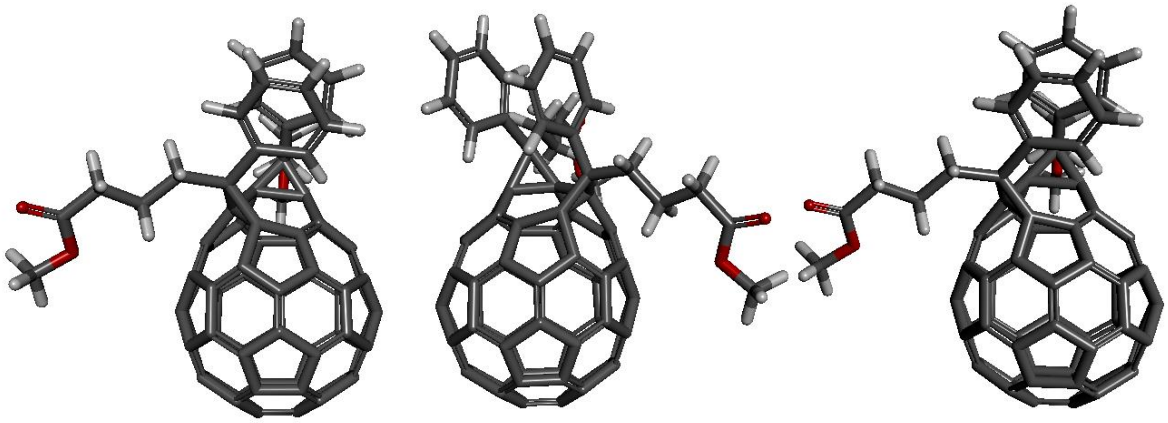

Figure 2.8 The representation on the left shows cis-2,12-bis$PC_{62}BM$ and that in the centre shows its mirror image cis-10,11-bisPC61BM. However, after interchanging two PCBM groups on mirror image we obtain the representation on the right, which is superimposable on the representation on the left. This demonstrates that cis-2,12-bis$PC_{62}BM$ is not chiral.

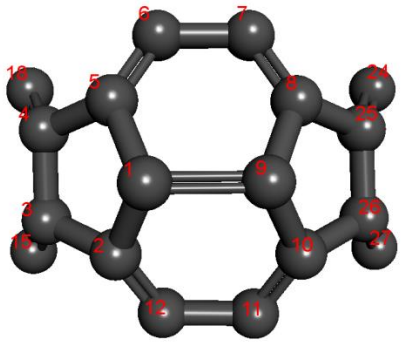

Figure 2.9 Carbons 1 and 9, which are bridges by the first PCBM group in all isomers of bis$PC_{62}BM$ join two pentagons. By inspection, it is found that only the cis isomers that bridge the double bonds that radiating from those two pentagons are achiral (i.e., 3,15; 4,18; 24,25 and 26,27). With the exception of the polar isomers, all other isomers, including trans isomers that bridge these carbons are chiral.

2.2.4 Conclusion

No.	Isomer	Symmetry equivalent of Isomer	Enantiomer of isomer	Enantiomer of the Symmetry equivalent Isomer
1	trans-2,12	trans-5,6	trans-10,11	trans-7,8
2	trans-3,15	trans-4,18	trans-26,27	trans-24,25
3	trans-13,14	-	trans-28,29	-
4	trans-19,20	-	trans-22,23	-
5	trans-32,33	trans-47,48	trans-38,39	trans-41,42
6	trans-34,35	-	trans-46,58	-
7	trans-36,37	-	trans-43,57	-
8	trans-49,59	trans-50,51	trans-53,54	trans-55,56
9	trans-52,60	-	-	-
10	cis-2,12	cis-10,11		
11	cis-3,15	cis-26,27		
12	cis-4,18	cis-24,25		
13	cis-5,6	cis-7,8		
14	cis-13,14	cis-22,23	cis-28,29	cis-19,20
15	cis-32,33	cis-47,48		
16	cis-34,35	cis-44,57	cis-46,58	cis-36,37
17	cis-38,39	cis-41,42		
18	cis-49,59		cis-53,54	
19	cis-50,51		cis-55,56	
20	cis-52,60			
21	21,40 (r,f)	44,45 (r,d)	21,40 (r,b)	16,17 (r,d).
22	30,31 (r,f)	16,17 (r,u)	30,31 (r,b)	44,45 (r,u).

Table 2.5 The 21 isomers of C_{60}bisPCBM are listed in the column on the left. The other columns show the symmetry equivalents and/or enantiomers as appropriate of these 21 isomers.

By the above analysis we finally conclude that there are in effect 22 methanofullerene isomers of bis$PC_{62}BM$, and these are listed in Table 2.5. According to the recent simulation from my colleague, we found that four double bonds ([2,12],[5,6],[7,8],[10,11]) in the same hexagonal ring with the [1,9] bond cannot be added with a second addend due to the steric hindrance. Basically, two addends are too close and interfere with each other to collide once the functional groups rotate or vibrate. It is also chemically energetically unfavourable to be synthesised as it is highly unstable. The total number of distinguished isomers is reduced to 19, which is almost consistent with the 18 isolated isomers from the purification in the next chapter. However, it cannot be concluded that the addends far from each other are favourably synthesised. The relative abundance of all the isomers will be fully demonstrated in the purification part.

2.3 Nomenclature on $PC_{71}BM$

C_{70} has a D_{5h} symmetry with C_5 axis through opposite pentagons, five σ_v planes and one σ_h plane. The symmetry determines a total of eight bond types of C_{70} from the equator to the pole, including 2.12, 1-2, 1-6, 1-9, 9-10, 8-9, 8-25 and 24-25, from the standard numbering system of fullerene. [100] As there are five different sets of symmetrically equivalent carbon atoms in C_{70} proved by the ^{13}C NMR with five lines (1:2:1:2:1), normally we have another way to name them instead of number from the pole to the equator as a, b, c, d and e in order, shown in Figure 2.10. Therefore, we can rename the bond as a-a (single bond), a-b (double bond), b-c (single bond), c-c (double bond), c-d (single bond), d-d (double bond), d-e (single bond) and e-e

(double bond). The PCBM addend, can be added onto the cage with two possible orientations, and this can produce 16 possible potential isomers. However, this number is reduced to 14 effective isomers for two reasons. (1) Symmetrical isomers. The two addend orientations involving the equator of C_{70} (bond 2.12 (e-e)) are symmetrically equivalent – they are interposable by the horizontal reflection. (2) Chiral isomers. With the 8-25 (a-b) bond lying along a vertical mirror plane of C_{70} the two orientations on this bond are mirror images of one another.

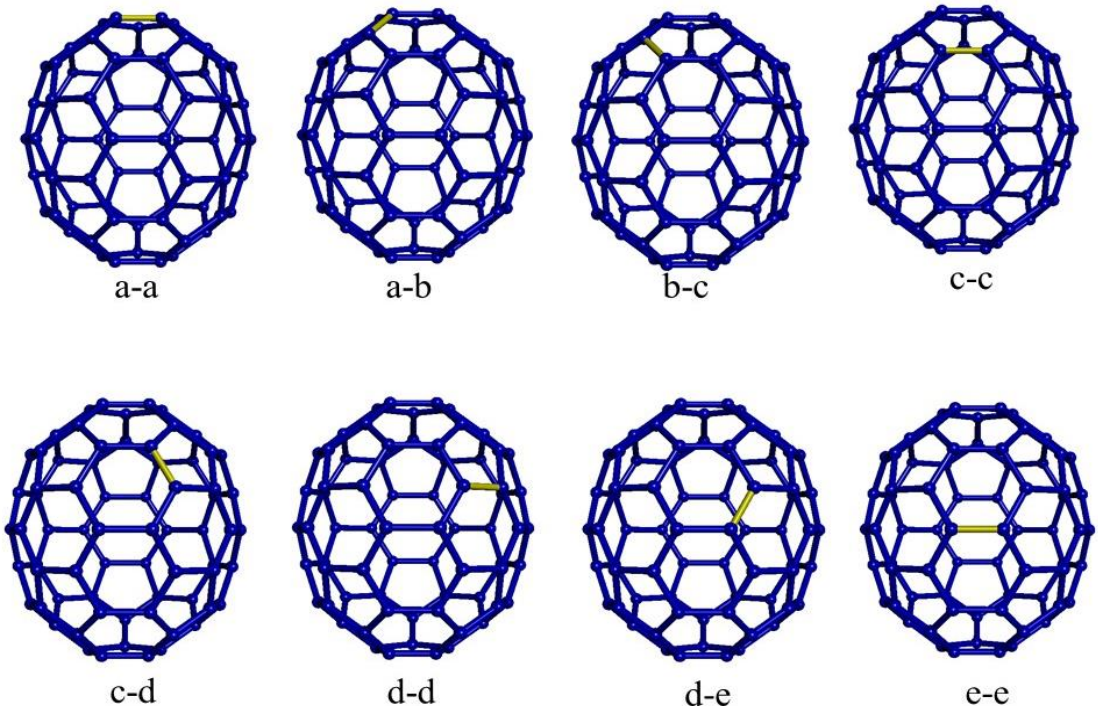

Figure 2.10: All eight types of bond between the five unique carbons a, b, c, d and e from the pole to the equator of C_{70}.

Similar to bis$PC_{62}BM$, $PC_{71}BM$ isomers may exist as homofullerenes or methanofullerenes. The homofullerenes are categorised by the breaking of a fullerene bond. Table 2.6 shows the calculated separations between the bridgehead carbons for all 14 isomers. It is seen that the bridgehead separations can be divided into two distinct groups. One group involves bridgehead separations in the range

1.55 – 1.65 Å, and the other in the range 2.15 – 2.30 Å. The former group involves double/aromatic bonds of C_{70}, and hence, these bonds lead to methanofullerenes on cyclo-addition involving the 1-2, 9-10 and 8-25 bonds, while the possible homofullerenes involve bridging of the 1-2, 2-12, 1-6, 8-9 and 24-25 bonds of C_{70} as they are single bond.

Bridgehead	**2.12 (e-e)**	**1-2 (d-e)**	**1-6 (d-d)**	**1-9 (c-d)**
Separation /Å	r = s = 1.65 (1.54)	r = s = 2.28 (1.41)	r = s = 1.64 (1.43)	r = s = 2.17 (1.47)
Bonding	Non-bonded	Non-bonded	Non-bonded	Non-bonded
Bridgehead	**9-10 (c-c)**	**8-9 (b-c)**	**8-25 (a-b)**	**24-25 (a-a)**
Separation /Å	r = s = 1.55 (1.38)	r = s = 2.15 (1.45)	r = s = 1.59 (1.38)	r = s = 2.16 (1.46)
Bonding	Single bond	Non-bonded	Single bond	Non-bonded

Table 2.6. B3LYP/6-31G(d,p) calculated C-C separations of the bridgehead carbons to three significant figures of all 16 nominal isomers of $PC_{71}BM$, together with the bridgehead bonding; the equivalent bond lengths for C_{70} is given in parentheses. The bridgehead separations for each r/s pair, with respect to carbon atom 71, were identical to this level of accuracy. The bridgehead carbons are labelled with their IUPAC numbering going from equator to pole, and with the commonly used trivial labelling from Taylor et al. in parentheses. [101]

It is noted that even the smallest of these bridgehead separations at 1.55 Å is a rather long single bond between sp^3-hybridised carbons. This causes steric constraints that are locked into the fullerene structure, and extra-long single bond lengths may exist, up to 1.7 Å. Nonetheless, the 8-25 (a-b) and 9-10 (c-c) bonds of C_{70} are much shorter than any other bond, and thereby, have the most double bond character and are likely to be the most reactive towards cyclo-addition, in order to release the strain from the cage and also follow the ordinary synthesis rules. Compared to the cyclo-addition onto a single bond (σ bond), the double bond is easier to break.

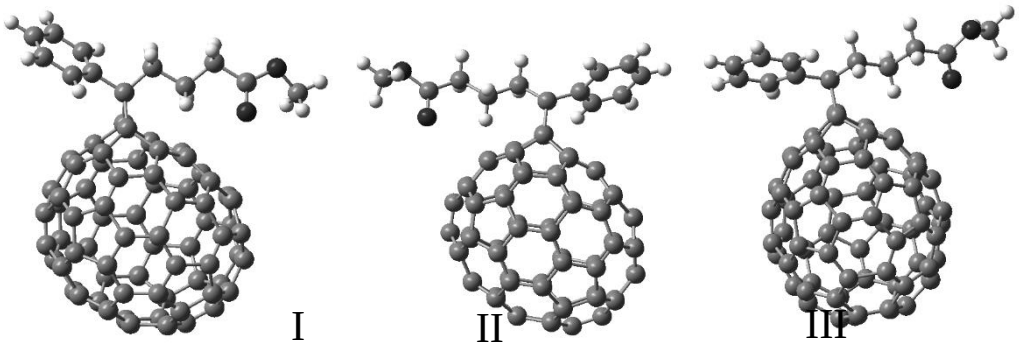

Figure 2.11: Only three isomers of $PC_{71}BM$ exist, III from the addend to a-b bond and I and II from the addend to c-c bond.

Based on previous research and the above analysis, the three isomers are confirmed to be built with addends only on the 8-25 (a-b) and 9-10 (c-c) bonds. The chirality analysis of the three isomers shows that C_{70} carbons 8 and 9 both have r symmetry, and that carbons 10 and 25 both have s symmetry. Hence, for the major isomer there is an rs pseudo-symmetry for the methano-bridging carbon (carbon 71), and for the minor isomers there is r-pseudo-symmetry for the isomer with the phenyl pointing up (Fr-1.1) and s-pseudo-symmetry for the isomer with the phenyl pointing down (Fr-1.2). As such, the recommended IUPAC nomenclature for the major isomer racemate is methyl 4-[(8R,25S,71rs)-71-phenyl-3´H-cyclopropa[8,25](C70-D5h(6))[5,6]fulleren-71-yl]butanoate. Whereas, the systematic names for each of the two minor isomers of $PC_{71}BM$ are methyl 4-[(9R,10S,71r)-71-phenyl-3'H-cyclopropa[9,10](C70-D5h(6))[5,6]fulleren-71-yl]butanoate and methyl 4-[(9R,10S,71s)-71-phenyl-3'H-cyclopropa[9,10](C70-D5h(6))[5,6]fulleren-71-yl]butanoate, respectively. These systematic names are necessary to unambiguously and uniquely define these three isomers. However, they are long and there is a large body of literature in which the isomer mixture is known by the trivial name $PC_{71}BM$, which is itself derived from the trivial name for

the more common C_{60}-based analogue of these molecules: PCBM. As such, in this work we suggest a trivial nomenclature that retains 'PCBM' and uniquely identifies the three isomers via the position and chirality of the 'cyclopropa' carbon atoms – the two bridgehead carbons and the bridging atom as follows: 8R,25S,71rs-$PC_{71}BM$, 9R,10S,71r-$PC_{71}BM$, and 9R,10S,71s-$PC_{71}BM$.

2.4 SUMMARY

According to the analysis and systematic nomenclature, there are 21 distinguished isomers of bis$PC_{62}BM$ after the comparison to find out the symmetry equivalent and the chiral isomers. This number is further narrowed down to 18, because of the steric hindrance, which is proved by the purification results in Chapter 3. All these isomers were named by the cis and trans methods along with the second addition bridge carbon number. For $PC_{71}BM$, there are 14 possible isomers, but according the bond length analysis as well as previous research, only three isomers exist due to the curvature causing strain on the cage. These are 8R,25S,71rs-$PC_{71}BM$, 9R,10S,71r-$PC_{71}BM$, and 9R,10S,71s-$PC_{71}BM$.

Chapter 3

Purification of bis$PC_{62}BM$ and $PC_{71}BM$

In this chapter, all the procedures of the isomer purification of bis$PC_{62}BM$ and $PC_{71}BM$ are described in detail. The purification of bis$PC_{62}BM$ is described first, including sample preparation, equipment parameter settings, column selection, initial pass stage, peak recycling stages and purity test stage. Finally the whole purification map is summarised, followed by an analysis of the relative abundance of isomers. This is followed by the purification details of $PC_{71}BM$.

3.1 Introduction

The purification is the most time-consuming stage of my project, and it took around two years to build the routes and purify all 21 isomers exceeding 99% purity. $PC_{71}BM$ and $bisPC_{62}BM$ mixtures were separately prepared into a nearly saturated solution in toluene. Various columns equipped with HPLC were tried to achieve the best efficiency for isomer separation.

The columns for HPLC are mainly divided into four groups, Reversed-Phase chromatography (RPC), Normal Phase Column chromatography (NPC), Ion-Exchange Column chromatography (IEC) and Size-exclusion chromatography (SEC) listed in table 3-a. RPC is applied for more than 50% of cases in purifying small molecules. Two RPC columns (Cosmosil 5PBB and Cosmosil 5PYE) and one NPC column (Waters Silica) were applied in purifying $bisPC_{62}BM$ and $PC_{71}BM$ (Table 3-b).

Column categories	*Stationary Phase*	*Main interaction*
Reversed-Phase (RPC)	Octadecyl, Octyl, Cyano and Phenyl	hydrophobic, Dispersion Force
Normal Phase (NPC)	Silica, Amino	hydrophilic interaction dipole–dipole interactions
Ion-Exchange (IEC)	Sulfo propyl, Carboxymethyl, Diethylaminopropyl	electrostatic interactions Absorption
Size-exclusion (SEC)	porous particles, such as silica, polystyrene	size exclusion, filtration, depending on Mw

Table 3-a: Four main categories of HPLC columns: RPC, NPC, IEC and SEC

Column Name	***Cosmosil 5PBB***	***Cosmosil 5PYE***	***Waters Silica***
Categories	RPC	RPC	NPC
Particle size	5 µm	5 µm	5 µm
Column Size	20.0 mm I.D. x 250 mm	20.0 mm I.D. x 250 mm	50 mm I.D. x 200mm
Stationary phase	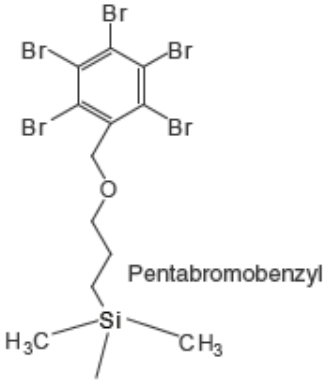 Pentabromobenzyl	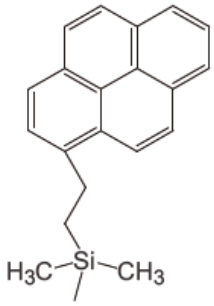 PYE	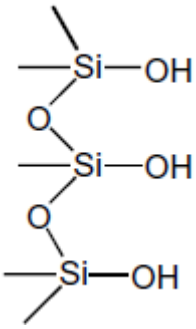
Main interaction	Hydrophobic Interaction, Dispersion Force	Hydrophobic Interaction π-π Interaction Charge Transfer Interaction Stereoselectivity	hydrogen bonding dipole–dipole interactions hydrophilic interaction
Application	Separation of structural isomers differing by double bond	Separation of structural isomers	Initial separation of compounds

Table 3-b: Columns applied in this research and their specifications.

3.2 PURIFICATION of bisPC$_{62}$BM

3.2.1 Preparation of samples

A 1000 mg sample mixture of full bisPC$_{62}$BM isomers was supplied to this project by our collaborator Prof. J. C. Hummelen from the Department of Chemistry at the University of Groningen. The synthesis of the bisPC$_{62}$BM was as for that of PCBM in chapter one, with the reactant ratio in the last steps changed from 1:1 to 2:1. 1000 mg of bisPC$_{62}$BM was dissolved in 700 ml of toluene to reach a concentration that was chosen because it was just enough for the detector to provide clear peaks and was not saturated by the sample. This solution was filtered through a 0.45 micron Teflon filter immediately before use. The purification was performed using a Japan Analytical Industry LC-908 peak recycling preparative HPLC. 3ml of the above

solution was injected into the column per run and delivered with a pure toluene (HPLC Grade 99.8%) mobile phase at a flow rate of 18 ml/min at room temperature. The chromatogram was monitored by a UV absorption detector operating at 312nm. After purification, all 18 isomers of bis$PC_{62}BM$ were obtained. The details of each separation are shown below.

3.2.2 Initial single pass HPLC of the full mixture

In order to test whether it is possible to separate any isomers from the full mixture, a single pass HPLC was initially used with a silica column (50 mm x 200 mm). The HPLC chromatogram, shown in Figure 3.1 shows that the sample consisted of at least eight fractions, each of which contains at least one isomer or more, excluding the first fraction that is mostly composed of impurities. By cutting at the positions of the dashed lines indicated in Figure 1, the sample was partially separated into those eight fractions. They are called residual, F1, F2, F3, F4, F5, F6 and F7. As the residuals are mainly composed of small amounts of impurities, the other fractions were prepared for further purification. To partially purify the entire sample the above procedure was repeated with more than 200 separate 3ml injections.

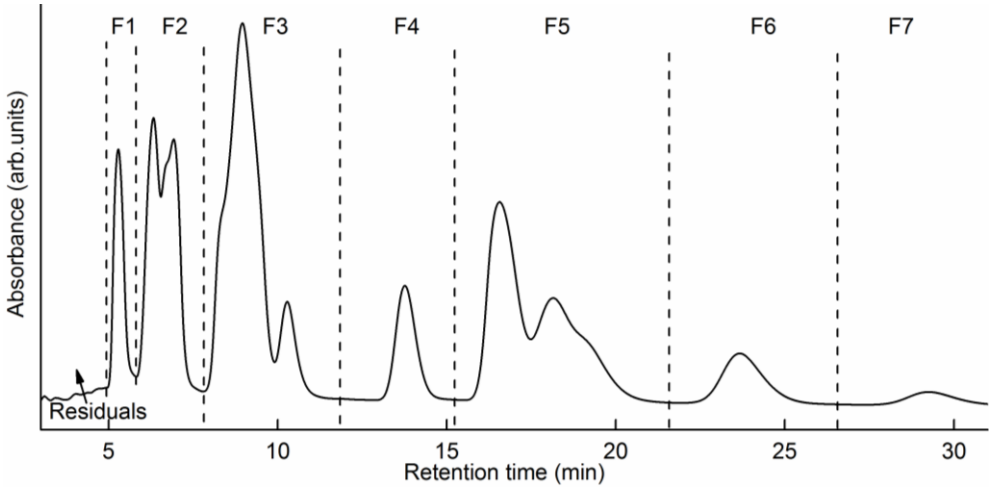

Figure 3.1: The initial single pass HPLC profile for the full mixture. The sample contains eight fractions, which are called, residual, F1, F2, F3, F4, F5, F6 and F7.

3.2.3 PURIFICATION OF BisPC$_{62}$BM F1

Following the initial single pass HPLC, fraction-[1] (F1) was subjected to one further recycling HPLC stage using a silica column (50 mm x 200 mm), from which a pure isomer bisPCBM F1 was finally obtained; the procedure involved peak recycling.

Figure 3.2 shows the recycling stage for F1. It can be seen that there are few impurities in the sample as there is a minor shoulder before the main peak in F1. Also there is some remaining F2 at the tail which becomes an obvious bump at the end of the third cycle. After four cycles, two gaps between F1 and the residual peak, and between F1 and the remaining F2 were seen. The three fractions were cut in between them after the fourth cycle (as indicated by the red dashed lines).The major peak (the second fraction), called F1 was collected and concentrated, waiting for the purity test. The last fraction, the right little shoulder was combined with F2. To purify the entire sample to this stage, the above recycling stage was repeated with around 40 separate 3 ml injections.

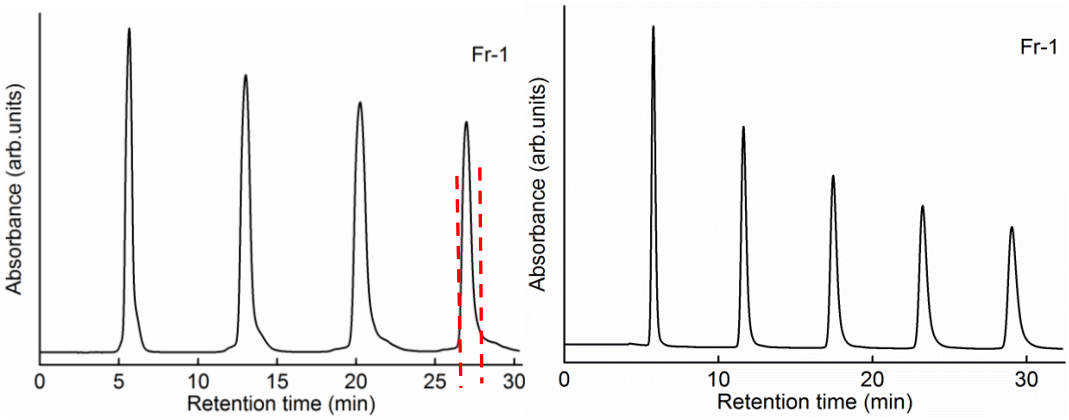

Figure 3.2: The first recycling HPLC profile of the separation of F1 and that for the purity test of F1.

For the purity test, the 40 samples from the previous stage were added together and concentrated down to around 100ml of nearly saturated solution. One testing

sample was subjected to more recycling HPLC for five cycles using a 5PBB column, with the same solvent flow rate and injection volumes as above, shown in figure 3.2. After five cycles, there was just only one peak there, and no evidence of other impurities. It can be concluded that F1 is pure.

3.2.4 PURIFICATION OF BisPC$_{62}$BM F2

Faction 2 contains several isomers, and they cannot be totally separated by one recycling. In stage 2, they are further cut into three sub-fractions, called F2.1 (in blue), F2.2 (in yellow), and F2.3 (in purple), (Figure 3-3). The steps for collecting the sub-fractions were as follows:

1. F2.1 was removed after the third cycle. The fraction was collected at the lowest point of the gap between the two peaks.
2. F2.2 and F2.3 were collected respectively on the ninth cycle, which is indicated in Figure 3.1.

This step was built to maximise the separation for F2.1, F2.2 and F2.3, especially for the latter two fractions. To partially purify the F2, the above procedure was repeated with around 50 separate 3ml injections.

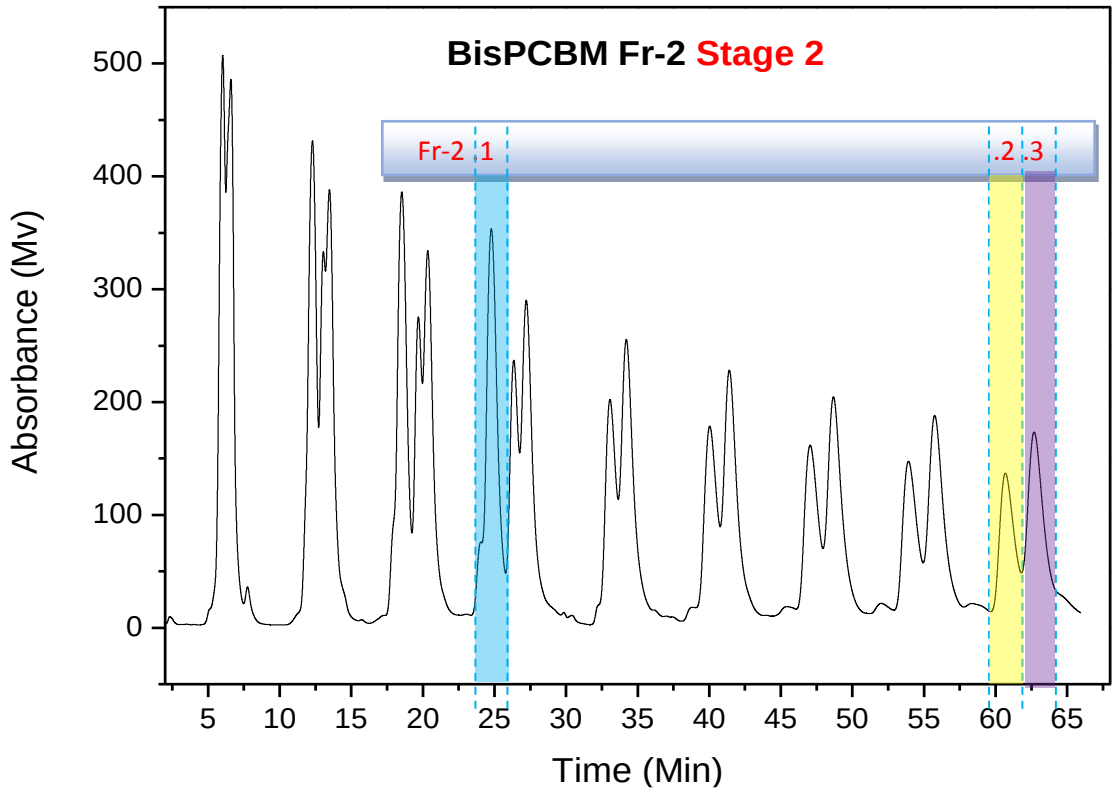

Figure 3.3: HPLC profile showing the recycling procedure for separating the bisPC$_{62}$BM F2 into F2.1, F2.2, and F2.3.

3.2.4.1 PURIFICATION OF BisPC$_{62}$BM F2.3

F2.3 was subjected to two further recycling HPLC stages, from which a pure sample of F2.3 was obtained. The two stages are shown below.

The first recycling stage for F2.3 – stage 3

The tiny residual peak on the left side of the main peak was removed on the third cycle, shown in Figure 3.4. After cycling F2.3 through the column eight times, the F2.3 and the residual F2.2 were collected separately at the minimum between the two peaks, marked by the dashed line. The residual F2.2 was concentrated and was combined with the F2.2 collected above. The nearly pure F2.3 was concentrated and was recycled again (below). In order to purify the entire sample collection to

purer F2.3 at this stage, the first recycling stage was repeated with about 30 separate 3ml injections.

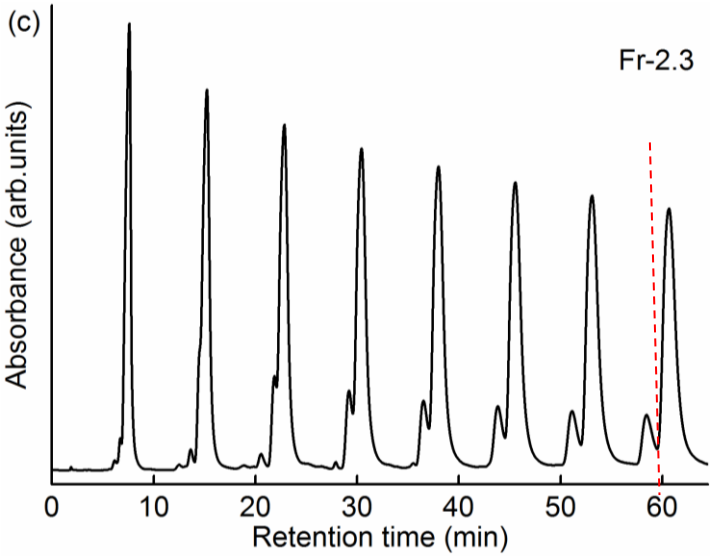

Figure 3.4: First recycling stage HPLC profile in the separation of BisPCBM F2.3

The second recycling stage for F2.3 – stage 4

In the next stage for F2.3 (Figure 3.5), the 30 samples from the previous stage were added together and concentrated down to around 70ml of nearly saturated solution. This sample was subjected to more recycling HPLC, with the same solvent flow rate and injection volumes as above.

After another seven-cycle treatment, F2.3 was separated from the tiny remnant of F2.2 from the previous stage by cutting the two peaks at the minimum between them. The amount of F2.2 going into this treatment is clearly much reduced from that seen in the first treatment. The next step is to investigate the purity of F2.3. It took about 25 repetitions of the above to purify the entire sample to this stage.

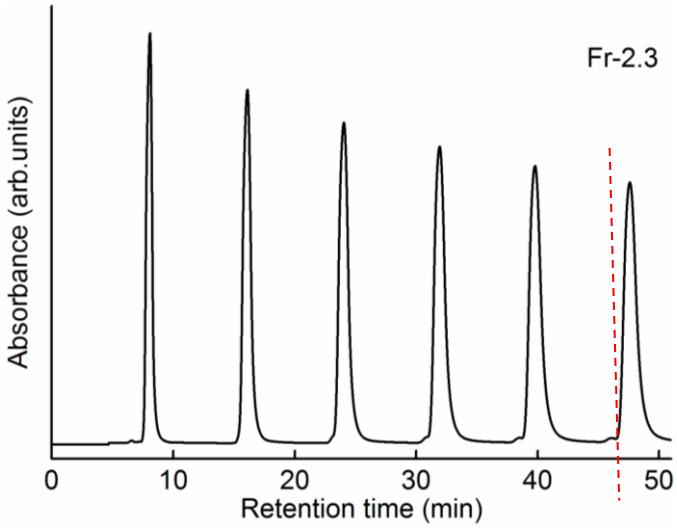

Figure 3.5: HPLC profile from the second recycling stage for separating F2.3

The purity test of F2.3

After the second recycling stage, 25 samples were added together and concentrated into 50ml. A 1ml F2.3 sample from the concentrated solution was diluted into 3ml by toluene, which was then injected into HPLC. The diluted sample can achieve a much clearer separation of components in the final solution. After it went through the column five times, shown in Figure 3.6 there is no sign of other minor peaks by the side of the main. It can be concluded that F2.3 is pure.

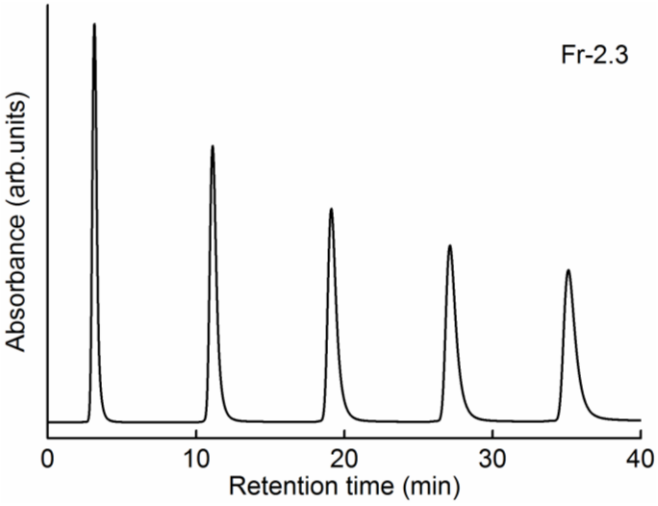

Figure 3.6: HPLC profile from the purity test of F2.3

3.2.4.2 PURIFICATION OF BisPC$_{62}$BM F2.2

The first recycling stage for F2.2 – stage 3

The bisPC$_{62}$BM F2.2 is fully separated by two further recycling stages. The first recycling was carried out as shown in Figure 3.6. The remaining F2.1 was the tiny peak before the major peak and was removed on the fourth cycle by cutting the two peaks at the minimum between them, shown by the red dashed line. After the solution went through the column for the eighth time, F2.2 and the remaining F2.3 (the shoulder on the right side of main peak) were collected separately. The remaining F2.3 was concentrated for further separating. The nearly pure F2.2 was concentrated and prepared for the next stage purification. It took about 30 repetitions of the above to purify the entire sample to this stage.

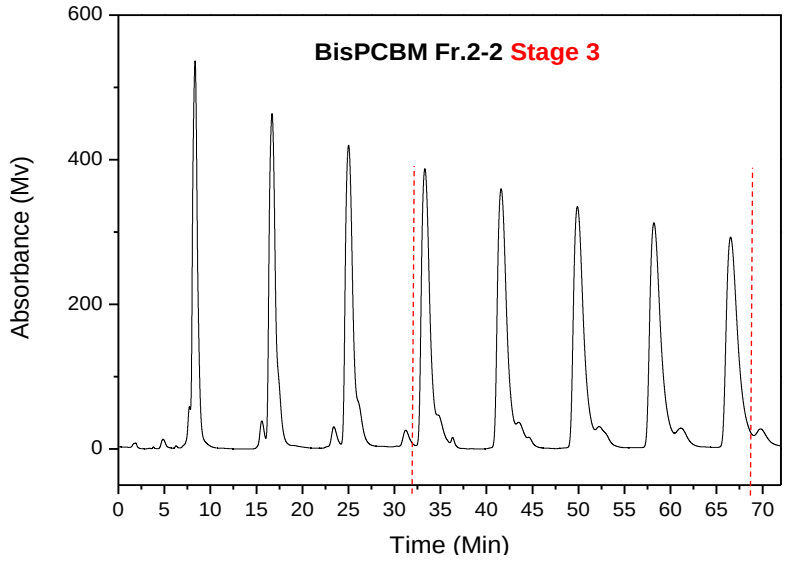

Figure 3.6: HPLC profile from the first recycling stage of separating F2.2

The second recycling stage for F2.2 – stage 4 and purity test

The collected F2.2 from stage 3 was concentrated for this stage of purification. From the spectrum, the impurities in this stage dropped to less than 1%. After the

fourth cycle, F2.2 with a high purity was collected when the minor peak was totally separated from the main peak. The procedure took 30 injections to be finished. The purity test of F2.2 followed. It was quite clear that there was no sign of impurity peaks and only a pure major peak, which proved F2.2 pure. The purification procedure was finished with a silica column. The purity test was carried out with a 5PBB column.

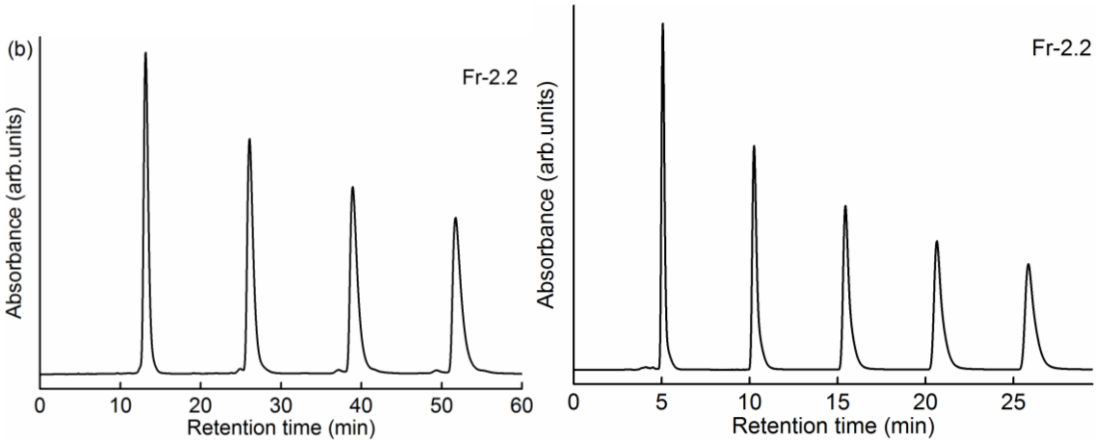

Figure 3.7: HPLC profiles from stage 4 of purifying F2.2 (left) and the purity test (right) for it.

3.2.4.3 PURIFICATION OF BisPC$_{62}$BM F2.1

The F2.1 mixture was collected and concentrated from F2 stage 2, when F2.1 was first separated from F2.2 and F2.3. From Figure 3.8, it is obvious there are at least two isomers in F2.1. There are two main steps to isolate the individual isomers from F2.1. The first is via a recycling method, where each isomer with a relatively high purity was roughly separated out from the mixture. According to the different purities, different recycling stages were applied until each isomer was pure. F2.1 was subjected to two more recycling HPLC stages, from which a pure sample of F2.1.1 and F2.1.2 was obtained.

The first recycling stage for F2.1 – stage 3

The tiny residual peaks on the left and right side of the main peak were removed on the second cycle, shown in Figure 3.8. On the second cycle, there was a bump on the second half of the main peak that was the residual of F2.2. The front peak F2.1.1 and F2.1.2 also start to separate on second cycle. After cycling F2.1 through the column six times, F2.1.1, F2.1.2 and the residual F2.2 were collected separately at the minimum between the two peaks and 10 seconds after the top of the main peak, marked by the red dashed line. The residual F2.2 was concentrated and was combined with the F2 mixture. The almost pure F2.1.1 and F2.1.2 were concentrated and recycled again (below). As with F2.1, to purify the entire sample to this stage, the first recycling stage was repeated with about 30 separate 3ml injections.

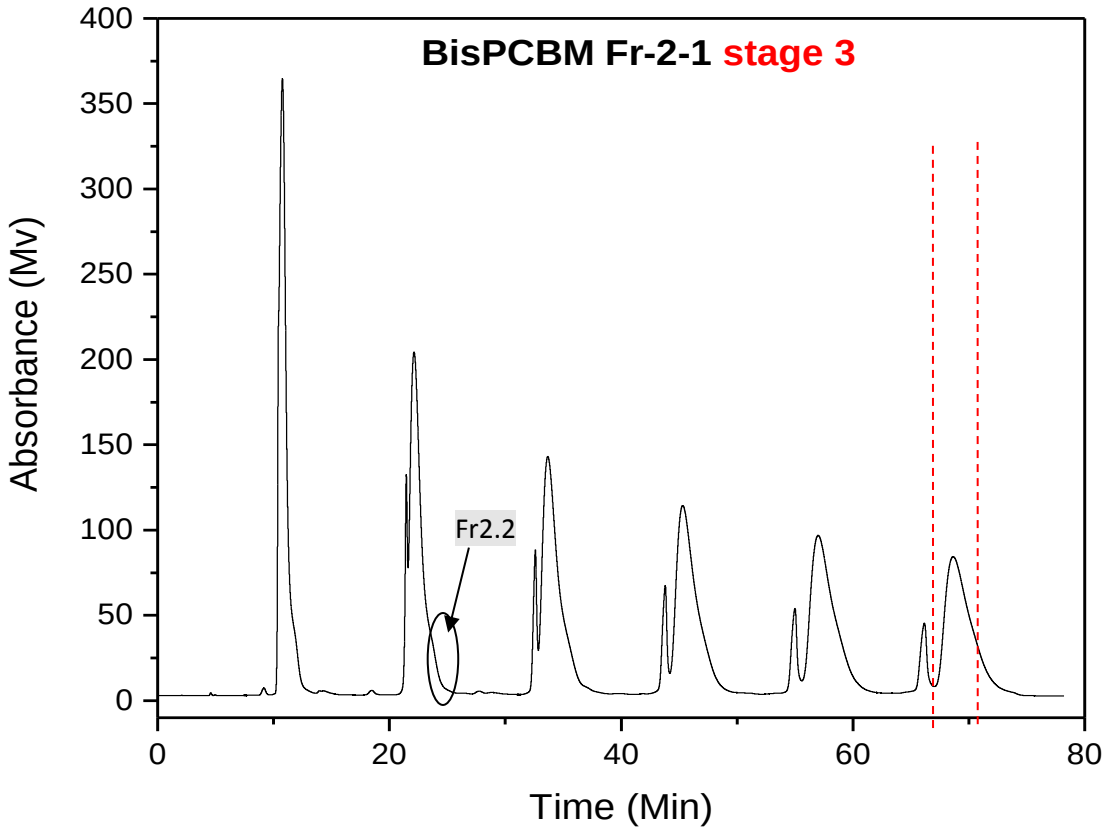

Figure 3.8: HPLC profile of first recycling stage in separating BisPCBM F2.3

The recycling stage for F2.1.1 and F2.1.2 – stage 4

In the next stage for F2.1.1 and F2.1.2 (Fig. 3-9), the 30 samples from the previous stage were added together and concentrated down to approximately a 50ml solution. F2.1.2 was subjected to more recycling HPLC first, with the same solvent flow rate and injection volumes as above. After another seven-cycle treatment, the F2.1.2 was separated from the small remnant of F2.1.2 from the previous stage by cutting the two peaks at the minimum between them. The amount of F2.1.1 going into this treatment was clearly much reduced from that seen in the first treatment, which was collected after five cycles and combined with F2.1.1. The next step was to investigate the purity of the F2.1.2. It took about 25 repetitions of the above to purify the entire sample to this stage. For F2.1.1, it also needed one more stage to become pure. The tail of F2.1.1 still contained some F2.1.2 and we cut the tail from a third of the height of the peak.

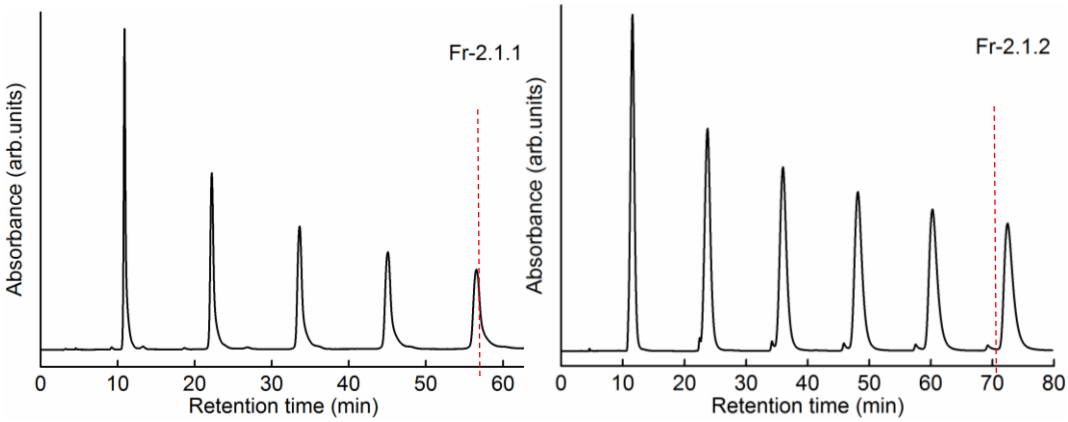

Figure 3.9: HPLC profiles from second recycling stage for separating the F2.1.1 (left) and F2.1.2 (right)

The purity test of F2.1.1 and F2.1.2

After the second recycling stage, 25 samples from F2.1.1 and F2.1.2 were added together separately and concentrated into 50ml, respectively. A 1ml F2.1.1 sample from the concentrated solution was diluted into 3ml by toluene, which was then injected into HPLC. A diluted sample can achieve a much clearer separation of different isomers. After it went through the column five times, shown in Figure 3.10 (left), there was no sign of other minor peaks by the side of the main. It can be concluded that F2.1.1 is pure. The same procedure was taken for F2.1.2, and Figure 3.10 (right) shows that after five cycles there is only one pure peak hence F2.1.2 is also pure.

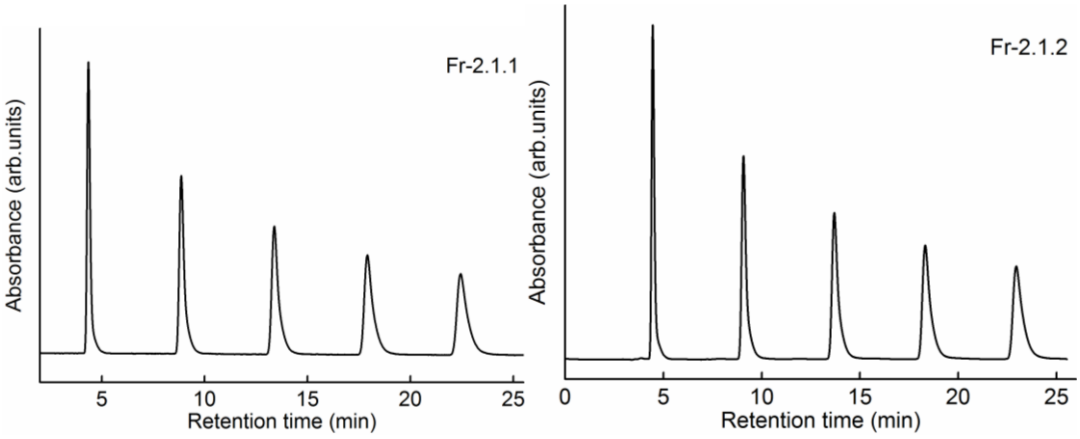

Figure 3.10: HPLC profiles from the purity tests of F2.1.1 and F2.1.2

3.2.5 PURIFICATION OF BisPC$_{62}$BM F3

The bisPCBM F3 collected from the whole mixture was concentrated into 150ml. There are more than five isomers in the mixture. The whole purification for this fraction contains two main procedures. The mixture was firstly purified into four fractions by the order of retention time, named as F3.1, F3.2, F3.3 and F3.4 through a silica column. The second main procedure was focused on each fraction until all

the isomers were isolated from each fraction via different columns and recycling procedures. According to Figure 3.11, F3 was injected and separated by HPLC through a silica column, which has better separation for the fractions than other columns, and the parameter was set at the same level as the previous one with a flow of 18ml/min. The pure F3.4 was collected at the second cycle end of F3.3 as it was already isolated from the mixture through the column twice. F3.1, 3.2, and 3.3 were collected respectively from the beginning to the end of the fourth cycle. All the cutting points are marked by the red dash line. This procedure was repeated 50 times. From the spectrum, it is also obvious that F3.1 is almost pure and F3.2 and F3.3 contain more than one isomer requiring further purification. F3.4 seems pure as well therefore the purification process was followed (below) for F3.1 and F3.4. The other sub-fractions were collected and concentrated for further separation.

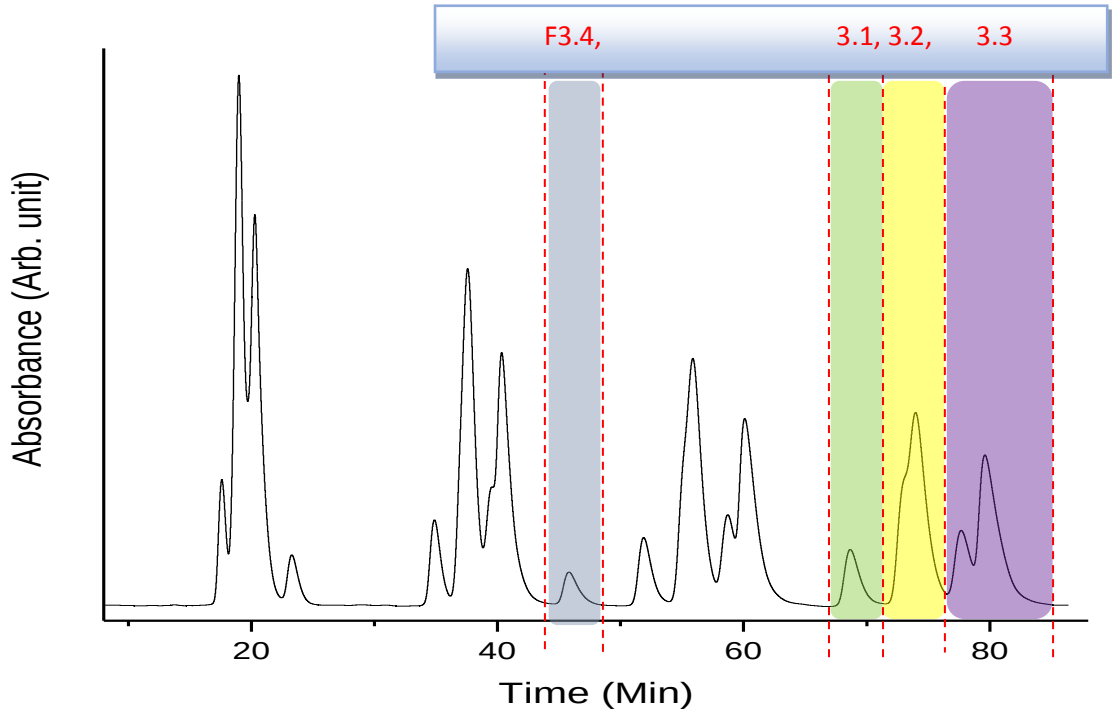

Figure 3.11: HPLC profile from the first purification stage of the BisPCBM F3

Purity test of F3.4

25 samples of F3.4 from the previous stage were added together separately and concentrated into 50ml. Diluted F3.4 from 1ml to 3ml was then injected into HPLC. After it went through the column five times, shown in Figure 3.12 there was no sign of other minor peaks by the side of the main. It can be concluded that F3.4 is pure.

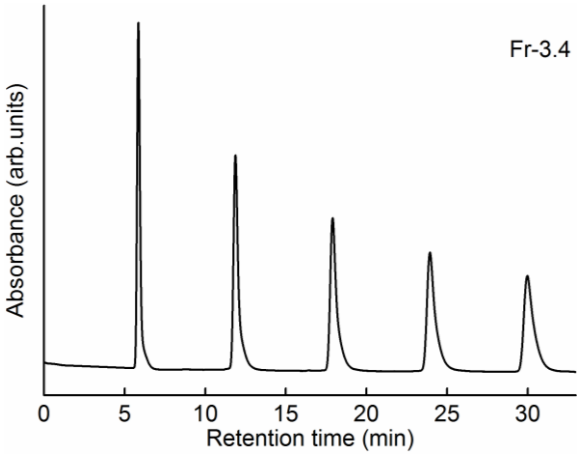

Figure 3.12: HPLC profile from the purity test of F3.4.

3.2.5.1 PURIFICATION OF BisPC$_{62}$BM F3.1

Following the first purification stage of F3, the fraction-[3]-1 was subjected to one further recycling HPLC stage through 5PPB columns, from which a pure isomer bisPCBM F3.1 was obtained; the procedure involved peak recycling.

Figure 3.13 (left) shows the recycling stage for F3.1. In the first cycle, there were some residuals in the sample as there are two minors before and after the main peak F3.1. The front minor peak was moved at the beginning of the first cycle by starting the peak recycling after it. Another minor peak was moved out of the

solution after the second cycle, cut between two dashed lines. The residuals were not collected and went to the waste bottle. After six cycles, the perfect pure peak F3.1 was collected and concentrated. From the second to the seventh cycle, the purity of the sample was proved to be around 100%. To purify the entire sample to this stage, the above recycling stage was repeated with about 20 separate 3ml injections. The purity test of F3.1 was followed to confirm it was completely pure, shown in Figure 3.13 which clearly displays that there are no tiny peaks around F3.1 after five cycles.

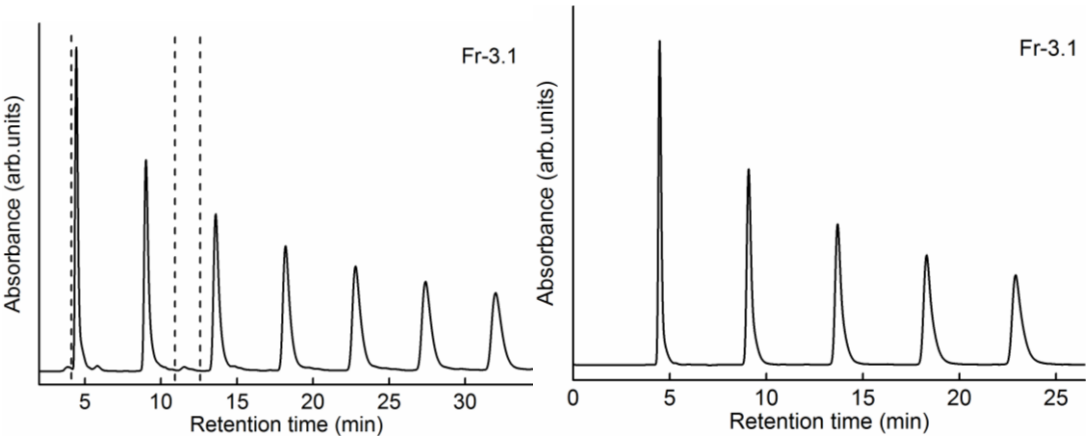

Figure 3.13: HPLC profiles from the second recycling stage for F3.1 and purity test of F3.1

3.2.5.2 PURIFICATION OF BisPC$_{62}$BM F3.2

The F3.2 collected from the F3 mixture in the first stage contains more than one isomer. Further purification was necessary to isolate individual isomers from the mixture. F3.2 was concentrated and injected into the HPLC. Those procedures were finished by a 5PPB column following the same settings as in the previous procedures. According to Figure 3.14, the two isomers started to separate in the second cycle. From the first cycle to the fourth cycle, two isomer peaks were largely

separated to almost maximum. However, from the fourth cycle to the sixth cycle, the peak separation was almost the same. The front peak contains most of one isomer named F3.2.1, while the second peak contains most of another isomer named F3.2.2. F3.2.1 was collected from the beginning of cycle seven and was finished at the lowest point between two peaks. The rest of cycle seven, starting from the onset of the second peak, was collected in another bottle. Both isomers were not pure and were prepared for further purification. To purify the entire sample to this stage, the above recycling stage was repeated with around 25 separate 3ml injections.

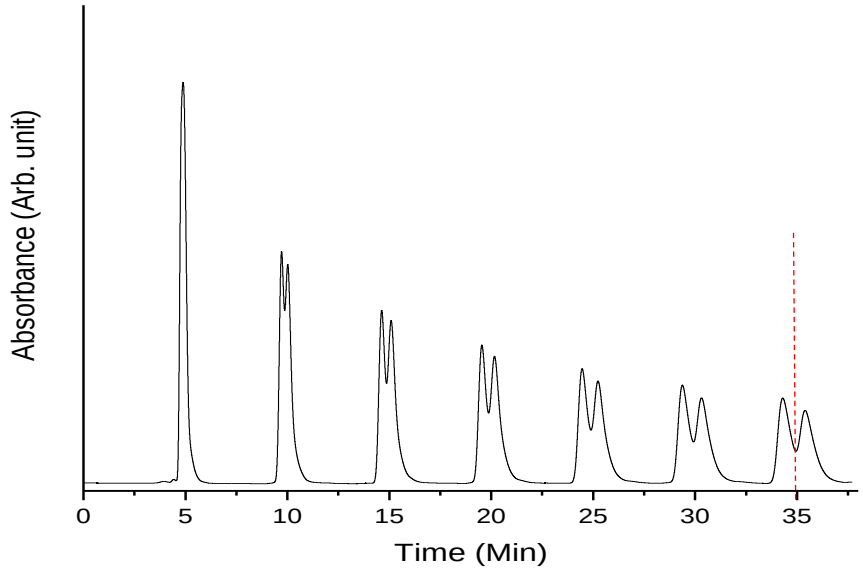

Figure 3.14: HPLC profile from the second recycling stage for F3.2

The impure F3.2.2 from the second stage was further purified first, with around 20% of F3.2.1 as seen in Figure 3.15 (left), while F3.2.1 was purer, so that the F3.2.1 residual from F3.2.2 during purification was added into the main F3.2.1 solution for further purification. The tiny peak in front of the main peak is F3.2.1 which was removed after the seventh cycle was cut from the lowest point and added into

F3.2.1. From the spectrum, the F3.2.2 collected from this stage still seemed impure, and the purity test showed it was around 99% pure. Therefore, one more recycling stage was needed to achieve a 100% pure sample. To purify the entire sample to this stage, the above recycling stage was repeated with around 25 separate 3ml injections.

The fourth stage for F3.2.2 followed the same procedure as the previous one. In this stage, it was obvious that the residual was around 1% less than that shown in Figure 3.15. In the sixth cycle, the tiny residual was separated from the main peak, so the residual was removed from the beginning of seventh cycle, ending at the intersection point of the dashed lines of the spectrum to ensure the 100% purity of F3.2.2, shown in Figure 3.15. The tiny residuals were also added into the F3.2.1 bottle. To purify the entire sample to this stage, the above recycling stage was repeated with around 23 separate 3ml injections. The purity test of F3.2.2 followed just after the fourth recycling stage in Figure 3.15 (right). After five cycles, the main peak was still clear without any minor peak, which proved that F3.2.2 is pure.

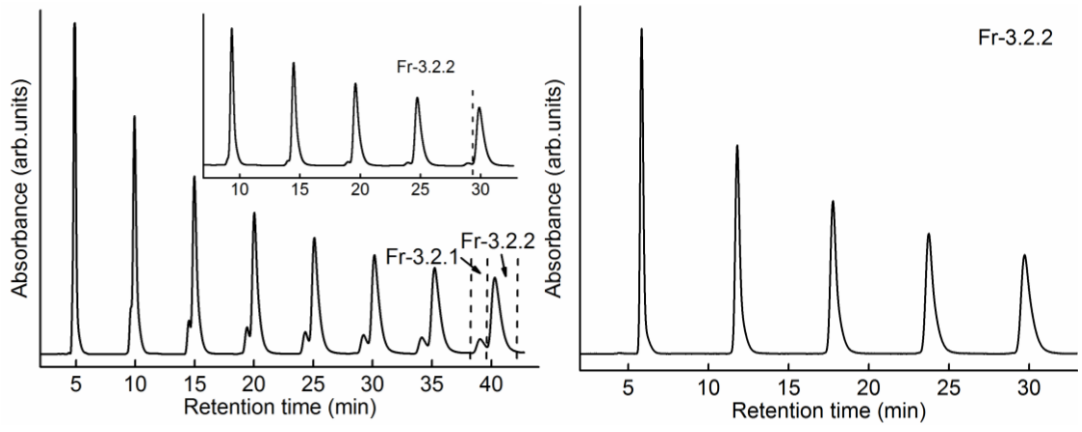

Figure 3.15: HPLC profiles from the third and fourth recycling stage for F3.2.2 and the purity of F3.2.2

All F3.2.1 from both stages were combined and concentrated for further purification. Since the front peak contained fewer impurities, it was easier for F3.2.1 to be fully purified. All the parameters of HPLC were set at the same level as the previous stage via a 5PBB column. From the spectrum, the sample was almost pure. The toluene flow of the fullerene isomers tended to diffuse backwards much more than they diffused forwards after many cycles, therefore the peaks maintained a fairly sharp attack, but the decay stretches backwards well after the peak maximum (look at the final cycle above for an example). The tailing would make it difficult to know when the very small remaining F3.2.2 sample was coming off the column. In order to ensure there were no impurities left, at the final cycle, the second half peak was cut at a third of the height, shown by the red line. The pure sample in front was collected and concentrated as pure F3.2.1. 20 separate 3ml injections were carried out.

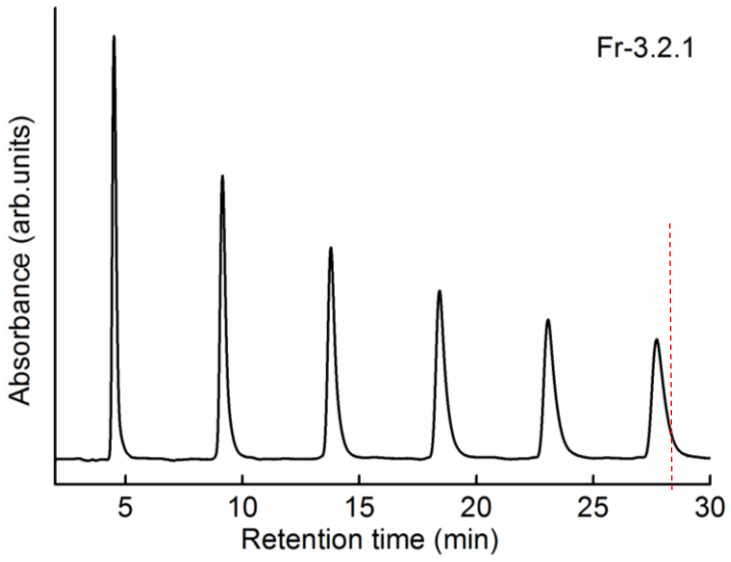

Figure 3.16: HPLC profile from the second recycling stage for F3.2.1

3.2.5.3 PURIFICATION OF BisPC$_{62}$BM F3.3

The final fraction from F3 is F3.3 with the second longest retention time in this fraction. Since a 5PPB column cannot effectively separate the two isomers from the mixture, a 5PYE column was tried as it has different hydrophobic, charge transfer and π-π interactions compared to the 5PPB column. Two isomers can be efficiently and more easily separated within three cycles through the 5PYE column as shown in Figure 3.17. At the beginning of the first cycle, there were some remaining residuals from other sub-fractions, which were removed before the onset of the first main peak, and also between the first cycle and the second cycle. The first isomer F3.3.2 was collected at the third cycle by cutting from the lowest point between the two peaks and at the end of the second peak, marked by the red lines. After another two cycles, the second pure isomer F3.3.1 was collected. After the purity test shown, both isomers were confirmed to be pure (Figure 3.18). To purify the entire sample, the above recycling stage was repeated with around 23 separate 3ml injections.

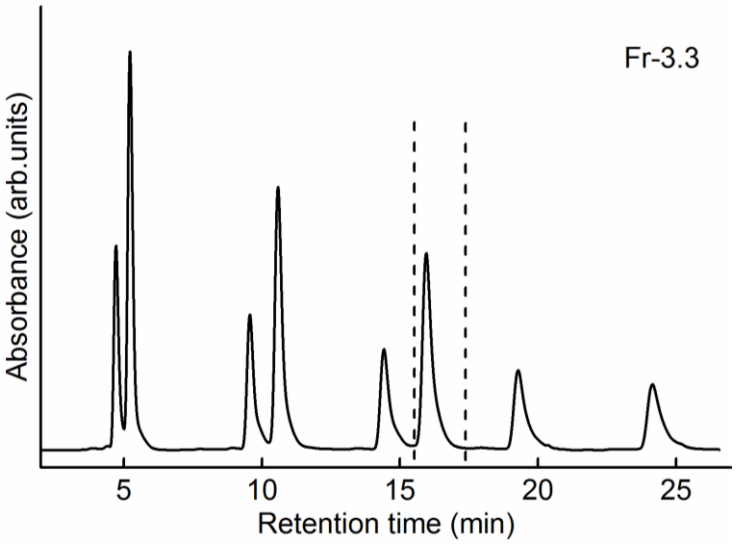

Figure 3.17: HPLC profile from the second recycling stage for F3.3 by 5PYE column

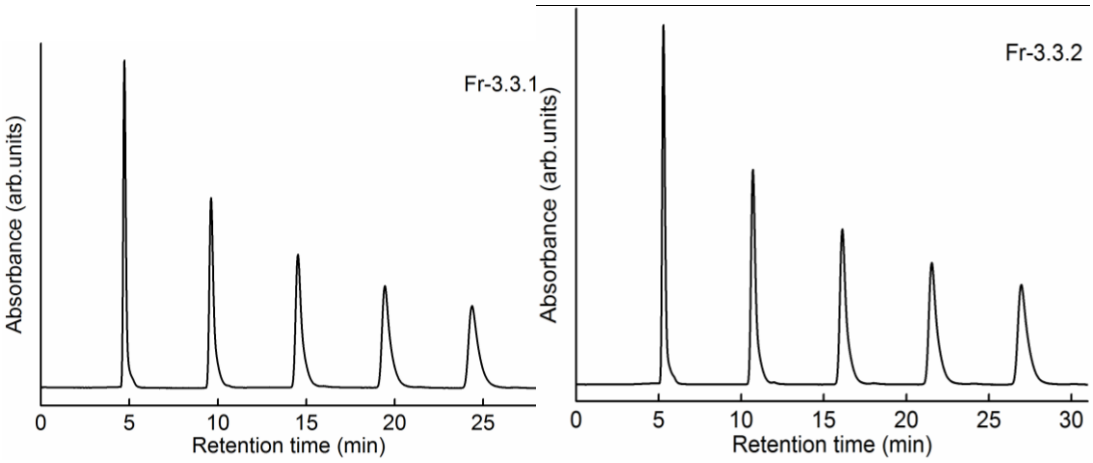

Figure 3.18: HPLC profile from the purity tests of F3.3.1 and F3.3.2

3.2.6 PURIFICATION OF BisPC$_{62}$BM F4

The F4 fraction collected was from a single pass of the whole bisPCBM mixture, but the purity of it was not clear even though it looked like a single isomer. A purity test was implemented via peak recycling. After five cycles, no shape change and peak separation for the only single peak proved that F4 is composed of only one isomer as seen in Figure 3.19 and is pure. This pure isomer solution was kept in a dark box to avoid decomposition for the structural and property investigations.

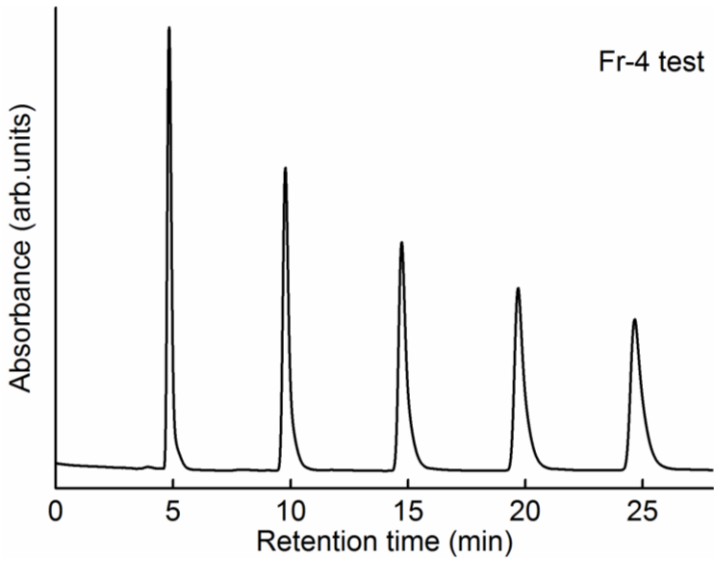

Figure 3.19: HPLC profile from the purity test of the F4 from the first stage purification

3.2.7 PURIFICATION OF BisPC$_{62}$BM F5

F5 had a relatively long retention time compared to the previous fractions. Since the silica column has better separation for the isomers of F5, the first procedure of purification still relies on the silica column to divide the fraction into three divisions. The sub-fractions will be further separated by other columns due to a short retention time and specific interaction with one isomer more than others. In Figure 3-20, the front peak was followed with a back peak with a shoulder in the first cycle, and the back peak separated into two after the second cycle. After four cycles, the three peaks were totally separated with a sufficient gap between them, named F5.1, F5.2 and F5.3 and marked with different colours. Thus, the different sub-fractions were collected at the fourth cycle, and concentrated for further purification since each sub-fraction may contain more than one isomer. 26 separate 3ml injections were taken to purify the whole sample to this stage.

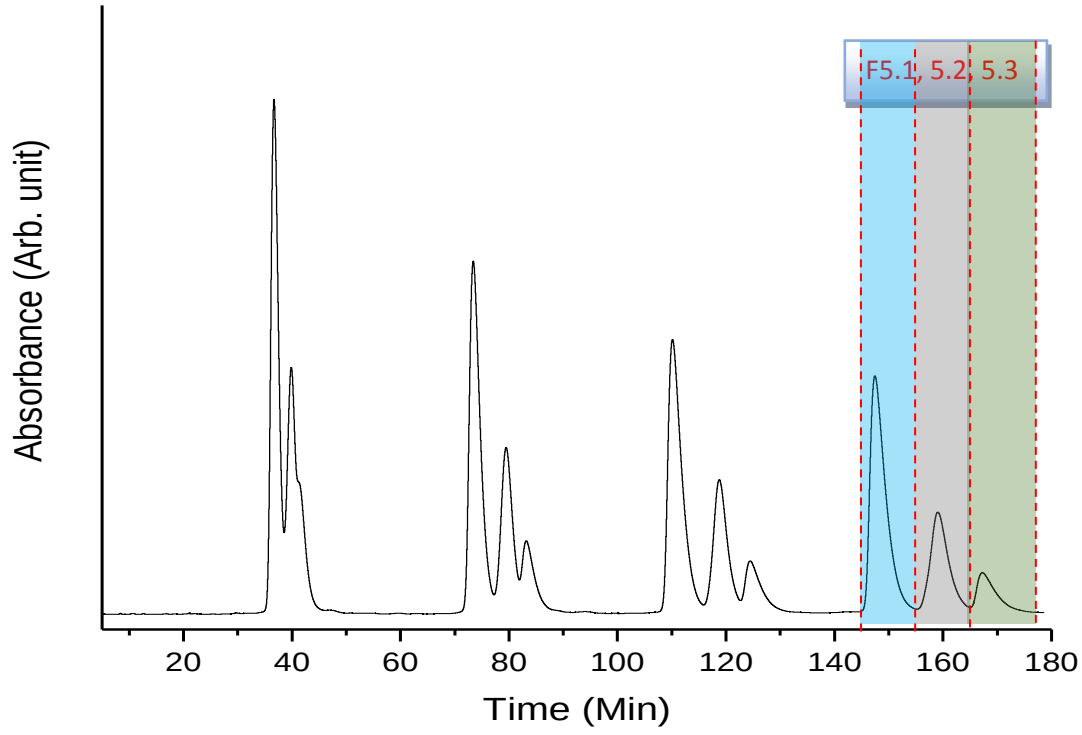

Figure 3.20: HPLC profile showing the second recycling stage of F5 using a silica column.

3.2.7.1 PURIFICATION OF BisPC62BM F5.1

The F5.1 was firstly tested by the PPB column, since PPB allows for much shorter retention times. After several cycles though the column, it was proved that the fraction is pure with a single peak, as shown in Figure 3.21.

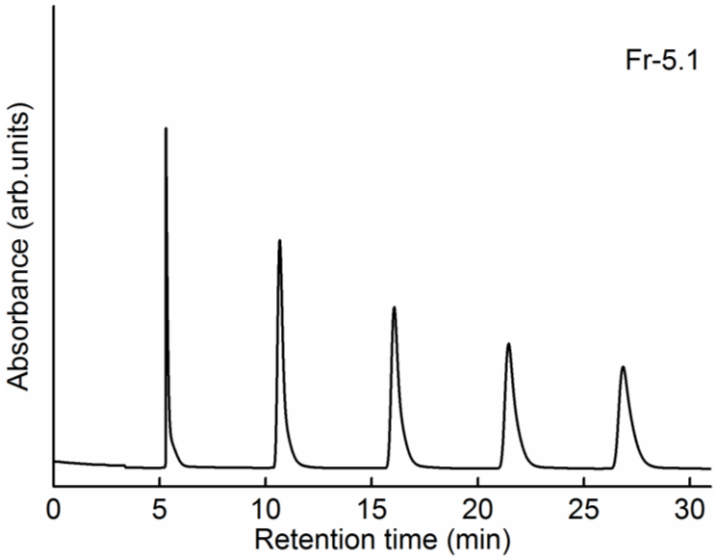

Figure 3.21: HPLC profile from the purity test of F5.1 through the PPB column

3.2.7.2 PURIFICATION OF BisPC$_{62}$BM F5.2

F5.2 was then tested by the PBB column as well. Figure 3.21 demonstrates that there were two isomers in F5.2. At the fourth cycle, the peak shoulder emerged and showed there was more than one isomer in the fraction. After 90 minutes peak recycling, it was still difficult for the column to separate the two peaks, therefore a PYE column was used. In Figure 3.22, the PYE worked much better than the PPB column for the separation of the two isomers, where the isomers started to separate from the second cycle and were totally separated at the seventh cycle. Therefore, the PYE column was applied to finish the purification of F5.2. F5.2.1 was

collected from the beginning of the seventh cycle to the lowest middle point between two peaks, while the rest was collected as F5.2.2. Through the purity test, both isomers were not pure. To complete this stage, 15 separate 3ml injections were done.

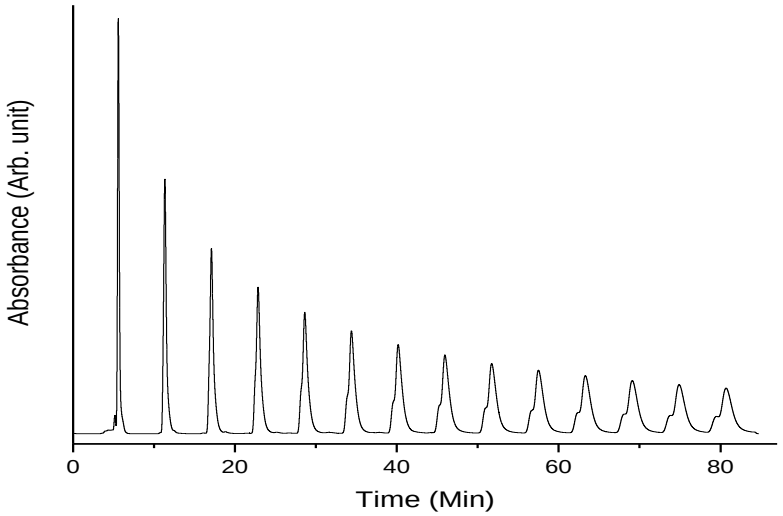

Figure 3.21: HPLC profile showing the third recycling stage of F5.2.2 through the 5PPB column.

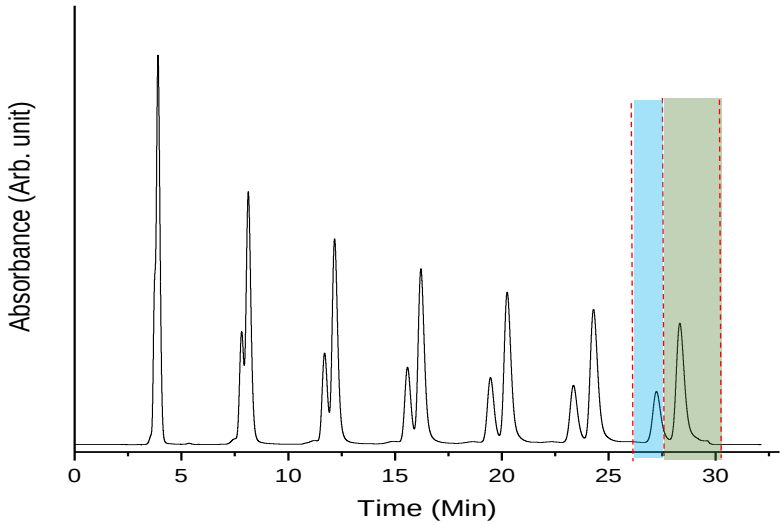

Figure 3.22: HPLC profile from the third recycling stage of F5.2.2 through the 5PYE column.

3.2.7.3 PURIFICATION OF BisPC$_{62}$BM F5.2.1

The F5.2.1 collected from the previous test was not pure enough, so another recycling stage was taken to purify it further. According to the spectrum, the

remaining F5.2.2 showed on the bottom right of the main peak, marked as red. After six cycles, the residuals were removed by cutting the peak at a third of the height of the back half peak to the end of the minor peak. After the purity test, F5.2.1 was shown to be quite pure, as illustrated in Figure 3.23 (right). The samples were concentrated for further characterisation. To finish this stage, 15 separate 3ml injections were done.

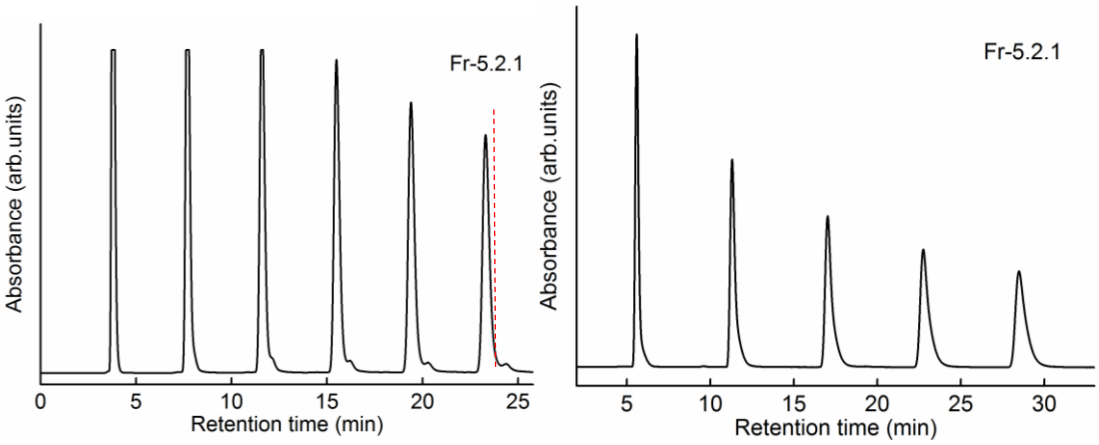

Figure 3.23: HPLC profiles from the fourth recycling stage and purity test of the F5.2.1

3.2.7.4 PURIFICATION OF BisPC$_{62}$BM F5.2.2

F5.2.2 obtained from previous tests contained some residual of F5.2.1, which could be removed by recycling. After several cycles, the minor peak gradually moved away from the main peak and there was no mixing until there was a big gap between them around the sixth cycle. The rubbish went to the waste bottle and the main peak for F5.2.2 was collected and concentrated. After the purity test, it was shown that F5.2.2 is pure, as seen in Figure 3.24. All of the F5.2.1 purified to this stage took eight separate 3ml injections.

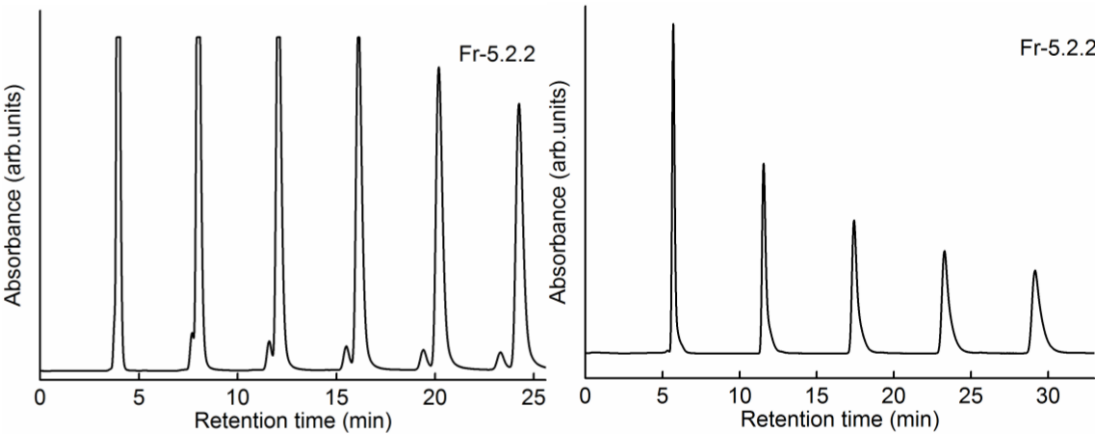

Figure 3.24: HPLC profiles from the fourth recycling stage and the purity of F5.2.2

3.2.7.5 PURIFICATION OF BisPC$_{62}$BM F5.3

F5.3 had some remaining residual in it after the first stage purification. From figure 3.25, a tiny peak front showed that one more stage was necessary to obtain the pure F5.3. At this stage, the PPB column was used to purify it. The tiny peak was too close to the main peak in the first cycle, while it was totally separate from and moved out from the main peak between the first and second recycling peak. After that, it was obvious that only one peak was there proving that the isomer is more than 99% pure. To finish this stage, eight separate 3ml injections were done.

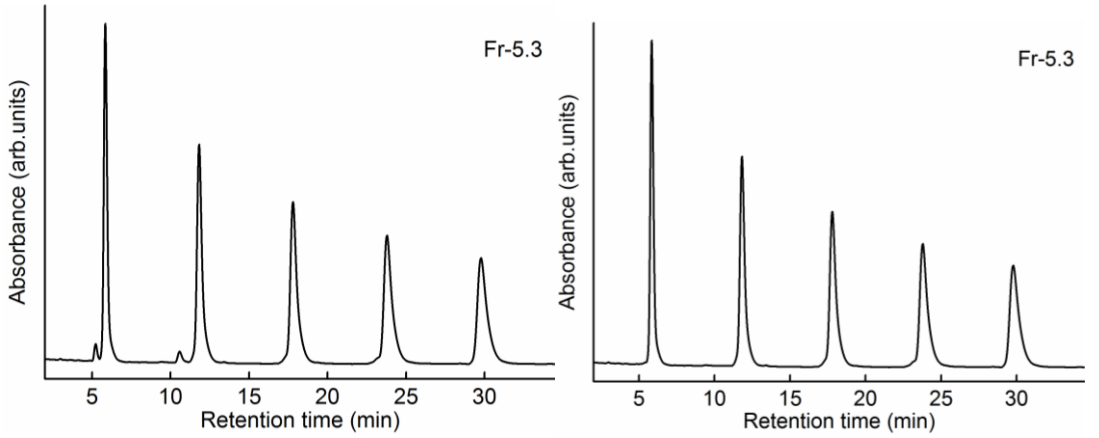

Figure 3.25: HPLC profiles from the second recycling stage the purity of F5.3

3.2.8 PURIFICATION OF BisPC$_{62}$BM F6

Since this fraction has a very long retention time in the silica column of around 20 minutes, the 5PPB column was used for further purification. The F6 collected from the previous test was from a single pass of the whole bisPCBM mixture, but the purity of it was not clear even though it looked like a single isomer. The purity test was implemented via peak recycling. After five cycles, no shape change and peak separation for the only single peak proved that F6 is composed of only one isomer as shown in Figure 3.26. Since there were some impurities in the sample, which were in front of the first peak, they were removed by cutting from the beginning of the injection to the onset of the main peak. After the purity test, the whole sample just went through the column once to move out the residuals. After purifying the sample, the sample was concentrated and stored for further characterisation.

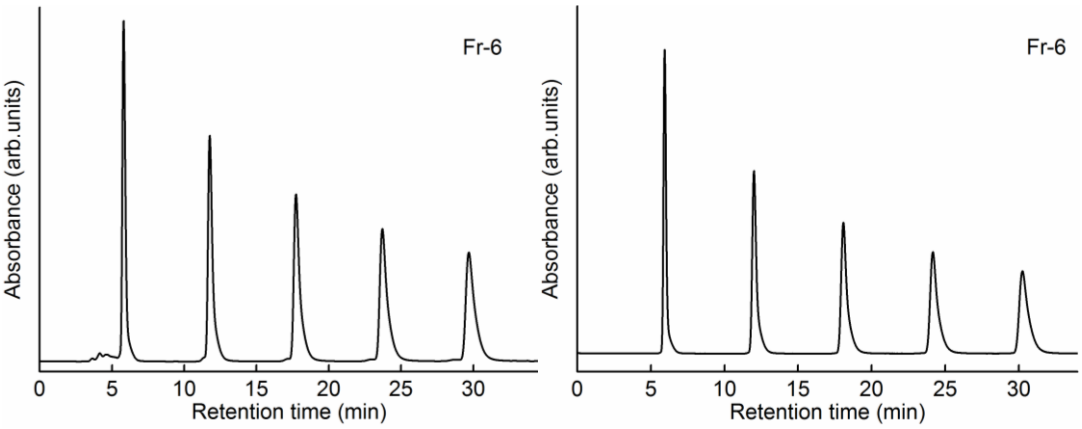

Figure 3.26: HPLC profiles from the first recycling stage and the purity test of F6

3.2.9 PURIFICATION OF BisPC$_{62}$BM F7

The F7 collected from the previous test was from a single pass of the whole bis[60]PCBM mixture, but the purity of it is not as clear as F4 and F6. The purity test was implemented via peak recycling. After five cycles, no shape change and peak separation for the only single peak proved that F7 is composed of only one isomer

and some residuals as one minor bump in front of the main peak in the first cycle. The residuals were moved out before the first cycle. The procedure was repeated until the whole sample was cleaned. The purity test shows that after this stage F7 was completely pure.

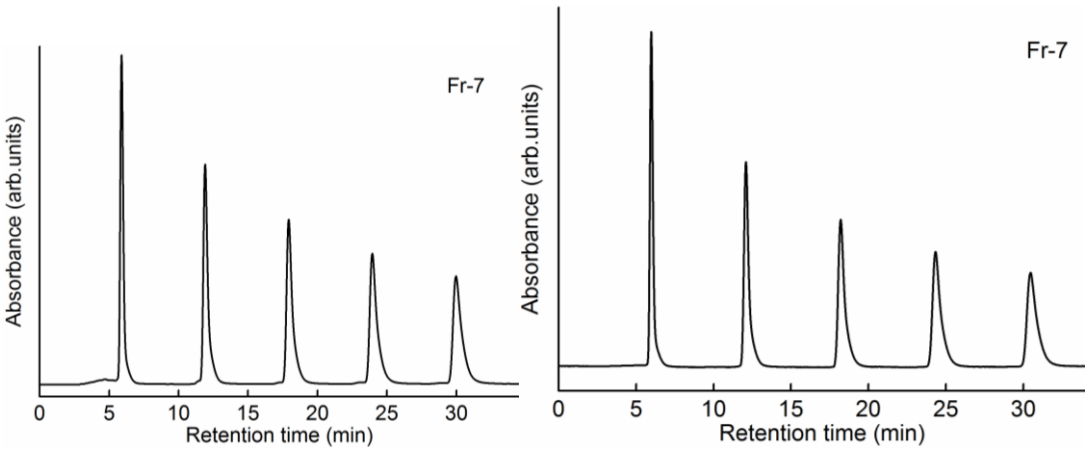

Figure 3.27: HPLC profiles from the first recycling stage and the purity test of F7

3.2.10 DISCUSSION and SUMMARY

This whole procedure was the first method to isolate 18 isomers of bisPCBM from the mixture. The complete flow chart of purification with the step details and applying columns is shown in Figure 3.28. Isomers took between one step to five steps to finally achieve completely pure samples. It is really time-consuming work, and the procedures could be optimised for a more effective way of separating them with shorter times and more quantities in future. The routine could be modified with different injection volumes, the number of fractions at the beginning, and the selection of columns. The 5ml samples were coloured from light brown to dark brown and from light purple to dark red in Figure 3.29. This means that the electronic structures and light absorption of the isomers are quite different from

each other, and this will be fully discussed in the electronic structure characterisation chapter.

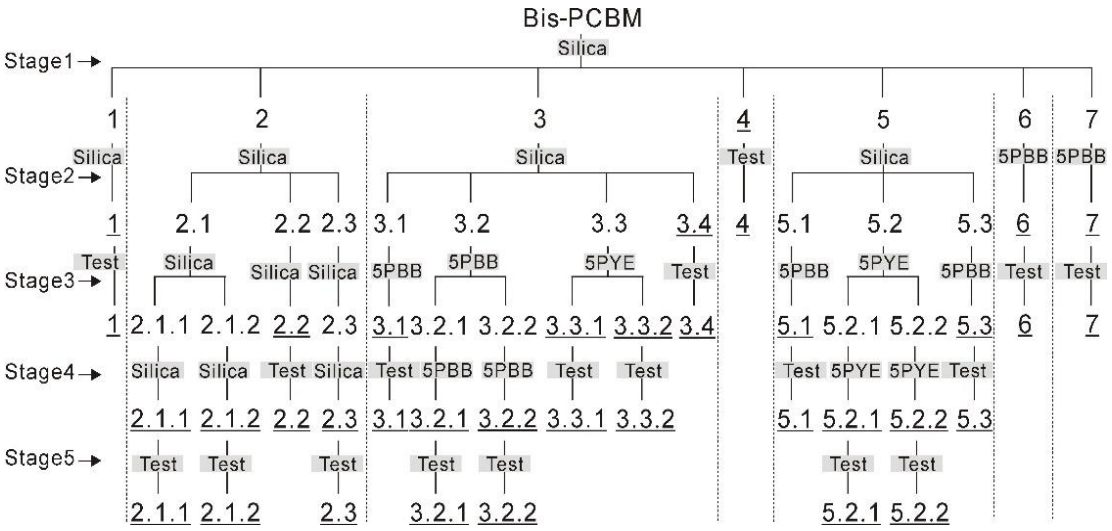

Figure 3.28: A complete flow chart for the purification of all stages for all 18 isomers. The column used at each stage is also shown.

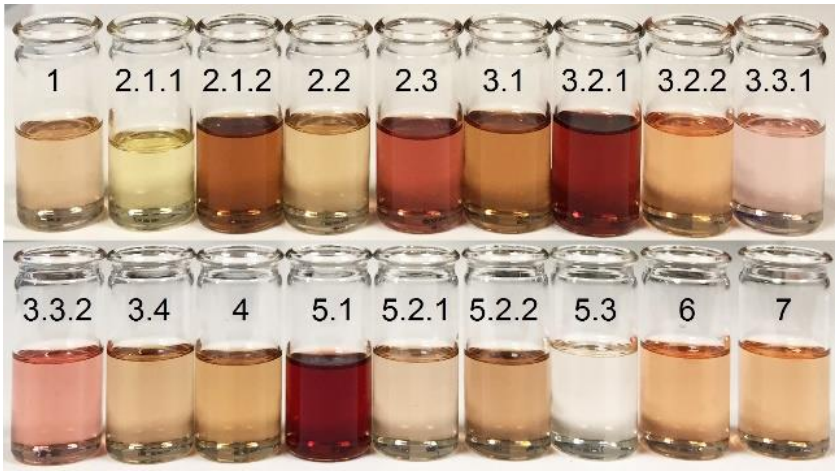

Figure 3.29: Pictures of all 18 isomers purified from BisPCBM

From the peak integration analysis of the resulting HPLC profiles, all the relative yield of 18 isomers and each fraction are shown in Table 3.1 (ranging from 1.2% to 15.6%). The top two most abundant isomers are F3.3.2 and F5.1 with 10.4% and 15.6% respectively. The lowest abundant sample is F2.1.1 with 1.2%. For the

fractions, F3 has the highest abundance out of the seven fractions. The difference of the relative abundance is within one order. Hirsch and co-workers have synthesised, HPLC purified and determined the relative abundances of a similar bis-adduct of C_{60} (as 3H,3H'-dicyclpropa-C60) and three other bis-adducts of C_{60}. They characterised all isomers and found the most abundant isomers are the e isomers. The second most abundant are the trans-3 isomers, while the lowest yield is from trans-1 isomers. This is because of steric hindrance (no cis-1 isomers) and statistical advantage (more e isomers) and disadvantage (fewer trans-1 isomers). There are two very high abundance isomers (F3.2.2 and F5.1) and three very low abundance isomers (F2.1.1, F3.4, F7). Hence, we tentatively assign F3.3.2 and F5.1 as the two equatorial isomers. However, for more certainty in the assignment, further characterisation, such as NMR, UV-Vis and X-ray diffraction analyses is required.

Fraction	**F1**	**F2**				**F3**			
Content/ %	6.7%	19.4				33.1			
Isomer		**F2.1.1**	**F2.1.2**	**F2.2**	**F2.3**	**F3.1**	**F3.2.1**	**F3.2.2**	**F3.3.1**
Content/ %		1.2	7.5	4.4	6.3	3.0	7.0	7.5	3.4
Fraction	F3		F4	F5				F6	F7
Content/ %	33.1		6.2	26.5				5.2	1.4
Isomer	**F3.3.2**	**F3.4**		**F5.1**	**F5.2.1**	**F5.2.2**	**F5.3**		
Content/ %	10.4	1.8		15.6	2.3	5.4	3.2		

PS: The content of residual is 1.4%.

Table 3.1: Relative abundance of BisPC_{62}BM isomers from obtained from integration analysis of the HPLC profiles

3.3 PURIFICATION of $PC_{71}BM$

A 1000mg sample mixture of full $PC_{71}BM$ isomer mixture was supplied to us by Prof. J. C. Hummelen. The synthesis procedures of $PC_{71}BM$ were the same as that of $PC_{61}BM$ only replacing the C_{60} with C_{70} in the reaction. As the solubility of $PC_{71}BM$ is lower than that of bis$PC_{62}BM$, the $PC_{71}BM$ sample was dissolved in toluene to give a concentration of 1000mg $PC_{71}BM$ in 1000L toluene. This solution was filtered through a 0.45 micron Teflon filter immediately before use. The purification was performed using peak recycling preparative HPLC (LC-908). 3ml of the above solution was injected into the column per run and delivered with a pure toluene (HPLC grade 99.8%) mobile phase at a flow rate of 18 ml/min at room temperature. The chromatogram was monitored by a UV absorption detector operating at 312nm. After preparation, all isomers in the mixture were fully isolated. The details of each separation are shown below.

3.3.1 The peak recycling trial of $PC_{71}BM$ full mixture

After the sample passed through the 5PBB column once, only one peak was shown in the HPLC chromatogram, however the long tail of the peak and the shoulder on the peak suggested there was more than one isomer in the mixture. The recycling stage was necessary to separate the isomers. As the width of peak is narrow at around two minutes, around seven more passes would be required in order to maximally separate the different peaks. By cutting at the positions of the dashed lines indicated in Figure 3.3.1, the sample was partially separated into two fractions: MAJOR and MINORS. The MAJOR is the main fraction of the $PC_{71}BM$ isomers, while the MINORS are the fractions with a relatively lower amount. According to the chromatogram, it is obvious that two fractions have to be collected for further purification. As the MINOR is in front and the MAJOR is at the back, it is easier to purify the MAJOR from the whole mixture first, since all the isomers have long tails of peak, which is caused by a tendency of the solute to catch the lower concentration part of solution. As a result, the purification of $PC_{71}BM$ can be divided into two parts: the purification of the MAJOR, and the purification of the MINOR. As mentioned, the MAJOR was purified first.

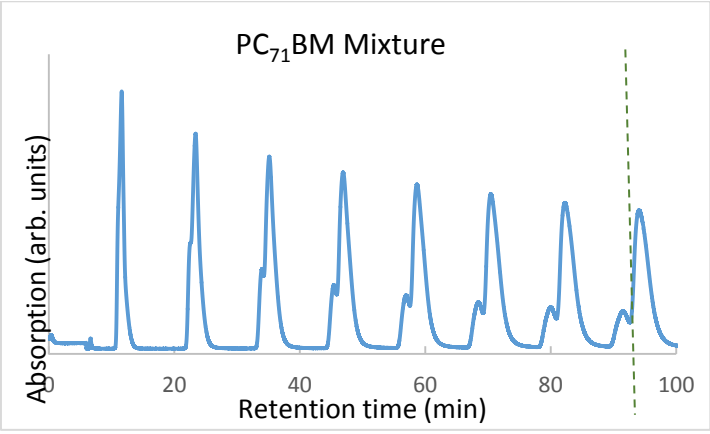

Figure 3.3.1: HPLC profile for the full mixture of $PC_{71}BM$ after 7 recycles.

3.3.2 PURIFICATION OF $PC_{71}BM$ MAJOR

According to the initial analysis of the $PC_{71}BM$ mixture, the MAJOR was subjected to two recycling HPLC stages, from which a pure isomer $PC_{71}BM$ MAJOR was finally obtained; the procedure involved peak recycling. Different columns were tried, and the 5PBB column was finally applied, as it gave a clear separation of the isomers.

Figure 3.3.2 shows the first recycling stage for the MAJOR. It can be seen that there were some residuals from the synthesis in the sample as there were several tiny peaks from zero to seven minutes. They were moved out from the sample at the first pass. In the first peak, some hidden peaks within can only be observed empirically. After three cycles, one obvious gap between the MINOR and the MAJOR emerged. After seven cycles, the gap between them was further enlarged, which was cut in between them after the seventh cycle (as indicated by the orange dashed line). The first fraction was collected and concentrated to be named MINORS. The MAJOR peak (the second fraction) was collected and concentrated for the second stage purification. To purify the entire sample to this stage, the above recycling stage was repeated with around 70 separate 3ml injections.

In the next stage for MAJOR, the 70 samples from the previous stage were added together and concentrated down to around 150ml of nearly saturated solution. This sample was subjected to more recycling HPLC, with the same solvent flow rate and injection volumes as above. After another eight-cycle treatment, the MAJOR was

separated from the small remnant of the MINORS from the previous stage by cutting the two peaks at the minimum between them. The amount of MINORS going into this treatment is clearly much reduced from that seen in the first treatment. The MINOR collected from this stage was concentrated and added into the previous MINOR bottle. The next step was to investigate the purity of the MAJOR. It took about 50 repetitions of the above to purify the entire sample to this stage.

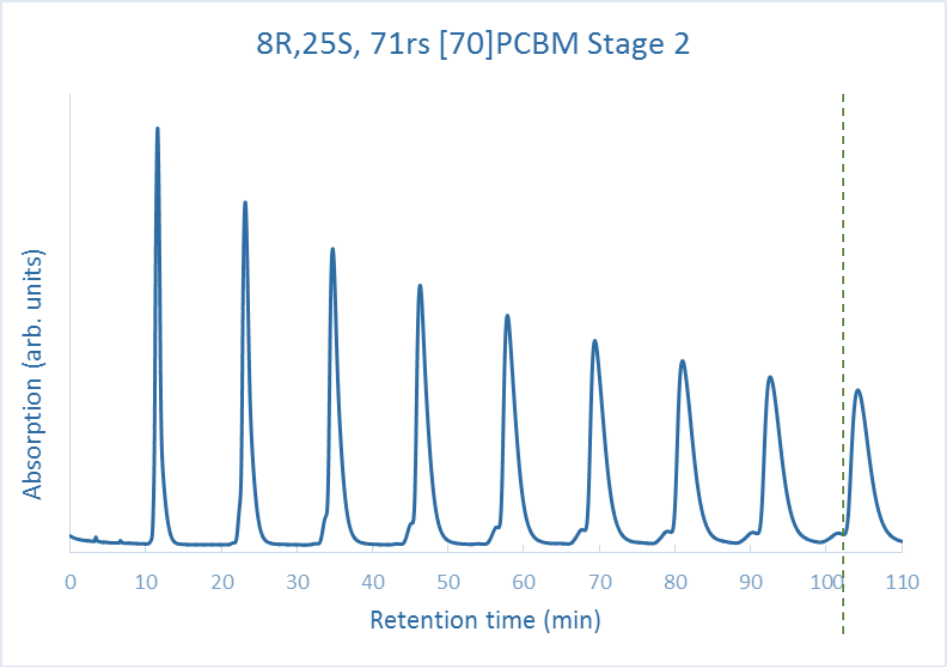

Figure 3.3.2: HPLC profile from the second stage of purification of MAJOR

Purity test

For the purity test, the 50 samples from the previous stage were added together and concentrated down to approximately 100ml of nearly saturated solution. One testing sample was subjected to more recycling HPLC for five cycles, with the same solvent flow rate and injection volumes as above. After five cycles, there was only

one peak, with no evidence of other impurities. It can be concluded that the MAJOR was pure.

3.3.3 PURIFICATION OF $PC_{71}BM$ MINORS

3.3.3.1 Obtaining the pure MINORS mixture

Since there was still some MAJOR in the MINOR mixture collected from the previous mixture, the pure MINOR mixture needed to be obtained first, before further purification of all MINOR isomers. The purification of pure MINORS includes two more recycling stages. This stage was conducted using a 5PBB column.

The first recycling stage for the pure MINORS

The tiny residual peaks on the left side of the main peak were removed on the first cycle, shown in Figure 3.3.3. After cycling MINORS through the column seven times, the MINORS and the residual MAJOR were collected separately at the minimum between the two peaks, marked by the dashed line. The residual MAJOR was concentrated and was stored for further use. The nearly pure MINORS were concentrated and recycled again (below). As with MINORS, to purify the entire sample to this stage, the first recycling stage was repeated using about 50 separate 3ml injections.

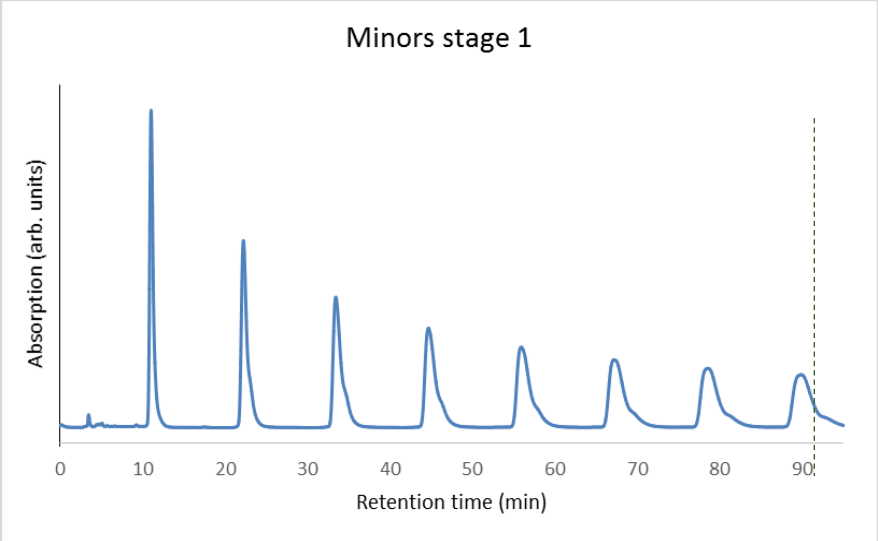

Figure 3.3.3: HPLC profile from the first recycling stage in separation of C70PCBM MINORS

The second recycling stage for pure MINORS –stage 2

In the next stage for MINORS (Fig. 3.3.4), the 50 samples from the previous stage were added together and concentrated down to around 150ml of nearly saturated solution. This sample was subjected to more recycling HPLC, with the same solvent flow rate and injection volumes as above.

After another nine-cycle treatment, it was obvious that the remaining MAJOR constituted less than 1% of the sample, hidden in the peak tails. The MINOR was separated from the small remnant of MAJOR from the previous stage by cutting the tail, which is indicated in Figure 3.3.4 by the dashed line. At the ninth cycle, the two MINOR isomers in the mixture can be observed from the peak shoulder. It took about 50 repetitions of the above to purify the entire sample to this stage.

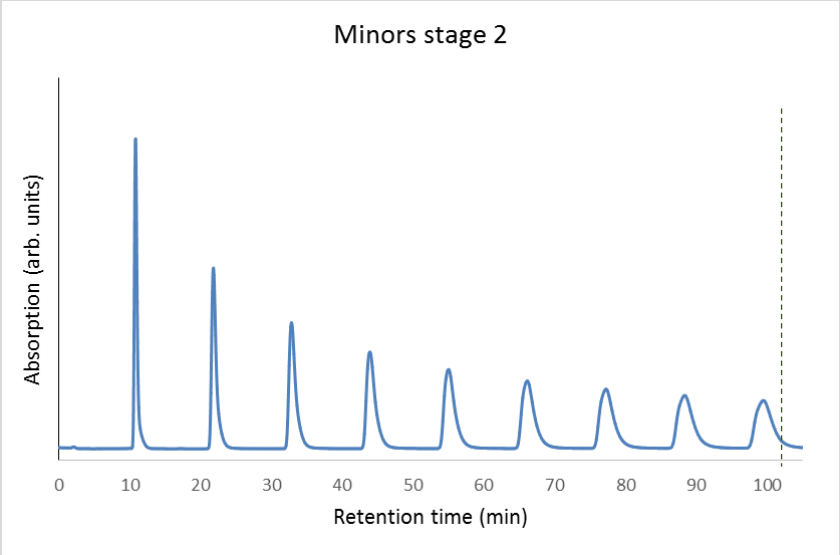

Figure 3.3.4: HPLC profile from the second recycling stage for separating the pure MINORS

The next step was to investigate the purity of the MINORS. After the second recycling stage, 50 samples were added together and concentrated into 150ml. A 1ml MINOR sample from the concentrated solution was diluted into 3ml by toluene, which was then injected into the HPLC. A diluted sample can achieve a much clearer separation of different isomers. After it went through the column five times, there was no sign of other peaks by the side of the main. It can be concluded that the MINOR was pure.

3.3.4 Initial stage of MINOR 1 and MINOR 2

The previous stage of purification was carried by the COSMOSIL 5PBB column, and other parameters are same. This column gives long retention times because of its long length, however the separation of MINOR isomers is ineffective with this column. A silica column was used for the further separation of both MINOR isomers. The following method was used to primarily obtain MINOR isomer solution, which

was prepared for further purification later. There are two MINOR isomers, which are called MINOR 1 and MINOR 2.

This stage is shown in Figure 3.3.5: after the fourth cycle, the gap between the two isomers emerged. The front one is defined as MINOR 1 and the back one is called MINOR 2. After the ninth cycle, the gap between the two isomers became wider. MINOR 1 and MINOR 2 were collected at the beginning of the peak and the lowest point of the gap respectively. The separation point was marked by the blue dashed line. Both isomer solutions were concentrated as original MINOR 1 and MINOR 2 solution for the individual purification, which will be fully demonstrated below. To finish this stage, 50 repetitions of 3ml injections were done.

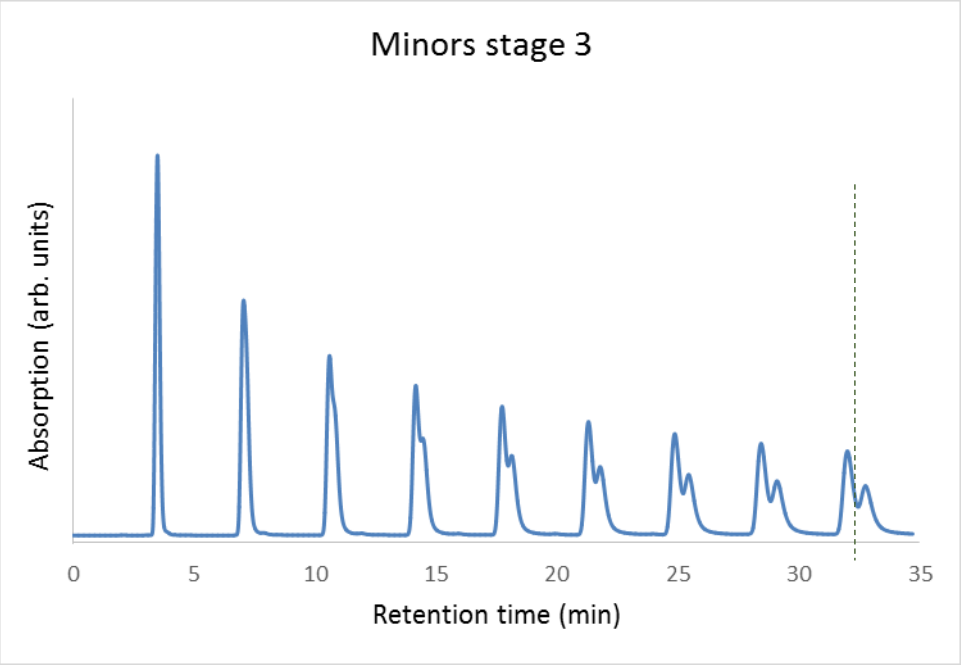

Figure 3.3.5: HPLC profile from the initial stage of MINOR 1 and MINOR 2 separation

3.3.5 PURIFICATION OF $PC_{71}BM$ MINOR 1

The $PC_{71}BM$ MINOR was fully separated by two further recycling stages. The first recycling was done, which is shown in Figure 3.3.6. After the solution went through the column for the ninth time, MINOR 1 and the remaining MINOR 2 (the shoulder on the right side of main peak) were collected separately. The remaining MINOR 2 was collected and added to the MINOR 2 bottle for further separating. The nearly pure MINOR 1 was concentrated and prepared for the next stage purification. It took about 40 repetitions of the above to purify the entire sample to this stage.

Since the MINOR 1 from the previous stage was around 99% pure, in order to make sure the sample was almost 100% pure, the 40 samples from the previous stage were added together and concentrated down to around 100ml of nearly saturated solution. This sample was subjected to more recycling HPLC, with the same solvent flow rate and injection volumes as above.

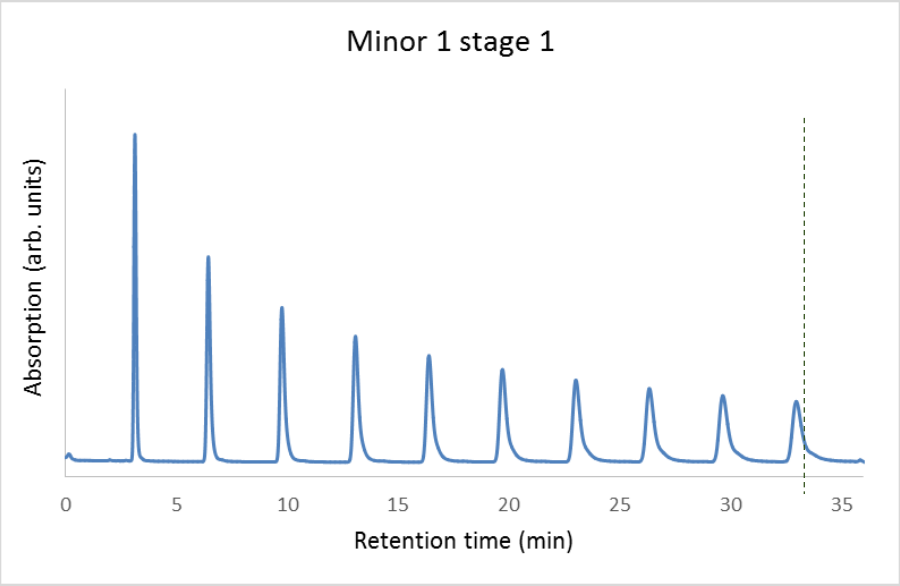

Figure 3.3.6: HPLC profile from the first recycling stage of separating MINOR 1

After another nine-cycle treatment, MINOR 1 was separated from the small remnant of MINOR 2 from the previous stage by cutting the tiny tail of the peak, shown in Figure 3.3.7. The amount of MINOR 2 going into this treatment was clearly reduced to an unviable level from that seen in the first treatment. The MINOR 2 collected from this stage was concentrated and added into the previous MINOR 2 bottle. The next step was to investigate the purity of MINOR 1. Through the purity test, MINOR 1 was more than 99.99% pure. It took about 35 repetitions of the above to purify the entire sample to this stage.

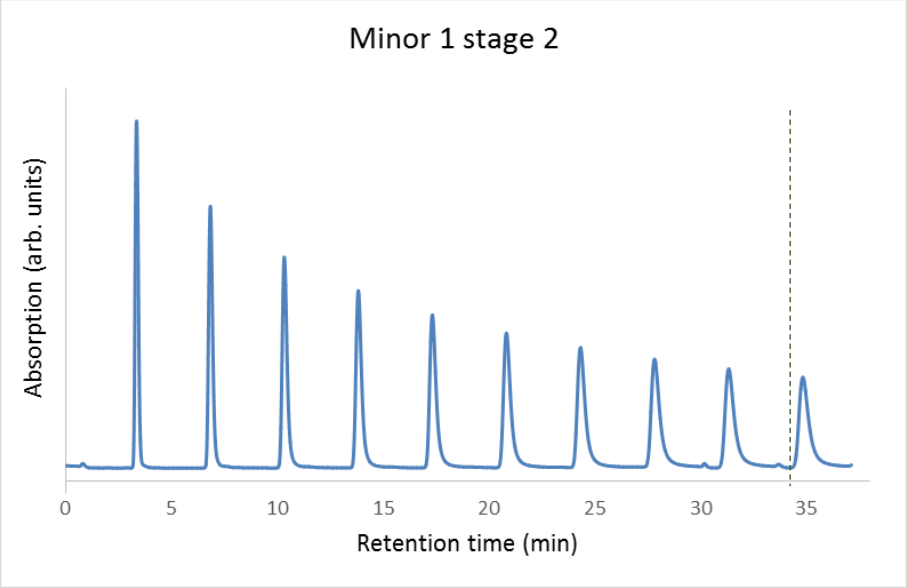

Figure 3.3.7: HPLC profile from the second recycling stage of purifying MINOR 1

3.3.6 PURIFICATION OF $PC_{71}BM$ MINOR 2

The MINOR 2 sample is from the initial stage of the separation of MINOR 1 and 2 and also from the previous purification stages of MINOR 1. The sample was purified by the silica column. The MINOR 2 was purified through three recycling stages. After that, the pure MINOR 2 was obtained.

Stage 1

Figure 3.3.8 shows the first recycling stage. After recycling MINOR 2 through the column seven times, the MINOR 2 and the residual MINOR 1 peaks were collected separately at the minimum between the two peaks. The purer MINOR 2 was concentrated and was recycled again. As with MINOR 2, to purify the entire sample to this stage, the first recycling stage was repeated using about 45 separate 3ml injections.

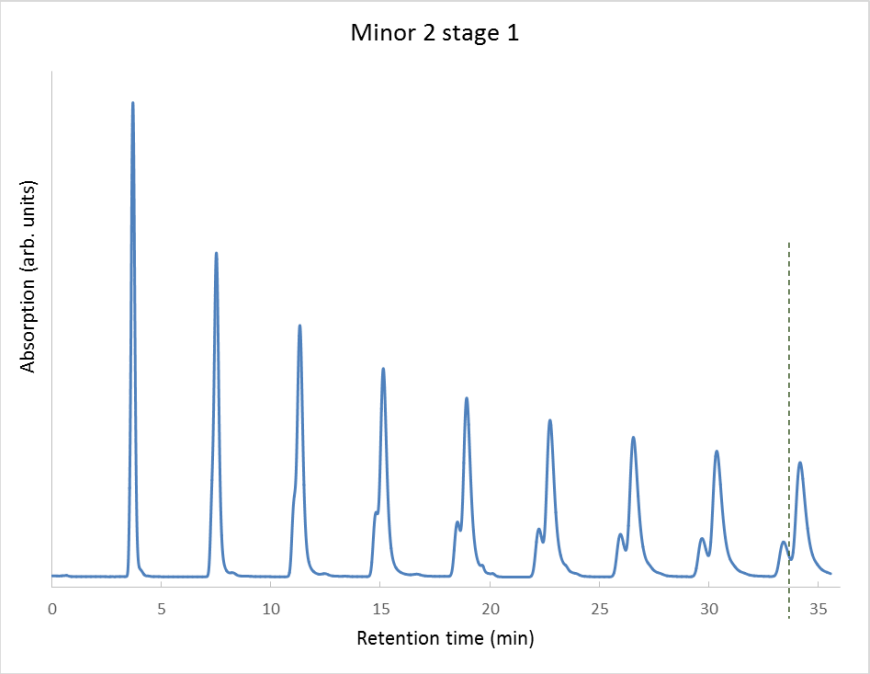

Figure 3.3.8: HPLC profile from the first recycling stage of separating MINOR 2.

Stage 2

In the next stage for MINOR 2 (Fig. 3.3.9), the 45 samples from the previous stage were added together and concentrated down to approximately 100ml of nearly saturated solution. This sample was subjected to more recycling HPLC, with the same solvent flow rate and injection volumes as above.

After another eight-cycle treatment, the MINOR 2 was separated from the small remnant of MINOR 1 from the previous stage by cutting the two peaks at the minimum between them. The amount of MINOR 1 going into this treatment was clearly much reduced from that seen in the first treatment, but there was still a tiny amount of MINOR 1 remaining in the MINOR 2 sample – necessitating another treatment. It took about 40 repetitions of the above to purify the entire sample to this stage.

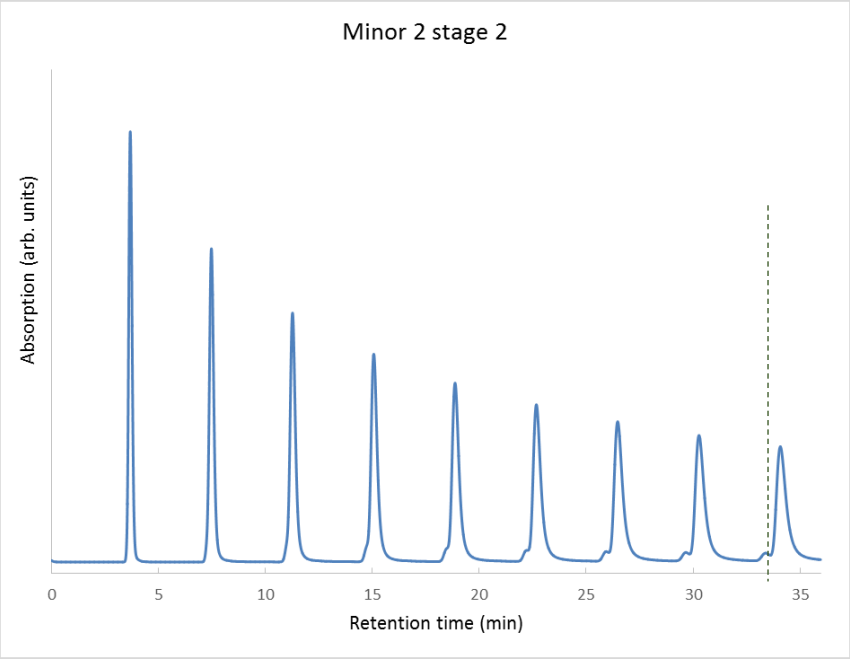

Figure 3.3.9: HPLC profile from the second recycling stage of separating MINOR 2

Stage 3

In the final stage for MINOR 2, the 40 samples from the previous stage were added together and concentrated down to around 75ml of solution. This sample was

subjected to yet more recycling HPLC, with the same solvent flow rate and injection volumes as above.

After nine cycles, the last tiny amount of MINOR 1 was moved out with 99% of MINOR 2 achieving 100% pure MINOR 2. The whole procedure is shown in Figure 3.3.10. MINOR 1 was cut after five seconds after the onset of the MINOR 2 peak. After purity tests, MINOR 1 and MINOR 2 were proved to be completely pure.

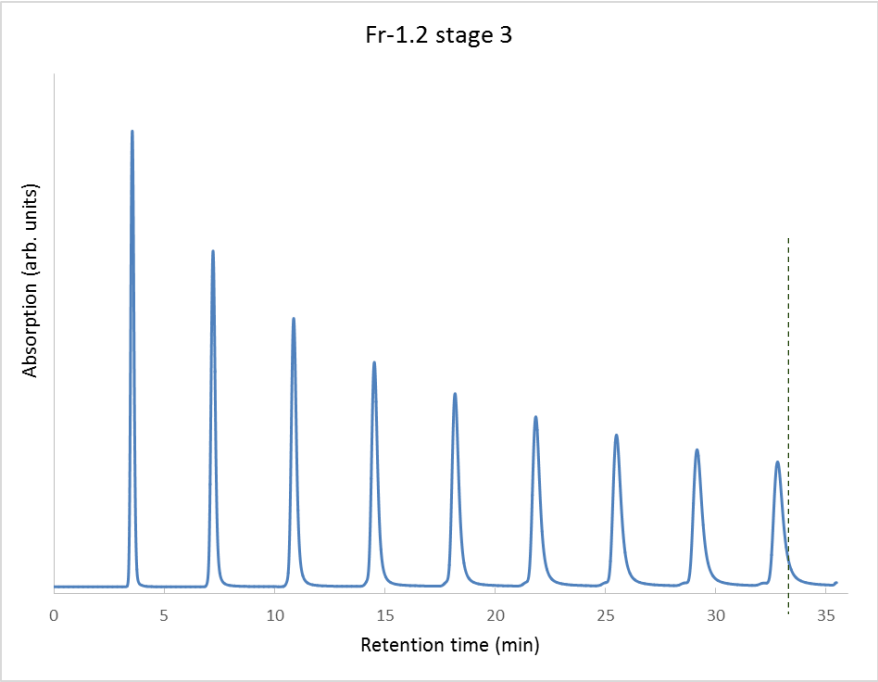

Figure 3.3.10: HPLC profiles from the third recycling stage of separating MINOR 2

3.3.7 Summary of $PC_{71}BM$ Purification

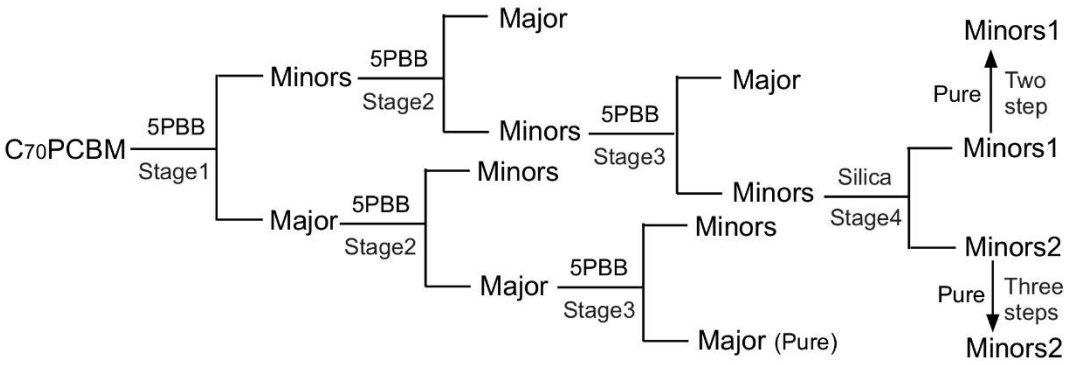

Figure 3.3.11: Purification flow chart for $PC_{71}BM$

The whole purification flow chart for $PC_{71}BM$ is displayed in Figure 3.3.11. Two columns (5PPB and silica) were applied to achieve the best efficiency of the separation. The MAJOR isomer took two stages to obtain a completely pure sample, while MINOR 1 and MINOR 2 took six to seven stages to achieve more than 99.9% purity. Furthermore, as the MAJOR isomer is most abundant with an 85% relative yield, its easy purification procedure makes it possible to produce isomer-pure OPVs based on the pure MAJOR for potential applications. On the other hand, both a low abundance of 6.4% to 8.6% and the time-consuming purification of the MINORS make it difficult for applications. The device building process on those pure isomers is in progress with our collaborator.

Isomers	Major	MINOR	
Content (%)	**85.0**	**15.0**	
Isomers		**MINOR 1**	**MINOR 2**
Content (%)		**8.6**	**6.4**

Table 3.2: Relative yields of all three isomers of $PC_{71}BM$

Chapter 4

STRUCTURAL CHARACTERISATION OF $PC_{71}BM$ ISOMERS

In this chapter, the ^{13}C NMR spectra and HF/DFT ab-initio calculations of the spectra for all three isomers of $PC_{71}BM$ are described, interpreted and compared for the structural assignment. The methanofullerene characters of all the isomers are determined first. The addition position of PCBM on each isomer has been identified by the original bond length and bond characters of the C_{70}. Furthermore, the orientation of the PCBM group of the two MINOR isomers is found by comparison between the simulated and real spectra.

The high-resolution neutron diffraction measurement of C_{70} (crystal phase) and e-ray diffraction (gas phase) shows that the original bond lengths for all bridged bonds of the calculated homo-fullerenes are in the range of 1.408 to 1.467 Å. [102], [103] As such, they would all have the substantial single bond character required to yield homofullerenes. Conversely, the original bond lengths (double bonds) for all bridged bonds of the calculated methanofullerenes in the range of 1.380 to 1.416 Å are consistent with the substantial double/aromatic-bond character required to yield methanofullerenes. These results are used in analysing the ^{13}C NMR spectra discussed later.

Bridgehead	**2.12 (e-e)**	**1-2 (d-e)**	**1-6 (d-d)**	**1-9 (c-d)**
Bond length /Å	1.467	1.416	1.408	1.453
Bridgehead	**9-10 (c-c)**	**8-9 (b-c)**	**8-25 (a-b)**	**24-25 (a-a)**
Bond length /Å	1.397	1.446	1.38	1.447

Table 4.1: The bond lengths of eight type bonds of C_{70}

NMR Spectroscopy: 80 mg of $PC_{71}BM$ major isomer (>99% purity), 35 mg for each $PC_{71}BM$ minor isomer (>99% purity) were dissolved separately in 5 mL CS_2, and transferred into NMR tubes with a few drops of Deuterated benzene, respectively. The ^{13}C NMR spectrum for each isomer was recorded using a Bruker Avance 600 MHz NMR spectrometer at ambient temperature using TMS as internal standard.

Figure 4.1 shows the measured ^{13}C NMR spectra of the MAJOR isomer (Fr-2). The observed chemical shifts can be divided into two regions. The spectrum comprises 75 resonances between 125 and 160 PPM, which are associated with sp^2 hybridised carbon, and seven resonances between 10 and 80 ppm, which are associated with sp^3 hybridised carbon.

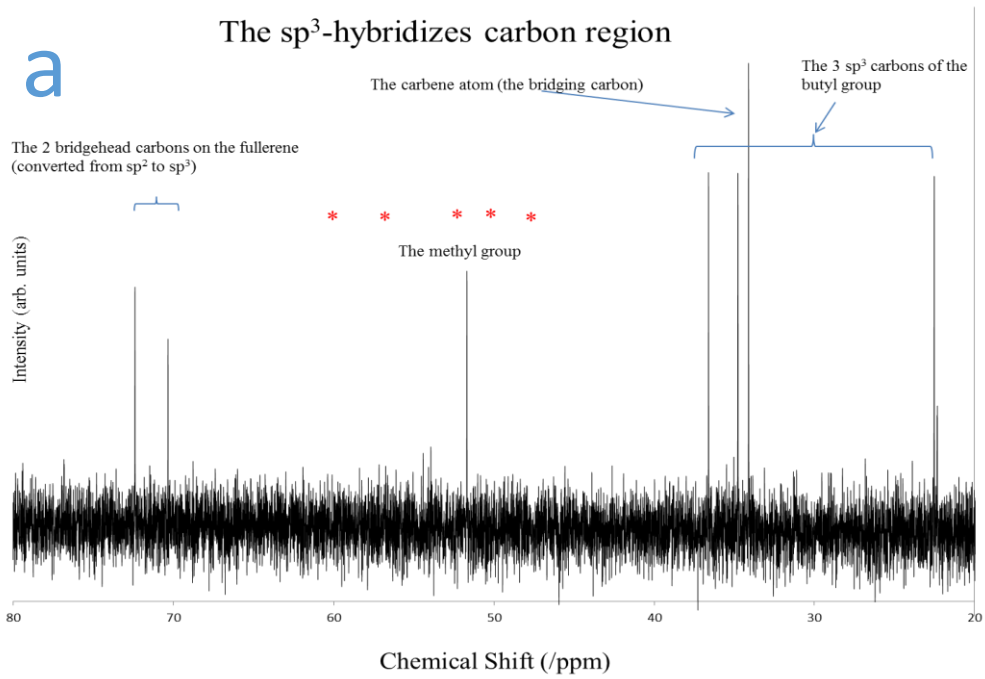
a
The sp3-hybridizes carbon region
The carbene atom (the bridging carbon)
The 3 sp3 carbons of the butyl group
The 2 bridgehead carbons on the fullerene (converted from sp2 to sp3)
The methyl group
Intensity (arb. units)
80
70
60
50
40
30
20
Chemical Shift (/ppm)

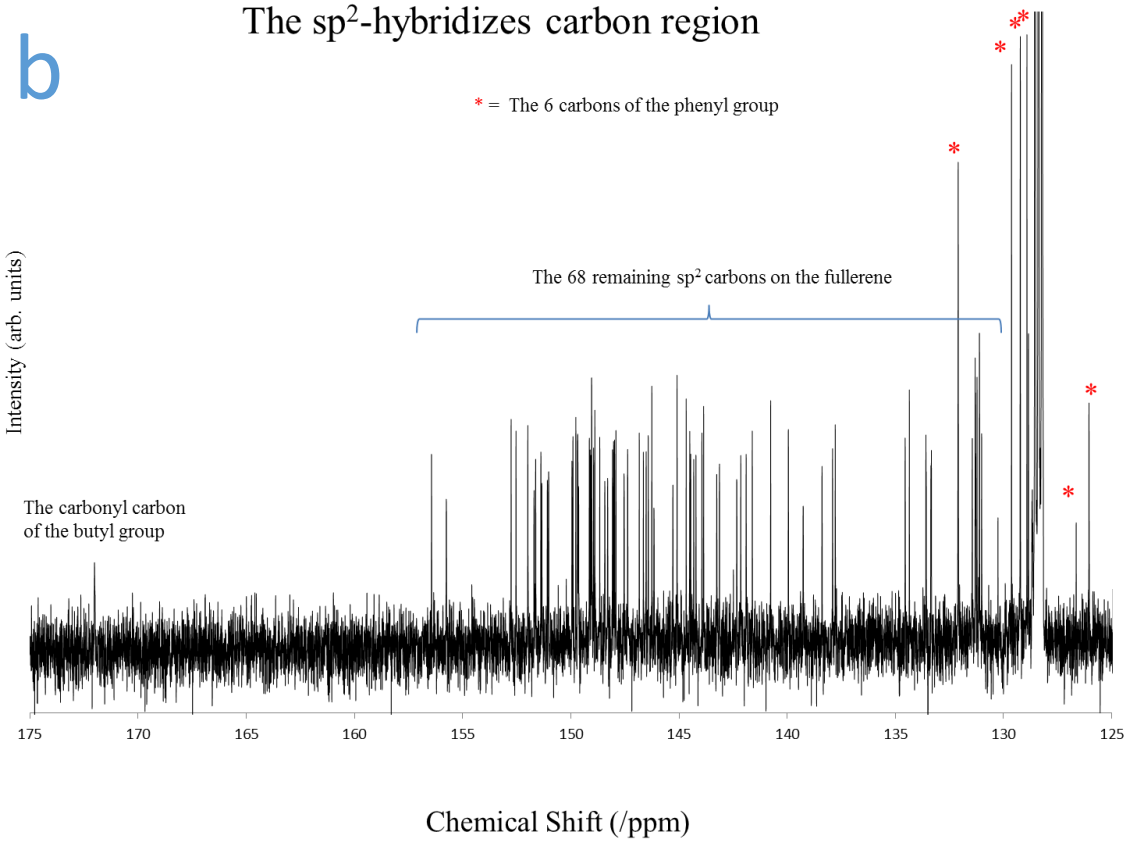
b
The sp2-hybridizes carbon region
* = The 6 carbons of the phenyl group
The 68 remaining sp2 carbons on the fullerene
Intensity (arb. units)
The carbonyl carbon of the butyl group
175
170
165
160
155
150
145
140
135
130
125
Chemical Shift (/ppm)

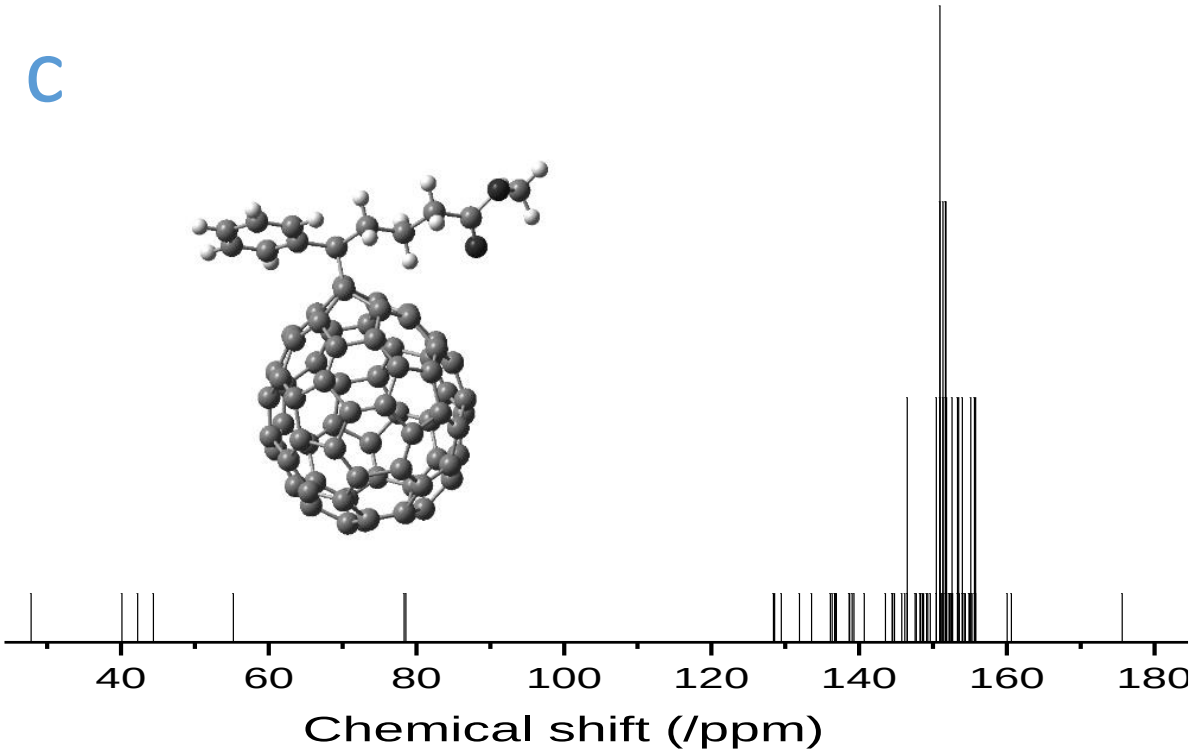

Figure 4.1: the ^{13}C NMR spectra of the Major isomer, showing (a) the sp^3 hybridised carbons, from 10-80 ppm, (b) the sp^2 hybridised carbons from 125 to 175 ppm and (c) a simulation of the ^{13}C NMR spectrum of the major.

The methylbutanoate group accounts for four of the seven sp^3 resonances. With no sp^3 carbons on the phenyl ring, we conclude that the MAJOR isomer must be a methanofullerene involving 'cyclopropa' bridging with a former double or aromatic bond of C_{70}, which converts to a single bond with the two fullerene 'bridgehead carbons' converted from sp^2 to sp^3 hybridisation. The last sp^3 carbon is a bridging carbon on the PCBM group. This must be the case as otherwise the bond would break and the bridgeheads would remain sp^2 hybridised. The methanofullerene conclusion is also consistent with there being only 75 sp^2 carbon resonances. These comprise one resonance from the methylbutanoate group and six resonances from the phenyl group. This leaves only 68 sp^2 resonances to come from the C_{70} fullerene; which is consistent with another two fullerene carbon atoms converting to sp^3

hybridisation on the cyclo-addition. With discreet resonances for all 82 carbon atoms of $PC_{71}BM$, this isomer must have C1 molecular point group symmetry, basically no symmetry.

Of the three expected methanofullerene isomers, only one of them would have a ^{13}C NMR spectrum consistent with C1 symmetry. This is because the two isomers involving the 9-10 (c-c) bond each have a mirror plane, and hence are of Cs symmetry, whereas the isomers involving 1-2 (d-e) and 8-25 (a-b) possess identity as their only symmetry element. The molecular structure of C_{70} as determined by neutron diffraction gives the bond length of the 1-2 bond as 1.416 Å and that of the 8-25 bond as 1.38 Å. Hence, the 8-25 bond has considerably more double bond character than the 1-2 bond, from which we conclude that the MAJOR isomer is a methanofullerene involving bridging of the 8-25 bond of C_{70}. Details of naming and possible methanofullerene isomers of $C_{71}BM$ have been fully described in Chapter 2.

Based on the above analysis we conclude that the MAJOR isomer of $PC_{71}BM$ consists of a methanofullerene racemate in which the addend is attached to the fullerene via the cyclopropa-bridging of the 8-25 bond of C_{70}. A B3LYP/6-31G(d,p) simulation of this spectrum using the GIAO method, on a geometry re-optimised at the same level of theory with tight cut-offs, is shown in Figure 4b. This is consistent with the experimental one, as it comprises seven resonances for sp^3 carbons from 20 to 80 ppm for proving its methanofullerene character. In this region, the first line for the butyl carbon is around 30 ppm and the last two for the bridgehead carbons are

round 78 ppm. The intervals between each line are similar. For example, both spectra have three quite close resonances for the butyl carbons from 30-50 ppm. This again supports our conclusion on the molecular structure. The conclusion that the MAJOR isomer involves the 8-25 bond is unsurprising. This is because the vast majority of cyclo-addition-based C_{70} derivatives involve the 8-25 bond, whereas there are virtually no derivatives that involve the only alternative for this isomer that would be consistent with the ^{13}C NMR spectrum and indeed this result had already been predicted in Chapter 2.

Figures 4.2 and 4.3 show the ^{13}C NMR spectra of (a) fraction Fr-1.1, and (b) Fr-1.2. As with the spectrum of the MAJOR isomer, the spectra of both MINOR isomers are also divided into sp^2 and sp^3 hybridised regions. Each of these spectra consists of 75 sp^2 resonances and six sp^3 resonances. It is also seen that seven of the sp^2 resonances are of a substantially lower intensity than the other 36. This is consistent with each of the MINOR isomers possessing a mirror plane. This conclusion is also supported by there being only six resonances in the sp^3 region – one less than that of the MAJOR isomer, with that resonance being approximately double in relative intensity. This is due to the resonances from the two bridgehead carbons on the fullerene lying either side of a mirror plane, and hence, appearing as a single doubly-degenerate line in each of the two MINOR isomer spectra. Of the eight distinguishable bonds on C_{70}, only the 2-12, 9-10 and 24-25 bonds straddle the mirror planes of C_{70}; of which only the 9-10 bonds are short enough to be classed as a double/aromatic bond. Hence, we conclude that both of the MINOR isomers of

$PC_{71}BM$ are methanofullerenes in which the addend is attached to the fullerene via cyclopropa-bridging of the 9-10 bond of C_{70} in two opposing orientations.

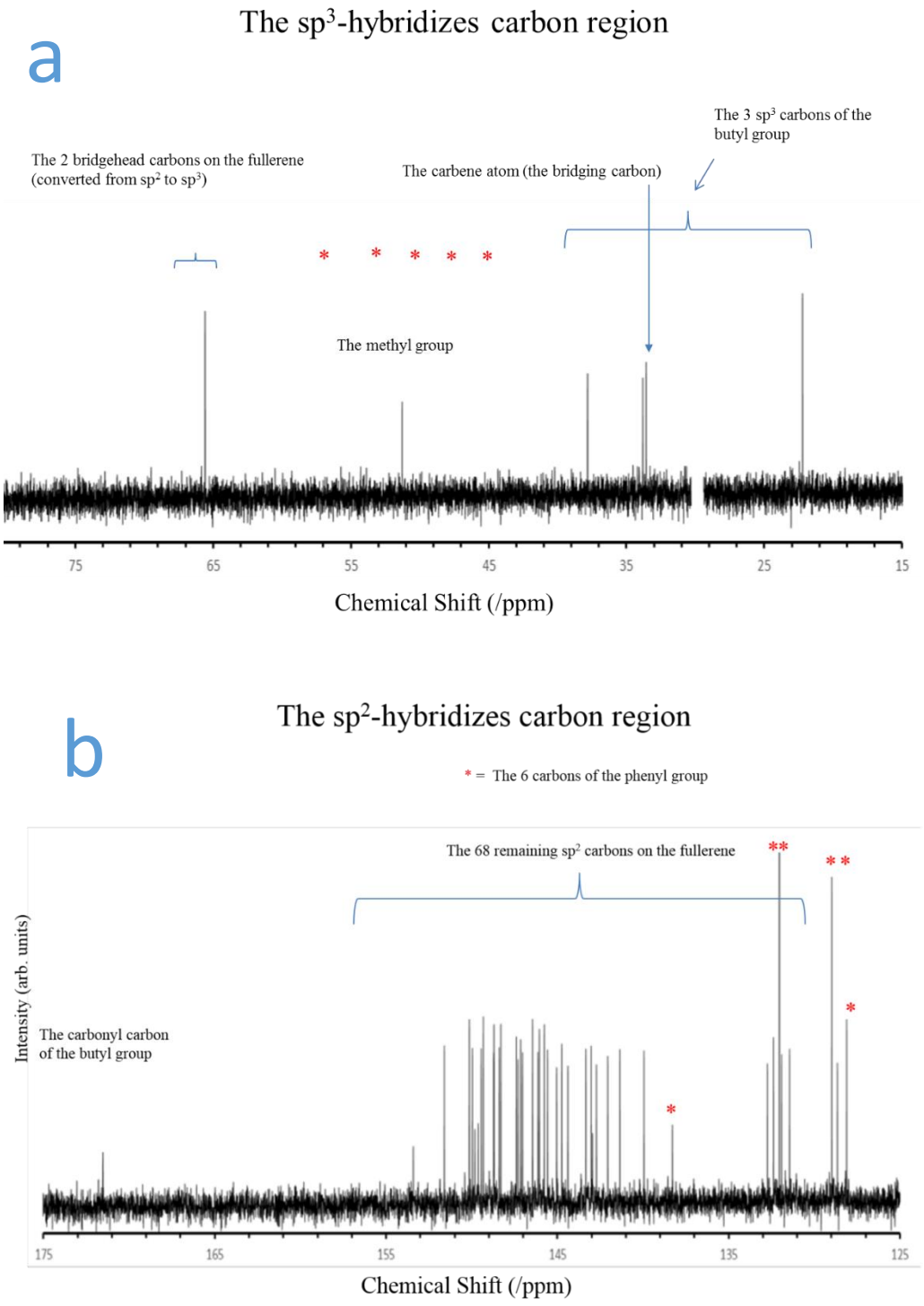

Figure 4.2: the ^{13}C NMR spectra of the minor 1 isomer, showing (a) the sp^3 hybridised carbons, from 10-80 ppm and (b) the sp^2 hybridised carbons from 125 to 175 ppm.

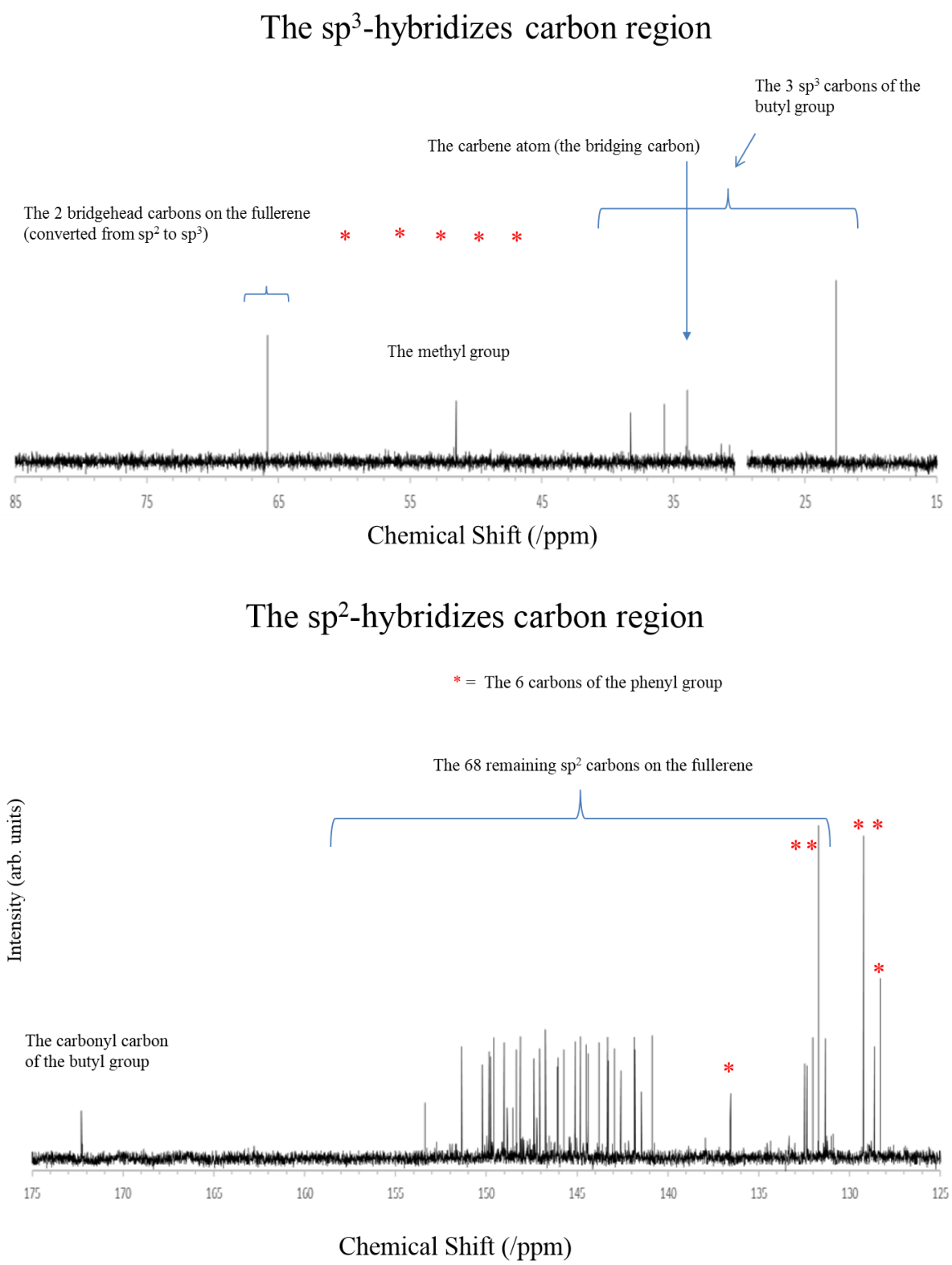

Figure 4.3: the ^{13}C NMR spectra of the MINOR 2 isomer, showing (a) the sp^3 hybridised carbons, from 10-80 ppm and (b) the sp^2 hybridised carbons from 125 to 175 ppm.

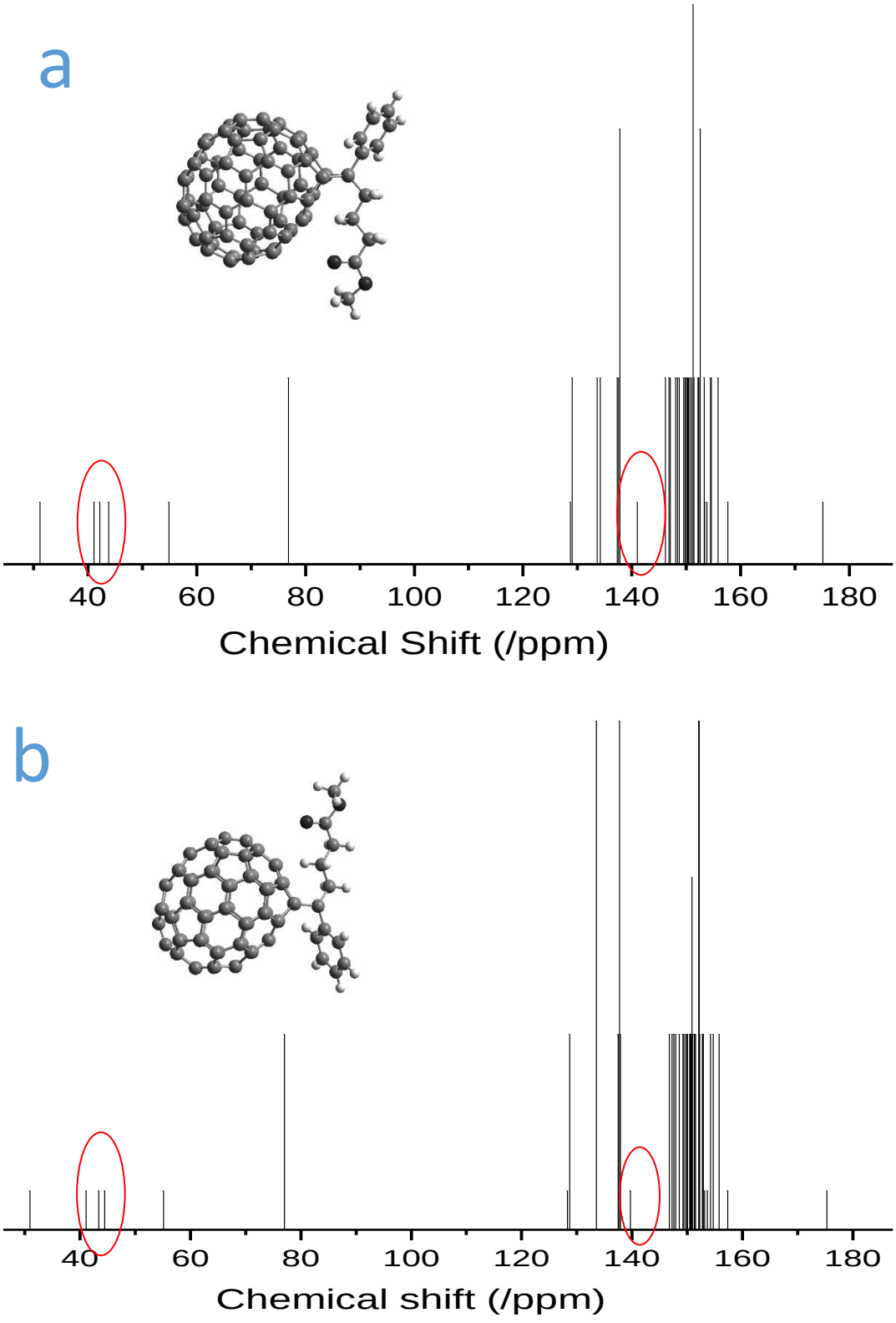

Figure 4.4: Simulated spectra of ^{13}C NMR for both minor isomers, showing (a) the spectrum from the isomer with phenyl group pointing up and (b) the spectrum from the isomer with phenyl group pointing down.

Unfortunately were are unable to definitively say which ^{13}C NMR spectrum corresponds to which MINOR isomer. This is because the form of the spectra for both isomers (numbers of lines and relative intensities) is identical. Furthermore, the simulated ^{13}C NMR is quite complicated in that there are not enough simulated/real similarities for a confident assignment one way or the other. The simulated NMR spectra based on B3LYP/6-31G(d,p) were also shown in Figure 4.4 for both MINOR isomers. Figure 4.4a is the MINOR isomer with the phenyl group pointing up, named 9R,10S,71r-$PC_{71}BM$, while the MINOR isomer with phenyl down is named 9R,10S,71s-$PC_{71}BM$.

Through comparison, most resonances are quite similar. However, there are two clear differences in the spectra that are useful for the structure assignment. Firstly, between the fullerene line forest and the lines for the phenyl group, there is only one resonance that represents the linking carbon on the phenyl group, which is connected to bridging carbon. For MINOR 1, the line of the real spectrum is located at 138 ppm and is close to the fullerene forest. MINOR 2 has an obvious shift of this resonance to a lower field around 136.5 ppm in the middle point of the gap. This difference is also shown in the simulated spectra. The 9R,10S,71r-$PC_{71}BM$ has a higher shift around 141 ppm for that resonance and 9R,10S,71s-$PC_{71}BM$ has the lower resonance around 139 ppm. Up to this point, we can say with some confidence that MINOR 1 is 9R,10S,71r-$PC_{71}BM$ and MINOR 2 is 9R,10S,71s-$PC_{71}BM$. This is supported by the second difference from the spectra. The second difference is from three butyl carbons with resonances from 30-50 ppm. The middle resonance

line has a different shift. The line of MINOR 2 shifts to a higher field, however there is a converse shift from MINOR 1 of the experimental spectra. The simulated resonance has the same difference with a similar shift. This is consistent with the structure assignment. According to these comparisons, it can be concluded that MINOR 1 is the 9R,10S,71r-$PC_{71}BM$, and MINOR 2 is 9R,10S,71s-$PC_{71}BM$.

SUMMARY

Through NMR characterisation and simulated spectra, the molecular structure of all the isomers of $PC_{71}BM$ was determined. The MAJOR isomer (8R,25S,71rs-$PC_{71}BM$) is the methanofullerene with the PCBM addend added to the 8-25 bond. As to the two MINOR isomers, MiNOR 1 (9R,10S,71r-$PC_{71}BM$) with the shorter retention time has a structure with PCBM attached onto the 9-10 bonds with the phenyl group pointing up, while the longer retained MINOR 2 (9R,10S,71s-$PC_{71}BM$) is with the phenyl group pointing down. The structural characterisation for the isomers of bis$PC_{62}BM$ is still ongoing. The isomer structures are already partially determined from the UV-Vis spectra, which are divided into seven bond groups in Chapter 5.

Chapter 5

Electronic Characterisation of bis$PC_{62}BM$ and $PC_{71}BM$

This chapter includes the UV-Vis characterisation and cyclic voltammetry (CV) for all the purified isomers of bis$PC_{62}BM$ and $PC_{71}BM$. The UV-Vis results are used for both structural assignment and band gap determination. LUMO values determined from the CV are important for potential OPV applications.

5.1 UV-Vis characterisation of BisPC$_{62}$BM

All the bisPCBM isomers were characterised using a UV spectrophotometer (SHIMADZU UV-2600) between 325 to 800 nm and 600-800 nm. The scanning rate and sampling intervals were set as 30 nm/min and 0.2 nm/s. The lower scanning rate was applied to achieve higher quality spectra in order to read the transition point more accurately. The samples for UV-Vis were prepared by a 3 ml injection into the HPLC with peak recycling of the pure bisPCBM isomer with pure toluene solution (HPLC Grade 99.8%) as the mobile phase. The collection of the sample was taken from the central part of the peak (marked in blue) in the second cycle to ensure 100% purity of the samples, which was transferred to the sample cell (10 mm x 10 mm) for the UV absorption test with the background toluene as the reference. The background toluene (reference) was collected from the eluate from the flat baseline of the curve.

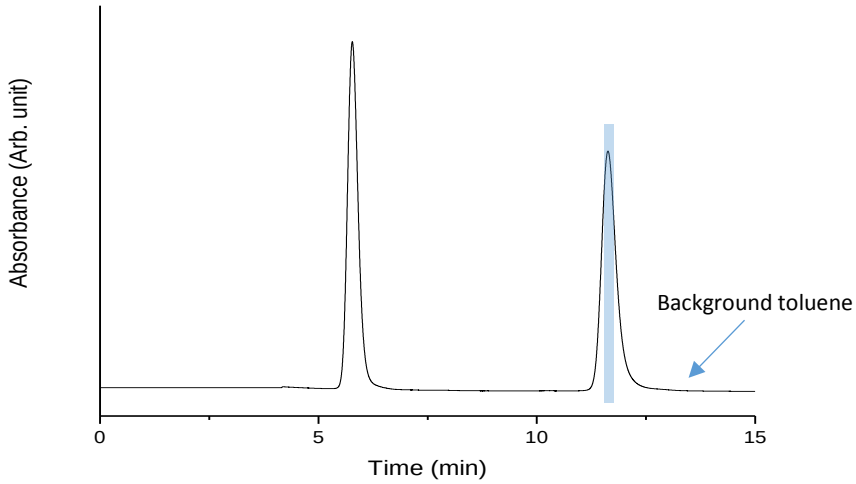

Figure 5.1: HPLC profile showing the isomer solution and reference sample for UV spectrometry.

As the scanning wavelength decreased from 780 nm to 375 nm, the distinct absorption range and characters of each isomer were displayed. The HOMO-LUMO

gap is the lowest excitation energy gap from the molecule non-bonding orbital to the anti-bonding orbital. Combined with the excitonic absorption peak, we can get the first transition point as shown in Figure 5.4 to Figure 5.10. The first onset is defined as the first intersection of two tangent lines drawn from the baseline and slope of the spectrum. According to these onset wavelengths (λ), the HOMO-LUMO gap (Eg) of each isomer can be calculated using the Planck Relation:

$$Eg=hc/\lambda$$

Where, h is the Planck constant and c is the speed of light in a vacuum. The onsets and the estimated HOMO-LUMO gaps for each isomer are given in Table 5.1. It shows that the Eg values of the isomers vary from 1.664 to 1.883 eV, where sample 5.1 has the largest value. The errors were calculated by the shifted intersections of tangent lines in possible locations.

Isomer	λ/nm	Eg/eV
Fr-1	727.3±0.3	1.705±0.001
Fr-2.1.1	721.5±2.5	1.718±0.005
Fr-2.1.2	724.1±0.3	1.712±0.001
Fr-2.2	722.0±0.3	1.717±0.001
Fr-2.3	732.9±1.3	1.692±0.002
Fr-3.1	720.2±0.3	1.721±0.001
Fr-3.2.1	725.4±1.5	1.709±0.002
Fr-3.2.2	740.8±2.4	1.674±0.004
Fr-3.3.1	722.3±1.0	1.717±0.002
Fr-3.3.2	659.5±0.2	1.880±0.001
Fr-3.4	745.2±0.4	1.664±0.001
Fr-4	721.9±0.2	1.717±0.001
Fr-5.1	658.4±0.2	1.883±0.001
Fr-5.2.1	734.9±0.3	1.687±0.001
Fr-5.2.2	741.7±0.4	1.672±0.001
Fr-5.3	717.9±2.3	1.727±0.005
Fr-6	707.1±2.4	1.754±0.005
Fr-7	704.9±2.3	1.759±0.005

Table 5.1: Transition onsets of UV-Vis spectra for isomers and the calculated HOMO-LUMO band gaps with errors

The absorption transitions of C_{60} and C_{70} are mainly focused on two regions. The peaks located from 190-410 nm are due to ^1T_1u-^1Ag transitions. [104] The absorption region from 410-620 nm are from orbital forbidden singlet-singlet transitions. Because of the complex structures of the derivative isomers, the molecular orbital splitting gets even more complicated, and the absorption can be simply divided into n- π*, π-π*,π-σ* and σ- π* transitions. An interesting phenomenon is that the isomers with a higher Eg value have a similar shape to their absorption spectra (like isomer 2.1.1, 3.2.2, 3.3.2, 5.1, 5.3, 6 and 7), while the ones with a lower Eg exhibit another kind of similar spectral shape. For deeper analysis, the 18 isomers can be divided into seven groups with extremely similar curve shapes and transition peaks in the range of 600 to 780 nm, presented below. These similar transition peaks correspond to similar electronic structures with close band gaps etc. In addition, the colour of the isomers in the four groups varies in an interesting trend with most of the isomers in the four-peak-group and the three-peak-group displaying a brown colour, and the two-peak-group and the one-peak-group showing pink and red colours. However, this is due to the absorption of the isomers in the visible region. These properties are relevant to their molecular configuration, such as two PCBM addends on C_{60} having similar symmetry, position and rotation direction. This is useful fundamental information for future research.

5.2 UV spectrum for structure assignment

Hirsch et al. have purified several bis-adducts of C_{60}, structurally identified them and recorded their UV-Vis absorption spectra. Comparing their UV-Vis spectra with

those of the 18 isomers in the present work shows very clear similarities, such that we may tentatively assign our spectra, and thereby the HPLC fraction. Before that, an introduction of the double bond system for bis-adducts from Hirsch et al. is shown below in Figure 5.2. They renamed the positions (the double bonds between two hexagons) for a second addition onto the C_{60}. The first addend (A1) is at the position for [1,9] double bonds. Also the different types of double bonds close to A1 were named cis-1 to cis-3, while those at the equator were named e, and those far from A1 were named trans-1 to trans-4. Accordingly, the double bonds and all isomers from our nomenclature system are put together with those eight bond types from Hirsch.

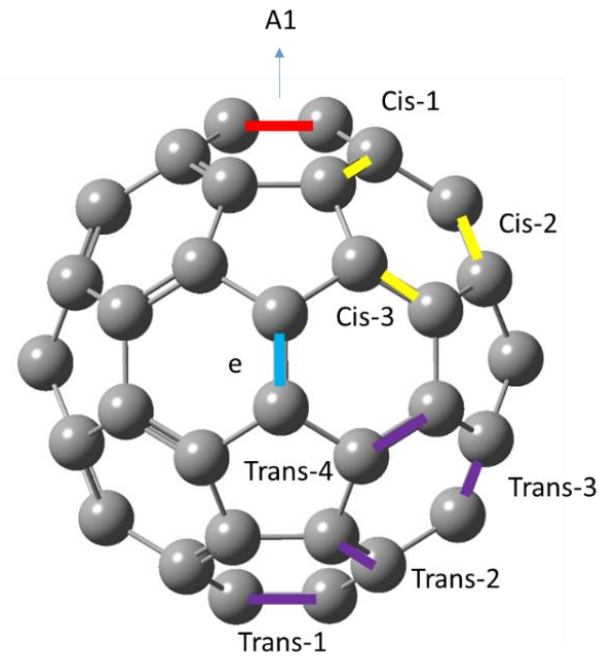

Figure 5.2: Nomenclature system of the double bonds for the second addition from Hirsch et al.

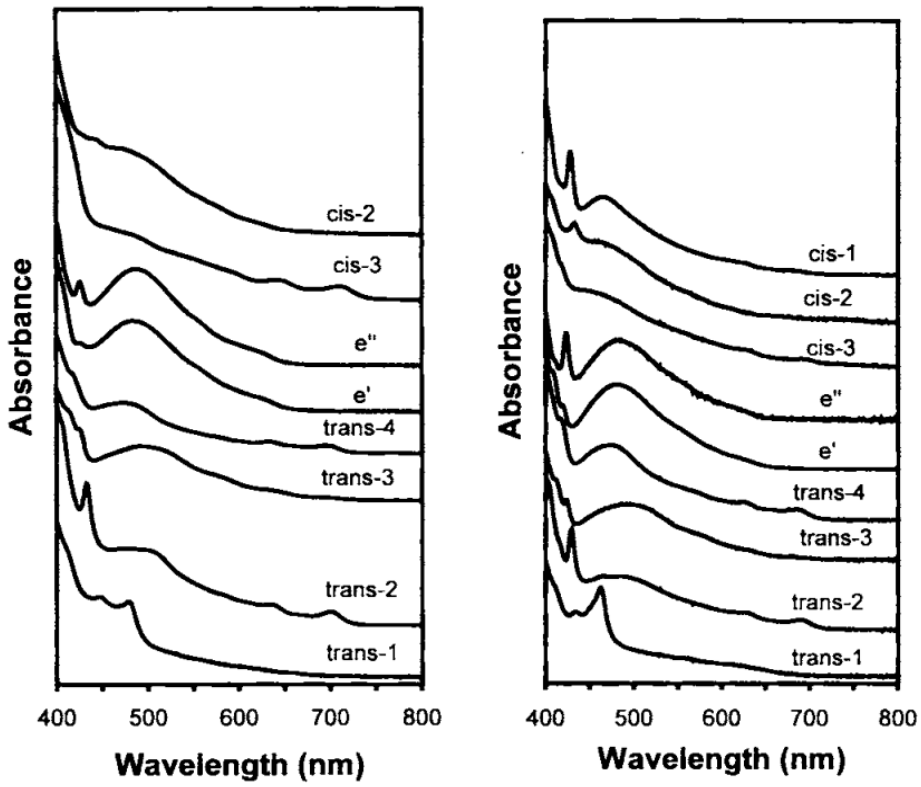

Figure 5.3 UV-Vis spectra of the isolated isomer of two bis-adducts compounds, C_{62} (anisyl)$_4$ and $C_{61}(COOEt)_2(NCOOEt)$. [93]

According to the spectra in Figure 5.3 from Hirsch, the isomers with a second addition on the same types of double bond of C_{62} (anisyl)$_4$ and $C_{61}(COOEt)_2(NCOOEt)$ have a high similarity of spectra. [93] In contract, the isomers from different bond types show obvious distinct characters. For example, all the cis-3 isomers have an L-shaped curve and all the trans-2 isomers have a peak near to 430 nm and two tiny bumps from 600 to 750 nm. These can be applied as fingerprints of the different bond type isomers. A comparison of all our isomers to this figure is given below. The assignment is listed in Table 5.2. All 18 isomers are assigned to the eight bond types and basically were divided into eight categories, where each group is composed of two to four isomers.

Bond types	Double bonds	Isomers
Cis-1	[2,12], [5,6], [10,11],[7,8]	trans-2,12, cis-2,12, cis-5,6
Cis-2	[3,15],[4.18],[26,27],[24,25]	trans-3,15, cis-3,15, cis-4,18
Cis-3	[13,14],[19,20],[22,23],[28,29]	trans-13,14, trans-19,20, cis-13,14
E	[21,40],[44,45], [16,17],[30,31]	21,40 (r,f), 30,31 (r,f)
Trans 1	[52,60]	trans-52,60, cis-52,60
Trans 2	[49,59],[50,51],[53,54],[55,56]	trans-49,59, cis-49,59, cis-50,51
Trans 3	[34,35],[46,59],[44,57],[36,37]	trans-34,35, trans-36,37, cis-34,35
Trans-4	[32,33],[47,58],[38,39],[41,42]	trans-32,33, cis-32,33

Table 5.2: Corresponding double bonds from our nomenclature to the eight double types from Hirsch. According to the similarity of UV-Vis spectra, all the 21 isomers from the theoretical analysis are assigned to the eight bond types.

The equatorial, e, isomers from Figure 5.4 show a pronounced sharp peak at about 420 nm, a broad and somewhat more intense peak at about 500 nm, and a smooth tail with a relatively low-wavelength onset. By reason of the asymmetry of the bridging carbons of bis$PC_{62}BM$, we expect two isomers to have these traits, and indeed they are found in two HLPC fractions: F3.3.2 and F5.1. They are quite similar to each other and also to the spectrum of the e type and are distinct with other spectra. Furthermore, the e isomers were found by Hirsch et al. to be the most abundant of their bis-adducts; and of our fractions, F3.3.2 and F5.1 are considerably more abundant than any other. Hence, we may assign F3.3.2 and F5.1 to be the two equatorial isomers of bis$PC_{62}BM$.[104]

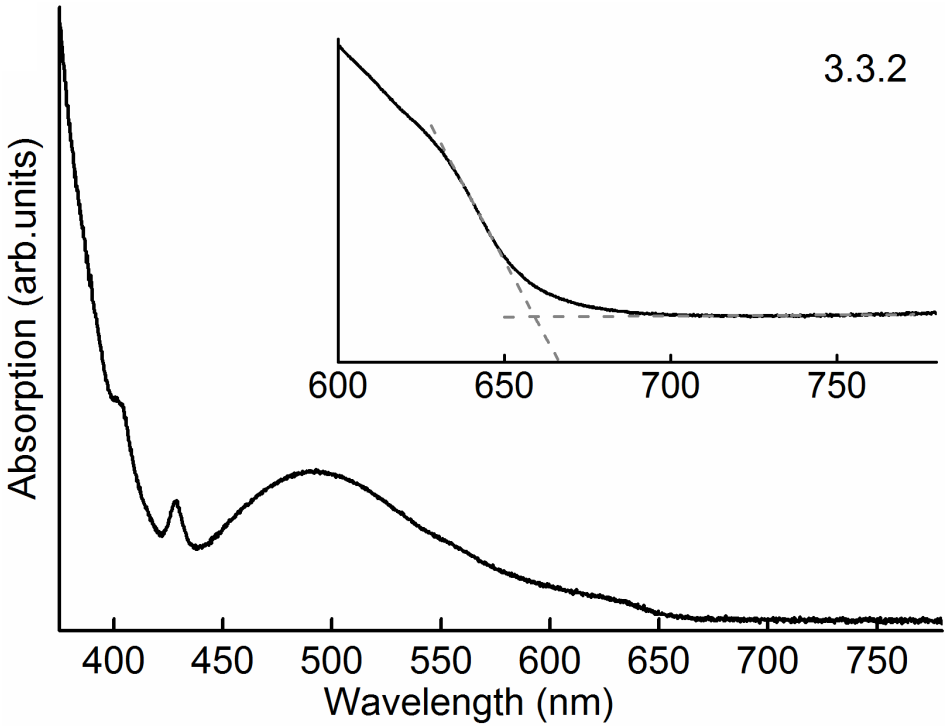

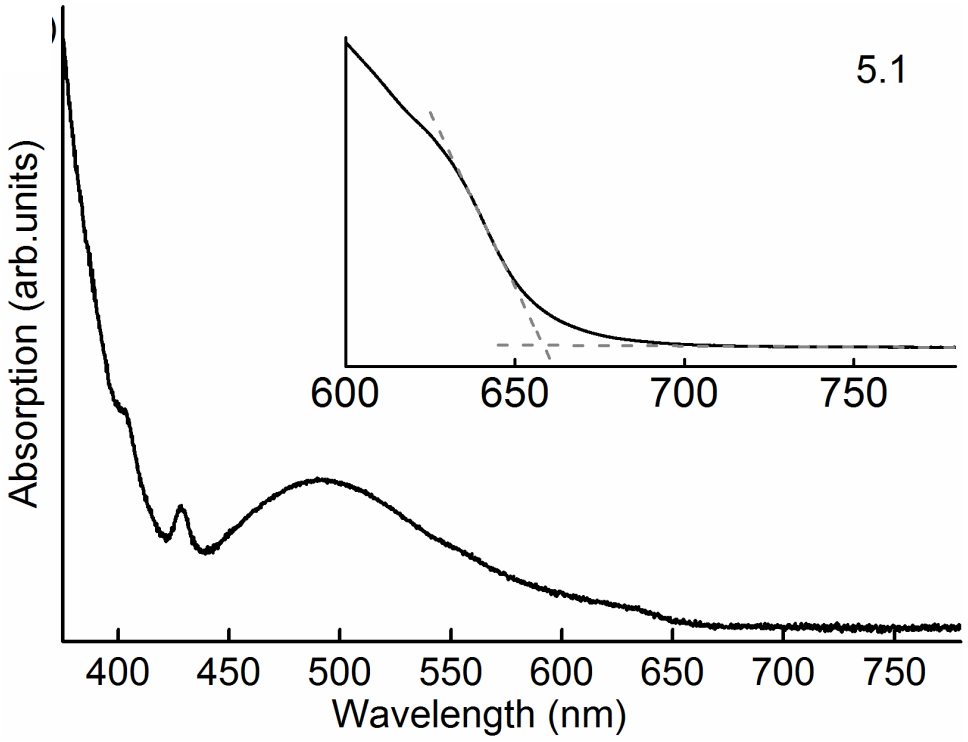

E

Figure 5.4: the UV-Vis spectra of F3.3.2 and F5.1, according to the comparison, both isomers belong to the e type isomers.

The spectra of the trans-2 isomers from Figure 5.5 have a shoulder near 410 nm, a pronounced sharp peak near 420 nm, a broad but this time less intense peak at about 500 nm and a bumpy tail with several weak peaks between 600 and 700 nm, and a relatively high-wavelength onset. This time we expect three isomers of bis$PC_{62}BM$ to have these traits; and find them in the spectra of only three fractions: F1, F2.1.2 and F3.1. Similar to the two e isomers, the spectra of these three fractions have the appropriate traits, are very similar to each other, and are distinctly different from the other spectra. The three isomers are assigned to the trans-2 group.

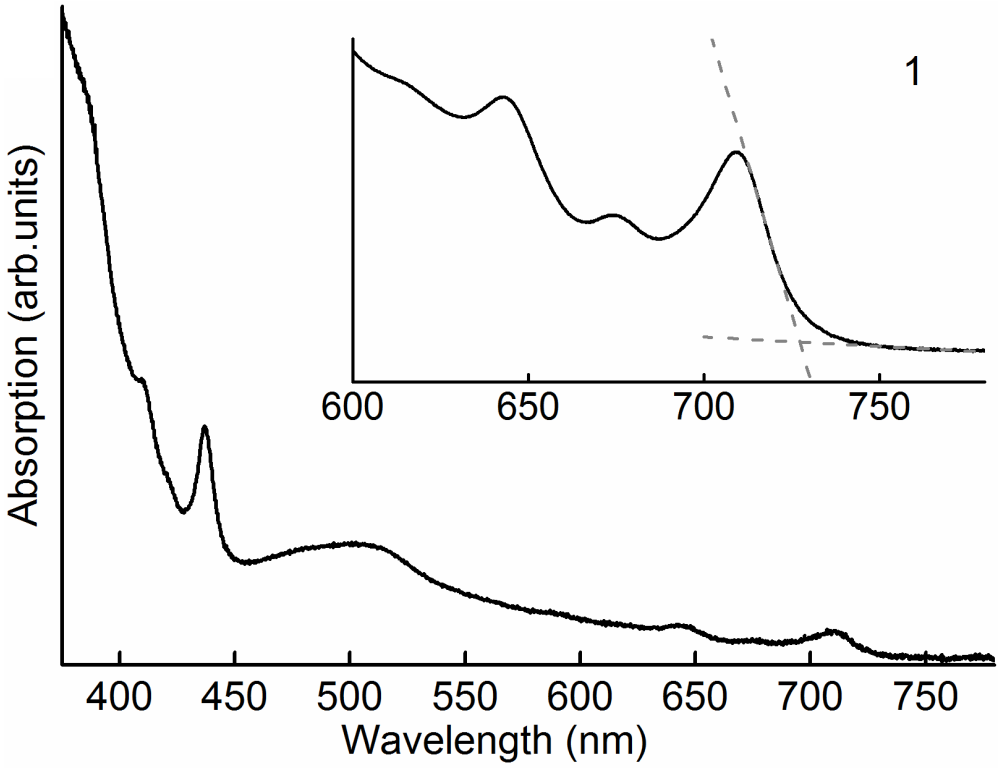

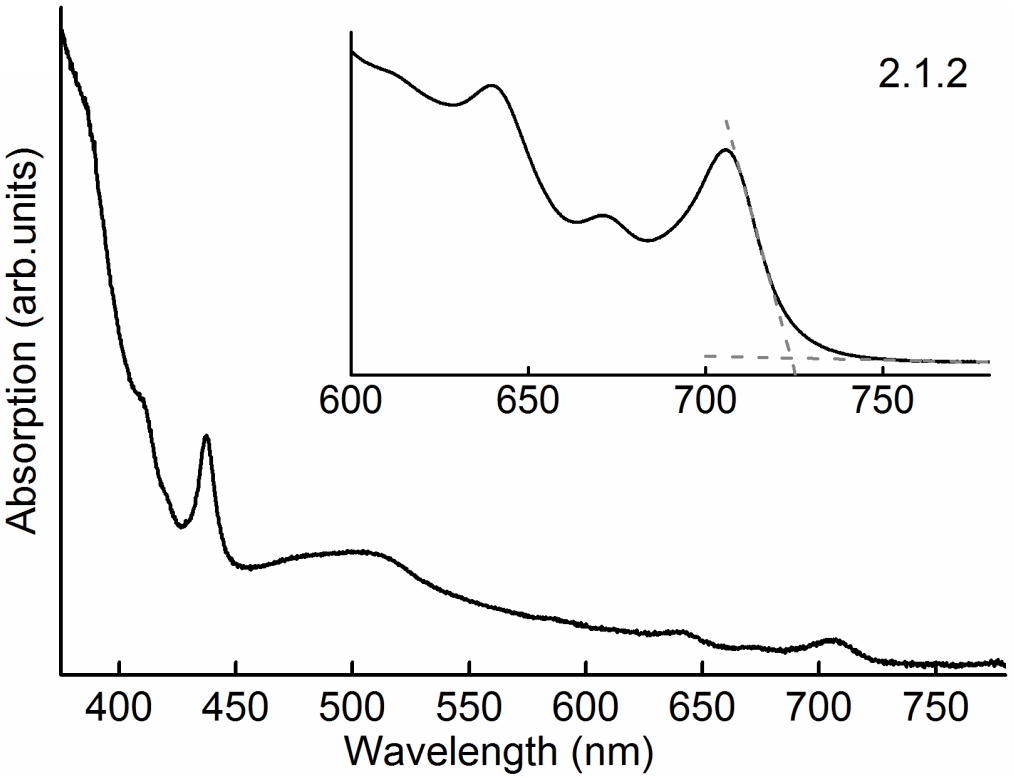

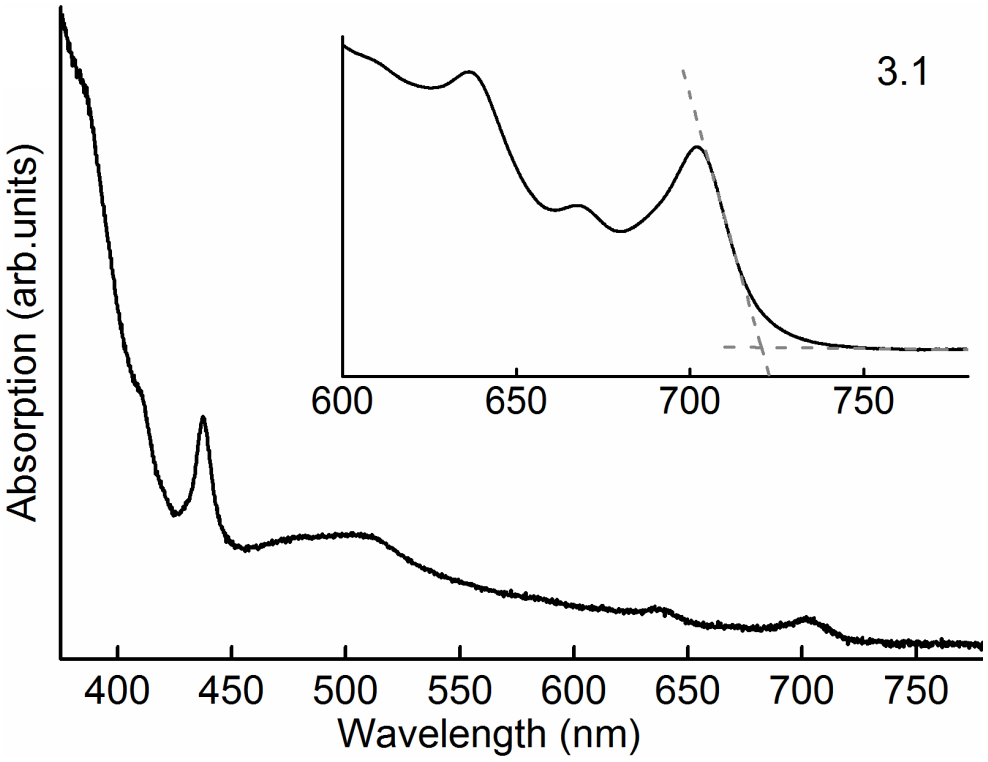

Trans-2

Figure 5.5: the UV-Vis spectra of F1, F2.1.2 and F3.1, according to analysis, the three isomers belongs to trans-2 group. The onsets of the first transition peaks were determined by the intersections of the two tangent lines.

The cis-2 spectra from Figure 5.6 show a unique broad and flat shoulder from 420 to 550 nm followed by a long tail, with a very small peak around 450 nm. After 410 nm, the absorption intensity increases sharply similar to other types of spectra. The spectra of F5.3, F6 and F7 show almost the same traits. We can assign F5.3, F6 and F7 to be the cis-2 type isomers.

The spectra of cis-3 are quite distinct showing an L-shape as compared to other types of spectra. The turning point of the L is around 430 nm. A broad bump from 450-550 nm is followed by the turning point. A series of very small peaks on the tail is seen from 600 to 750 nm. Before the turning point, a bump with a sharp increase is seen from 430-380 nm. Compared with our spectra, the spectra of F3.4 and F5.2.1 are extremely similar to this spectrum. The two isomers can be assigned to the cis-3 group.

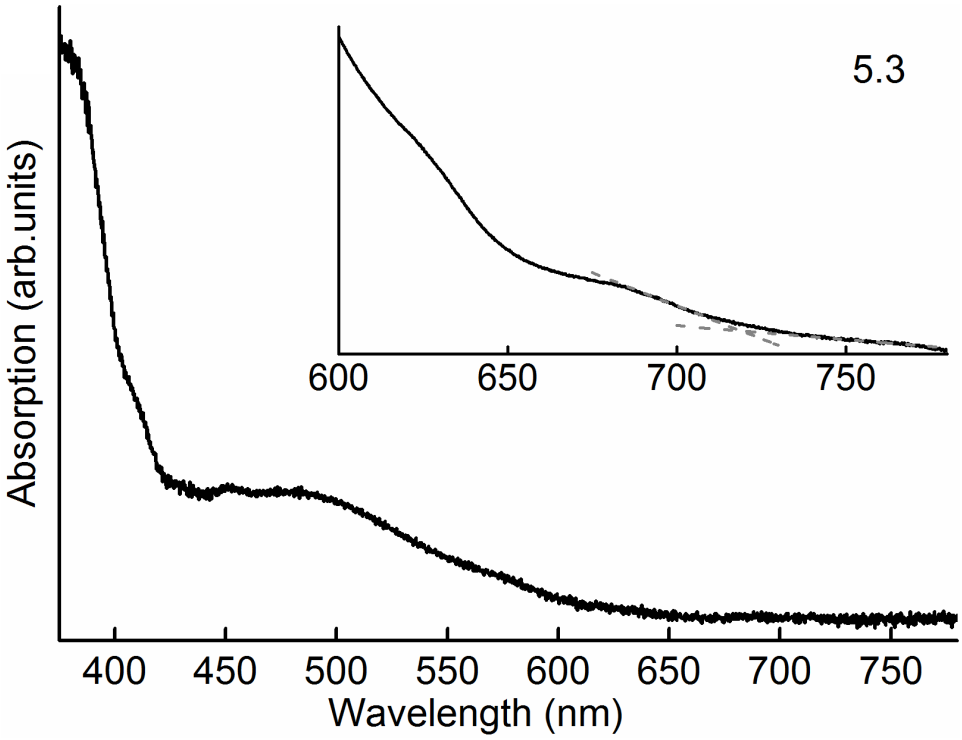

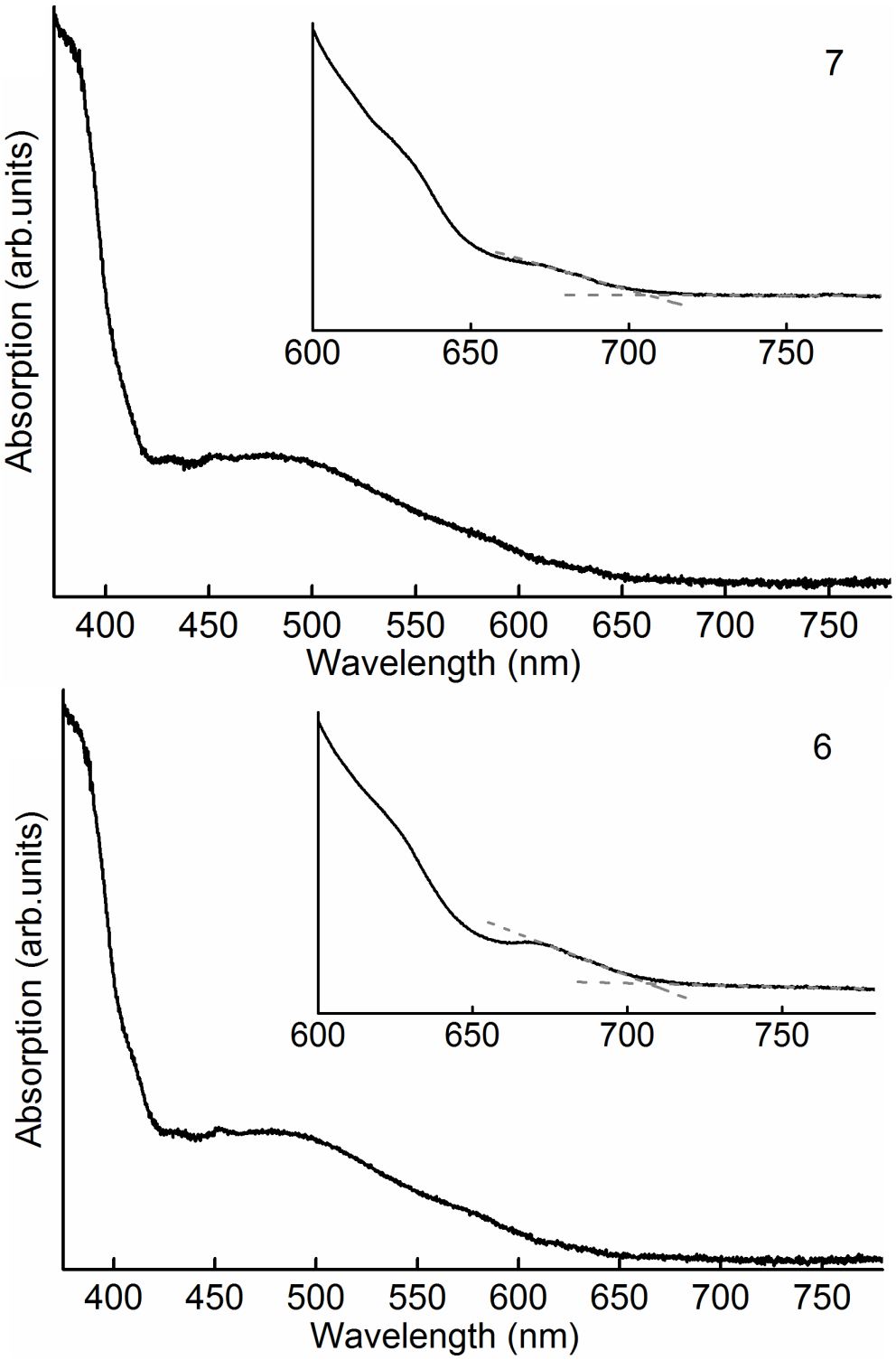

Cis-2

Figure 5.6: UV-Vis spectra of F5.3, F6 and F7. According to the analysis, the three isomers belong to the cis-2 group. The onsets of the first transition peaks were determined by the intersections of the two tangent lines.

The trans-4 type isomers show spectra with shoulders at around 400 nm, and a very small peak around 410 nm. A large bump is located from 450 to 550 nm with a long tail. Additionally, some very small peaks are observed along the tail from 640 to 720 nm. Through comparison with our spectra, the F2.2 and F4 have the same traits. They are assigned to the trans-4 type. Trans-3 type spectra have similar trends with trans-4 spectra. The differences are trans-3 spectra have a smoother tail and a tiny peak around 410 nm by the side of the peak around 425 nm, compared to the trans-4 spectra. The spectra of F2.3, F3.2.1 and F3.3.1 are displayed in Figure 5.8 and show clearly the same trends and characters. The three isomers are assigned to the trans-3 group.

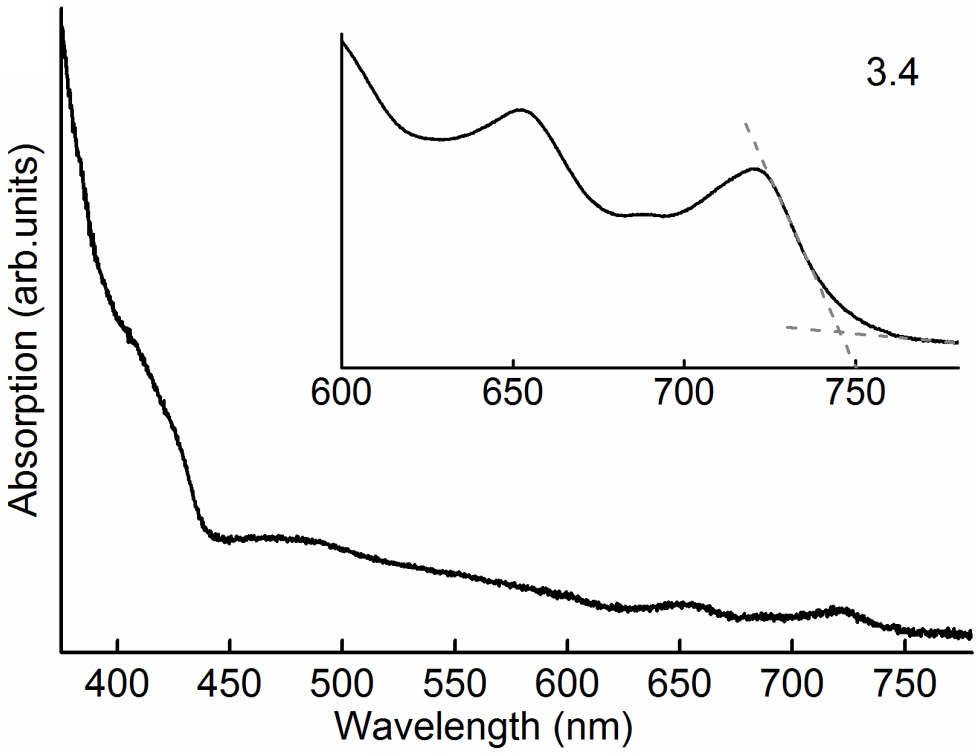

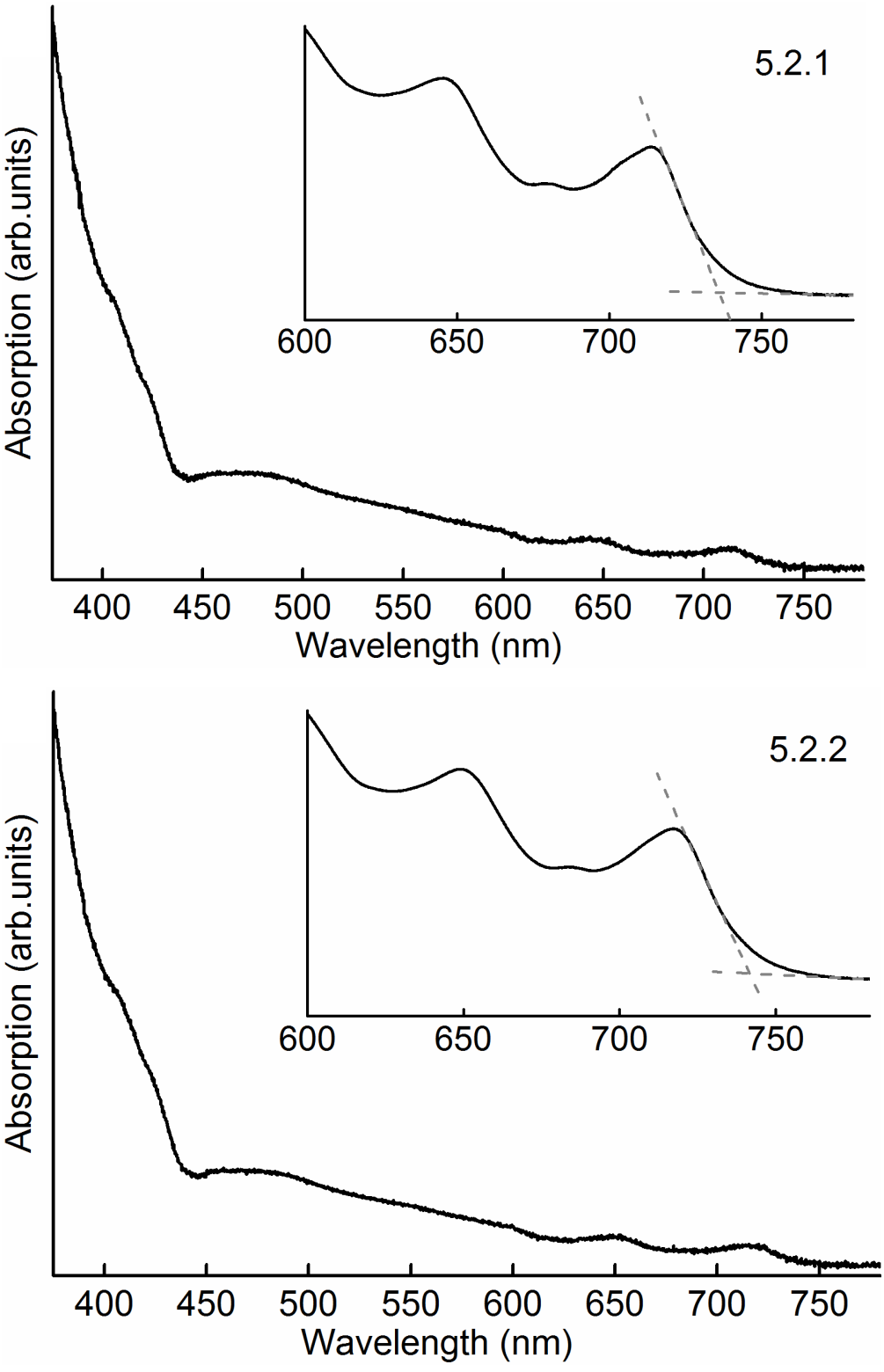

Figure 5.7: UV-Vis spectra of F3.4, F5.2.1 and F5.2.2. According to the analysis, the three isomers belong to cis-3 group. The onsets of the first transition peaks were determined by the intersections of the two tangent lines.

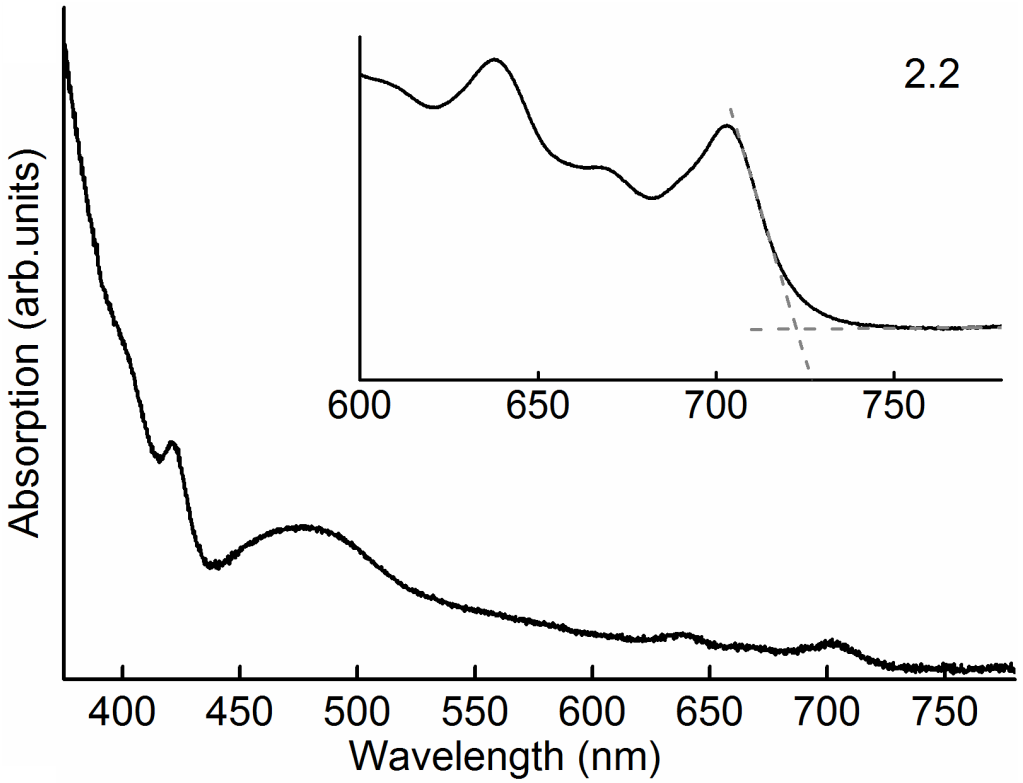
2.2
Absorption (arb.units)
600
650
700
750
400
450
500
550
600
650
700
750
Wavelength (nm)

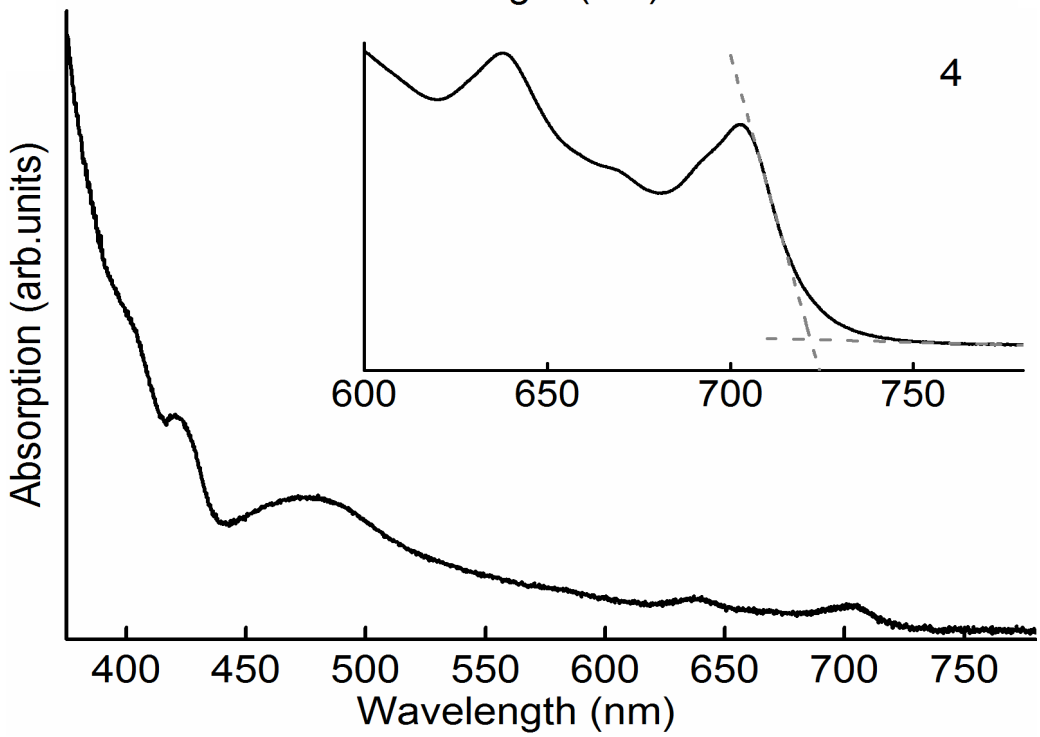
4
Absorption (arb.units)
600
650
700
750
400
450
500
550
600
650
700
750
Wavelength (nm)

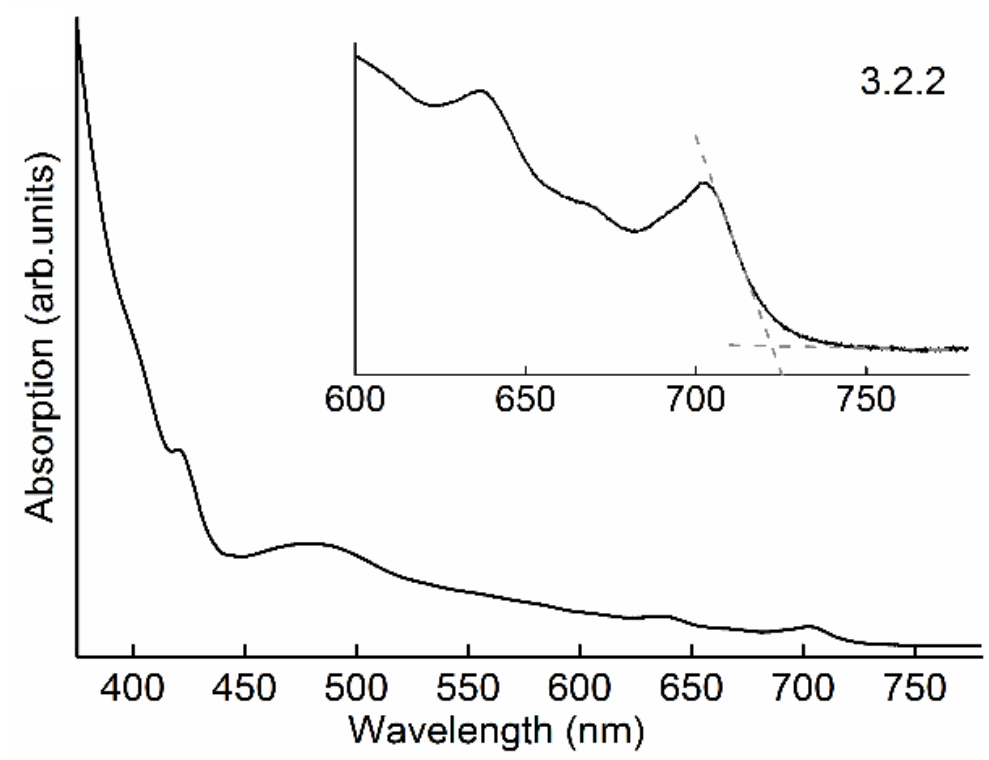

Trans 4

Figure 5.8: UV-Vis spectra of F2.2, F4, and F3.2.2. According to the analysis, the three isomers belong to the tran-4 group. The onsets of the first transition peaks were determined by the intersections of the two tangent lines.

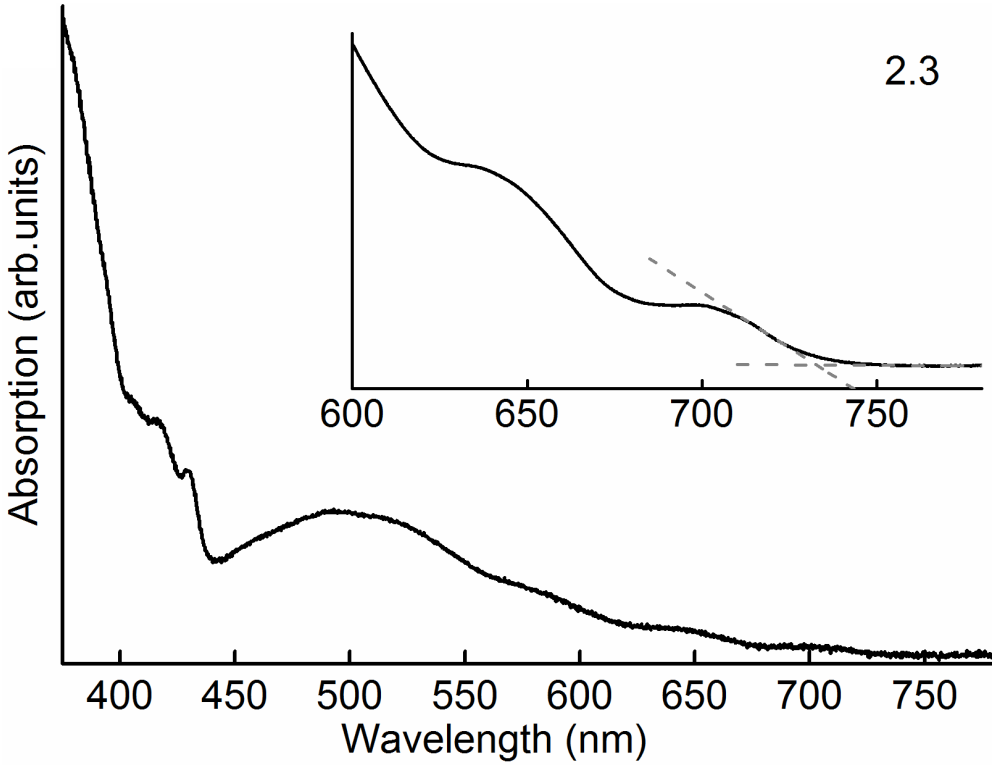

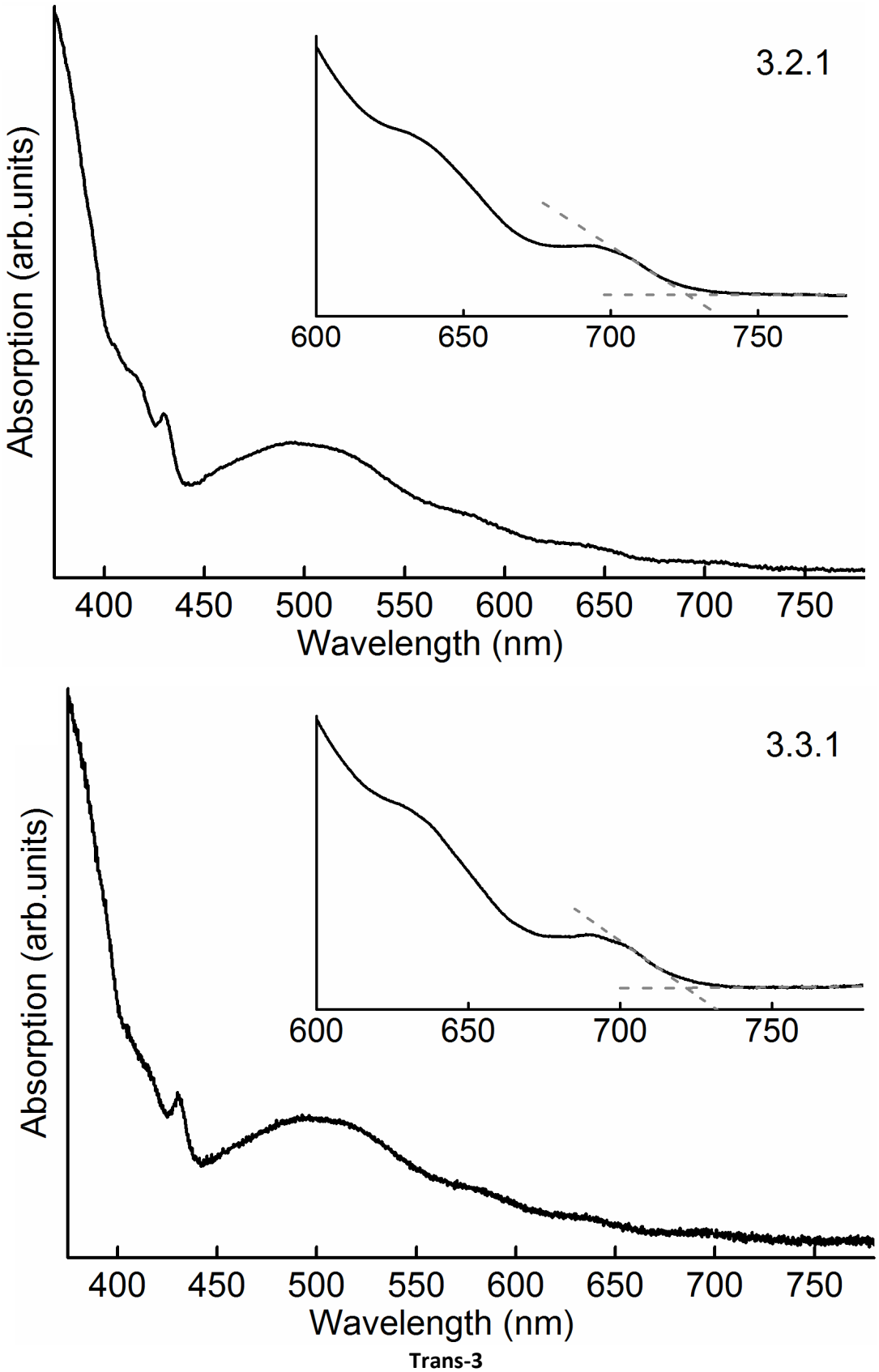

Figure 5.9: UV-Vis spectra of F2.3, F3.2.1 and F3.3.1. According to the analysis, the three isomers belong to the trans-3 group. The onsets of the first transition peaks were determined by the intersections of the two tangent lines.

For the trans-1 group, there is a bump from 400-420 nm. Two peaks are adjacent to each other at 450 and 475 nm. The latter one has a higher peak maximum and bigger peak width. The spectrum shows a clear tail from 500-700 nm. Compared to other spectra, it has a sharp increase around 500 nm. The only spectrum we found with similar traits is that for F2.1.1. We can therefore assign it to this group. However, from our analysis there should be two isomers in this group. We assume that F3.2.2 would be this group as well, and this is also the only isomer we found difficult to assign and fit it into the trans-1 group. The assignment of all isomers to the eight bond types is listed in Table 5.3. Further structure assignments of each isomer in each group are currently being conducted by my colleagues Xueyan Hou and Tong Liu.

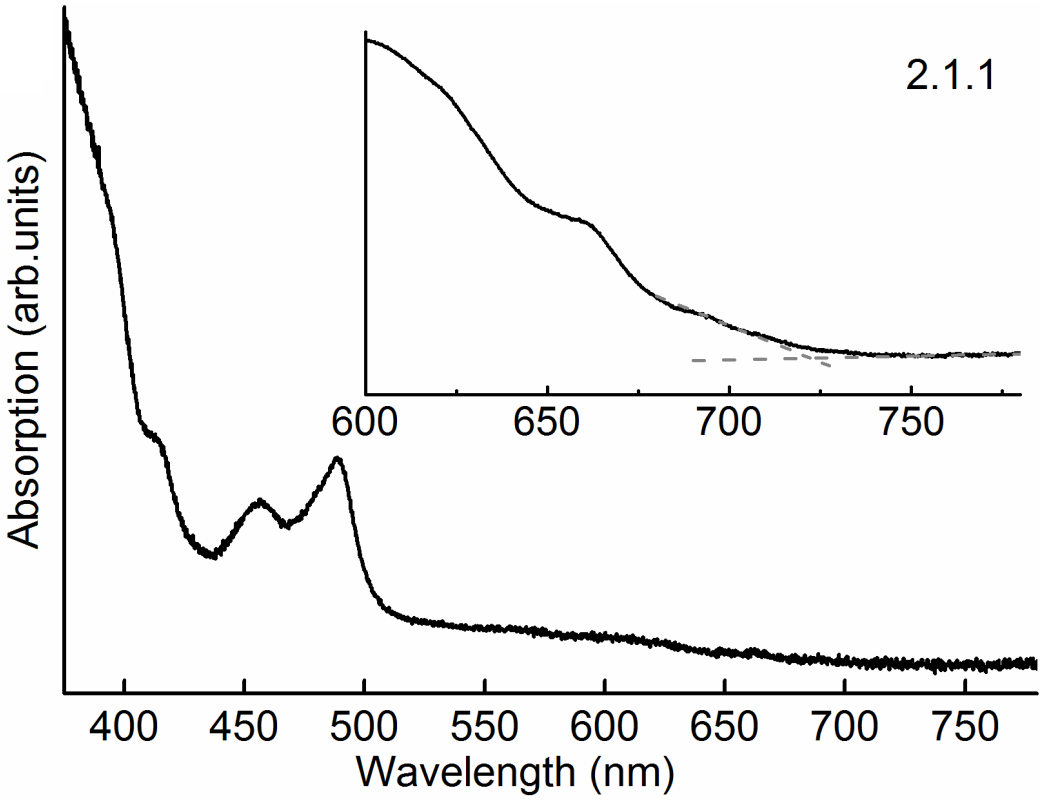

Trans-1

Figure 5.10: UV-Vis spectra of F5.3, F6 and F7. According to the analysis, the three isomers belong to the cis-2 group. The onsets of the first transition peaks were determined by the intersections of the two tangent lines.

If this assumption is right, the trans and cis isomers in the same bond type have almost the same spectrum. This would suggest that the addition position determines the main electronic structure of the width, height and shape of the light absorption spectrum without any effect from addend orientation. However, the onsets of the first transition peak of the trans and cis are varied, as shown by the Eg values in the table 5.1. The orientations of the two addends affect the Eg value and the electronic microstructure.

5.3 The relationship between the retention time with the eight bond types isomers

Based on these assignments, there is an apparent correlation between HPLC retention time and the relative positions of the two addends in Table 1. The trans-1 and trans-2 isomers tend to elute first, followed by trans-3 and trans-4, then the equatorial isomers and finally, cis-3 comes off the column before cis-2 in Table 5.3, except two isomers that do not strictly adhere to this order. According to the silica column instructions, a shorter retention time is normally due to a lower polarity of the isomers hence there is less interaction with the silica particles inside, belonging to trans-1,-2,-3,-4 groups, while longer retention times due to higher polarity, belong to the cis-2,-3 group. E group isomers are located in the middle retention time. This different kind of polarity is from the relative positions of the two addends. Trans groups have two addends far from each other, which can spread electrons well and achieve an even electron distribution so that there is a lower polarity. On the other hand, cis groups have two addends quite close to each other. As the two

addends are electron rich groups, this can cause electron concentration on one side of the C_{60} cage, resulting in higher polarity.

Isomer	**F1**	**F2.1.1**	**F2.1.2**	**F2.2**	**F2.3**	**F3.1**
Assignment	*trans*-2	*trans*-1	*trans*-2	*trans*-4	*trans*-3	*trans*-2
Isomer	**F3.2.1**	**F3.2.2**	**F3.3.1**	**F3.3.2**	**F3.4**	**F4**
Assignment	*trans*-3	*trans*-4	*trans*-3	*e*	*cis*-3	*trans*-4
Isomer	**F5.1**	**F5.2.1**	**F5.2.2**	**F5.3**	**F6**	**F7**
Assignment	*e*	*cis*-3	*cis*-3	*cis*-2	*cis*-2	*cis*-2

Table 5.3: Structural assignment of 18 isomers into seven bond types, listed by the retention time from the shortest to the longest.

The reason for the close but non-strict adherence is likely to stem from the asymmetry of the PCBM addends. Apart from the two trans-1 isomers, the asymmetry results in two distinguishable bonds of each bond type according to whether the second addend is closer to the phenyl or the methyl butanoate group of the first addend, the so-called configuration from different rotations of chains. Another reason for the non-strict adherence comes from most bond types giving two orientations of the two attends (trans and cis). Nonetheless, there is a clear trend in the above-mentioned direction; from which we conclude that in general for this type of bis-adduct, the closer the two addends are to each other the longer the retention time of that isomer.

5.4 UV-Vis characterisation of $PC_{71}BM$

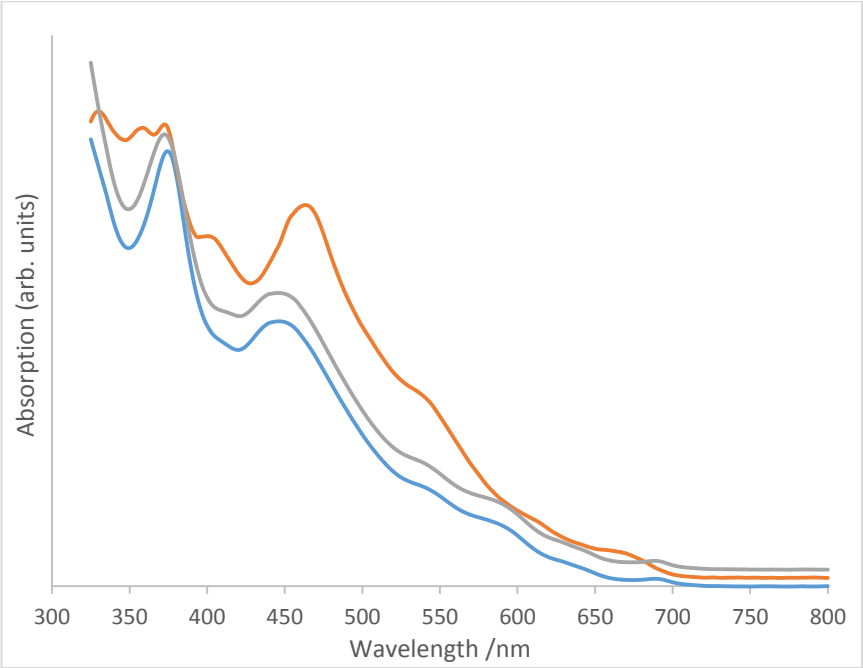

Figure 5.11: UV-Vis spectra of three isomers of $PC_{71}BM$ from 325-800nm

All three isomers were characterised by a UV-Vis spectrophotometer (SHIMADZU UV-2600) between 325 to 800 nm and 600-800 nm. The scanning rate and sampling intervals were set as 30 nm/min and 0.2 nm/s, respectively. The same sampling procedure was taken from the centre of the peaks as for bis$PC_{62}BM$. The spectra are displayed in Figure 5.11. A higher extinction coefficient can be achieved by $PC_{71}BM$ especially for higher absorption intensity from 400 to 700 nm, compared to C_{60} derivatives, as the high structural symmetry in C_{60} forbids the low energy transition, hence the absorption spectrum is narrower than that of $PC_{71}BM$. [105]

The spectrum of the MAJOR isomer, has a weak absorption from 700 to 800 nm. Several tiny peaks show along with a quickly increasing slope from 500-700 nm. A clear peak was shown around 470 nm and a shoulder appears around 410 nm. A high absorption plateau is located above 370 nm. Compared to the MAJOR, the

spectra of the two MINOR isomers have a lower absorption from 400 to 600 nm. The peak is also smaller with a round top around 450 nm. However, the peak around 410 nm is clearer than that in the spectrum of the MAJOR isomer. It is also interesting that the spectra of the MINORS have the same traits. This also proves the conclusion from the bisPCBM spectra that the relative orientation of addends to each other (trans or cis) affects the main electronic structure of the molecules a little, with small changes in the energy levels, hence there is a slight difference in HOMO and LUMO levels, discussed below.

The HOMO-LUMO gaps of the three isomers were calculated based on the onset of the first transition peaks. The onsets were also determined by the intersection of two tangent lines from baseline and slope, in Table 5-4. The two MINOR isomers have similar onsets with a 2 nm difference. The MAJOR isomer has a lower onset of around 700 nm. Hence the MINOR isomers have slightly lower band gaps than that of the MAJOR. Compared to $PC_{61}BM$ and $bisPC_{62}BM$, the HOMO- LUMO gap is 30-50 meV slightly higher.

Isomer	9R,10S,71r	9S,10S,71s	8R,25S, 71rs
Onset wavelength	709.23 nm	706.77 nm	699.79 nm
HOMO – LUMO gap	1.748 eV	1.754 eV	1.772 eV

Table 5.4: The onsets and experimental HOMO-LUMO gaps of the three isomers of $PC_{71}BM$

SUMMARY

The MAJOR isomer has stronger absorption than the two MINOR isomers, especially for the range from 400-600 nm. Their band gaps are quite close, and the HOMO-

LUMO gap of the MAJOR is slightly larger. In terms of light absorption efficiency, the MAJOR isomer would be favoured for applications as well as because of its higher abundance and ease of purification.

5.5 Cyclic voltammetry tests for Bis$PC_{62}BM$ and $PC_{71}BM$

Introduction

Cyclic voltammetry is one of the most commonly used methods to determine the energy levels of organic semiconductors. The electrolytes are formed with the samples dissolved in a solvent with a high dielectric constant, such as acetonitrile and an inert salt is dissolved in it to conduct the charge. The reactant is normally with a low concentration, in this case around 0.1 mg/ml. A modern three electrode system with working electrode, counter electrode and reference electrode is normally used. The working electrode has the controlled potential for charge transfer from the electrode to the molecule. The Fermi-level of the working electrode material is altered by applying voltage; when the level is raised up to the LUMO of the molecule, an electron jumps to the LUMO of the molecule. The counter electrode is for the charge flowing from the working electrode to the electrolyte and then back to the external circuit via it. Due to the difficulty of maintaining a constant potential from the working electrode during the redox reaction, a reference electrode such as Ag/AgCl can measure and control the potential of the working electrode with no current flow through it.

In order to calculate the LUMO of $PC_{71}BM$ isomers and bis$PC_{62}BM$ isomers, the cyclic voltammetry measurement was conducted for all the isomers under the same experimental conditions, and the details are described below. The isomers in the solution were in a redox process under a triangular voltage waveform. The voltammograms display the different redox process of each isomer as the various positions of the redox peaks reveal the different electron affinities of the isomers. The first reduction peaks of the reversible voltammograms reveal the LUMO levels of the isomers. The comparison within the bis$PC_{62}BM$ isomers and the external comparison between PCBMs (C_{60}, C_{70}) and bis$PC_{62}BM$ will be fully discussed below along with simulation results and application suggestions.

5.6 Cyclic voltammetry for $PC_{71}BM$ isomers

5.6.1 Experimental procedure

Step 1

Making the electrolyte

The isomer solutions (200 ml) contained toluene, and were dried via a rotary evaporator separately. It took around 20 minutes to form the completely dried fullerene at the bottom of each flask. In order to form the electrolyte, the $PC_{71}BM$ MAJOR was dissolved in 200 ml ortho-dichlorobenzene, and 50 ml acetonitrile was added with 0.1 M $(NBu)_4BF_4$, the inert salt to allow the current to pass through the solution, in total around 250 ml. Once the electrolyte was made, it was better to start the measurement immediately, or some tiny red precipitate (tiny dust size particles) would come out after five minutes. The MINOR 1 and MINOR 2 solutions

were made in the same way. The concentration of the fullerene is around 0.1 mg/ml.

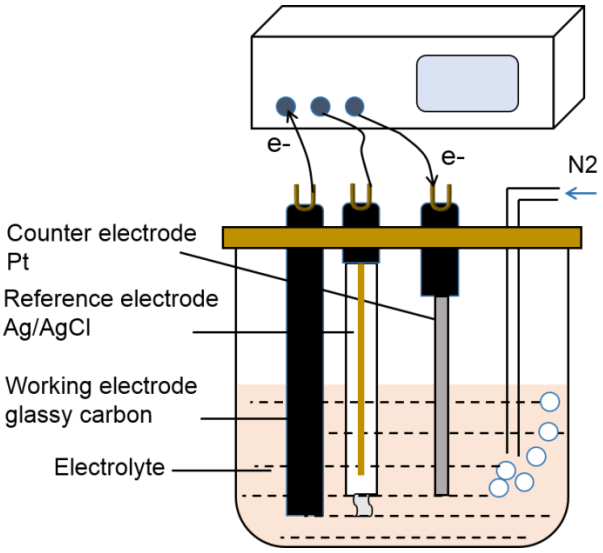

Figure 5.12: Diagram showing the cyclic voltammetry test for the isomers. Electrode 1 is a glassy carbon-working electrode, electrode 2 is the platinum mesh counter electrode, and electrode 3 is Ag/Ag+ reference electrode.

Step 2

Assembling the test equipment

In order to save the sample, a 50 ml beaker was put into a 200 ml test container with a four-holed black lip. Three electrodes, a glassy carbon-working electrode (7.1 mm^2), a platinum mesh counter electrode and a non-aqueous Ag/Ag^+ reference electrode were used and fitted into the container, while a small air tap was put through the black lip, far away from the counter electrode to avoid interference from the bubbles. The final assembled test container is shown below. The electrodes were connected to an Autolab PGSTAT 302N. Only 30 ml of solution was used for the measurement.

Step 3

Parameter setting and procedure details

The whole experiment was conducted with a scan rate of 50 mV/s, and a scan range from -2.5 to 2 V, while other parameters were set as default. The flow argon was controlled by a flow meter to keep it at a constant flow rate. The CV curve of each isomer was measured three times. As the half-cell potential of the reference electrode can drift from time to time and was influenced by the surrounding solution, ferrocene was added to each isomer solution as an internal standard referring to all CV results. A second CV curve which reveals the ferrocene peak was recorded after the original CV response was measured three times. Between the measurements of each fullerene, the working electrode was polished with 0.05 micro alumina to a mirror finish, followed by rinsing with deionised water then sonicated in fresh deionised water for 15 minutes, and the water was changed at five-minute intervals. The three isomers were measured sequentially. All the results are analysed in the next section.

5.6.2 Cyclic voltammetry results

The cyclic voltammograms of all three isomer are shown in Figs 5.13 and 5.14. The voltammagrams show a total of four reversible oxidation and reduction peaks in a negative voltage region for the isomers. The peak minimum of the lower half of the curve represents the redox process for adding an electron to the isomers and the peak maximum of the upper half represents the oxidation process as an electron is taken away from the isomers. The first and second reduction and oxidation peaks of isomers are located lower than zero volts around -0.7 to -0.9 V and -1.0 to -2.0 V,

respectively. The reduction-oxidation peak couples around 0.4-0.5 V belong to the ferrocene, which is the reversible process between Fe^{2+} and Fe^{3+}. All the graphs show a clear redox process with similar peak numbers and peak characters, and the obvious differences are the relative peak positions.

The first reduction-oxidation peak couple is quite reproducible on cycling. Here the LUMOs of the isomers were measured and defined by the middle point method, by Richard Beal in the Renewable and Environment Group of Oxford University [86]. The LUMO is defined as the average value of the first oxidation minimum and first reduction peak maximum that is the average voltage of moving the first electron and adding the first electron to the species. The main advantage of this method is for the measurement of LUMOs of the molecules with any tiny difference, as the LUMOs of the three isomers are very close. If the middle point moves towards a more negative voltage, it means a higher LUMO of the isomer. The following is an example showing calculation of the LUMO level of the MAJOR isomer. The ferrocene peaks are reversible with similar oxidation and reduction peaks marked in pink. The average of the oxidation and reduction peak maxima is around 0.4717 V, marked by the red arrow. The average for the first reduction peak couple of the MAJOR isomer is -0.8067 V. The LUMO level here for the MAJOR is the difference between the two average values, taking the ferrocene peak as the zero point. Hence, the LUMOs of MAJOR isomer is obtained as -1.2784 eV. Based on this method, the LUMOs of the three isomers were measured and calculated as listed in Table 5.5.

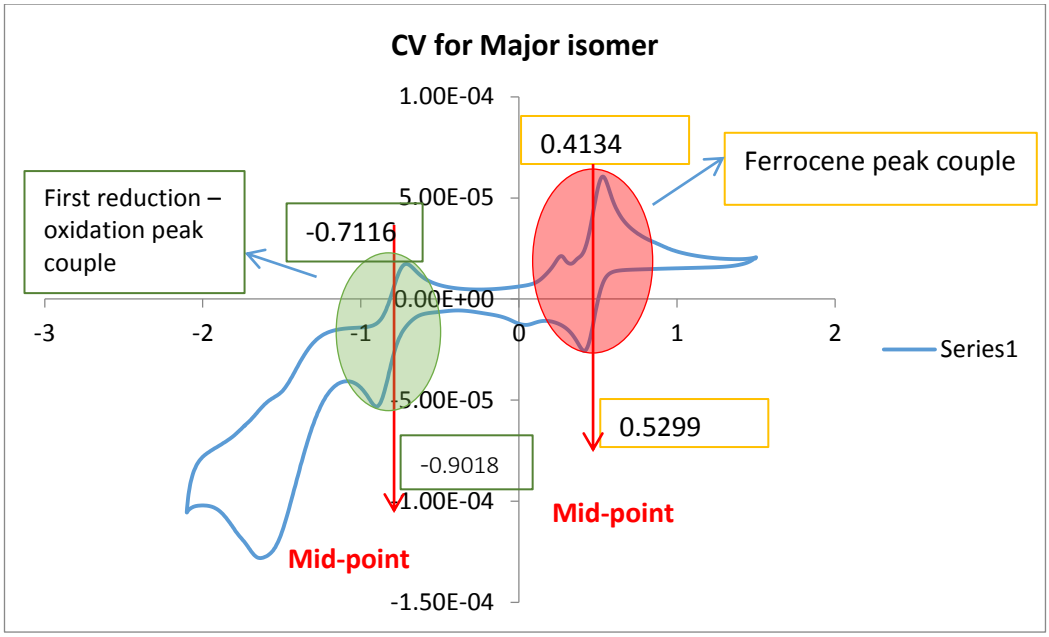

Figure 5.13: The cyclic voltammetry graph of the MAJOR isomer of C70PCBM. The coupled middle points of the peak couples are the average value of the oxidation and reduction peak maximums marked with a red arrow.

	C70PCBM Major isomer	Ferrocene (Major)	C70PCBM MINOR 1	Ferrocene (MINOR 1)	C70PCBM MINOR 2	Ferrocene (MINOR 2)	C60PCBM
Upper oxidation peak (V)	-0.7116	0.4134	0.726559	0.483551	-0.7382	0.4312	
Lower reduction peak (V)	-0.9018	0.5299	0.887759	0.483551	-0.8844	0.5268	
Couple middle point (V)	-0.8067	0.4717	0.807159	0.483551	0.8113	0.4790	
LUMO level of Major isomer (eV)	-1.2784	n/a	-1.2907	n/a	-1.2903	n/a	-1.2930
LUMO level to vacuum level (ev)	-3.9316	n/a	-3.9194	n/a	-3.9197	n/a	-3.9170

Table 5.5: The LUMOs of the three isomers of C70PCBM. The oxidation and reduction peak positions for each isomer, and the corresponding positions from ferrocene in the same graph for each isomers.

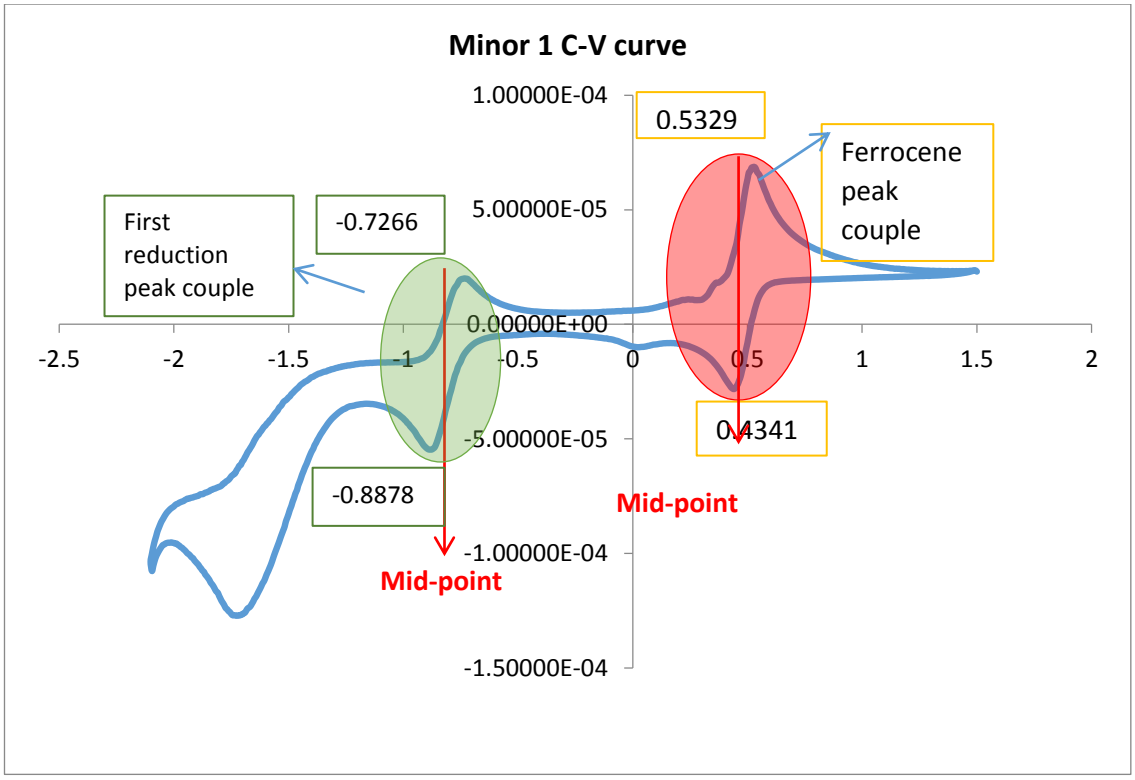

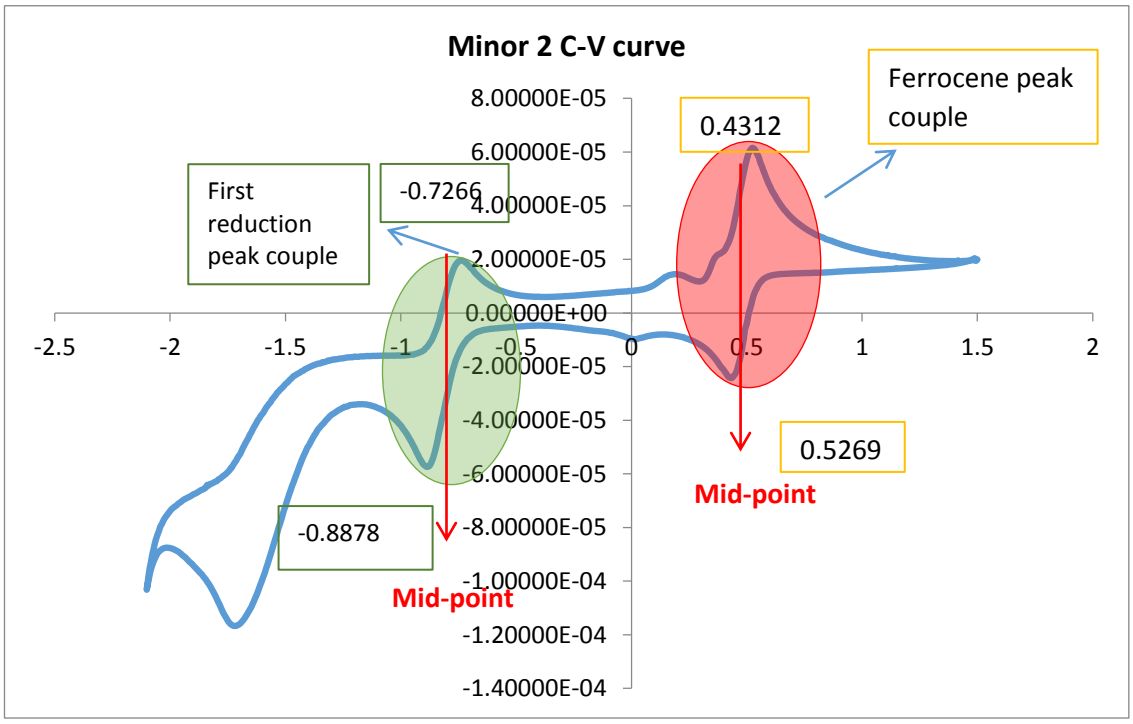

Figure 5.14: Cyclic voltammagrams of the two MINOR isomers of C70PCBM. The coupled middle points of the peak couples are the average value of the oxidation and reduction peak maximums marked by a red arrow.

The similarity and difference of the LUMO levels of the isomers are vividly demonstrated in Figure 5.15. The cyclic voltammograms are from the corrected potential of the isomers, which are the original values of isomers minus the values of ferrocene. Basically the curves were left shifted by treating the potential level of ferrocene as the zero point. The two MINOR isomers have almost the same trace of curves in grey and yellow that overlapped at 90% of the range and also have the extremely close LUMOs with only a 0.4 meV difference. The voltammagram for the MAJOR isomer is relatively different compared to the high similarity of the MINORS. Both the reduction and oxidation peaks of the MAJOR are distinguishable from the MINORS, the LUMO of which is 12 meV lower and is consistent with simulation results from the literature. [106] The LUMO of the $PC_{71}BM$ mixture is almost same as that of $PC_{61}BM$ according to the previous research. [16] All the isomers from our research have quite similar LUMOs to $PC_{61}BM$. The LUMOs of the MINOR isomers are the same as $PC_{61}BM$ with a 2 meV difference, within the error of the measurement. The HOMOs of the isomers determined using HOMO = LUMO – Eg are listed in Table 5.6.

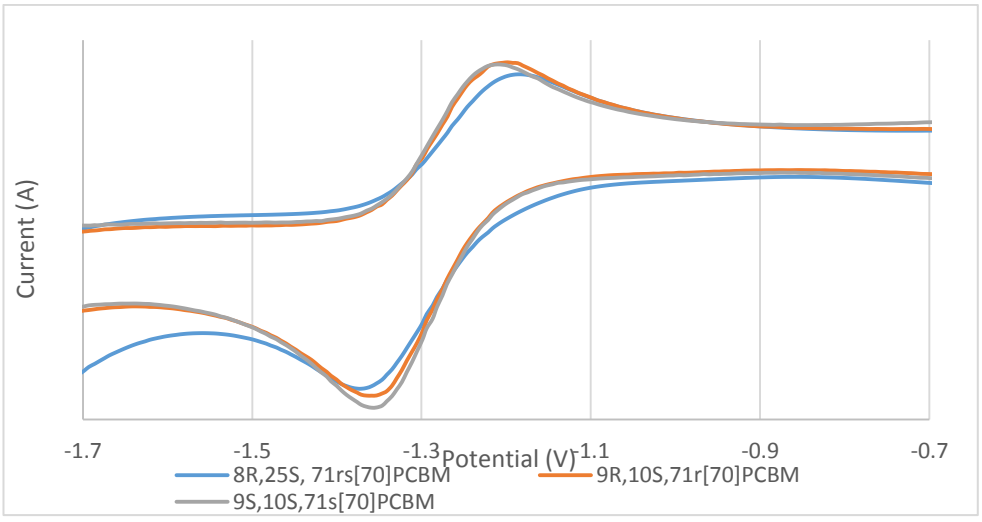

Figure 5.15: The first reduction-oxidation peak couple of the three isomers of $PC_{71}BM$

Isomer	MINOR 1	MINOR 2	The Major	$PC_{71}BM$
HOMO (eV)	-5.6678	-5.6742	-5.7036	-5.6390
LUMO (eV)	-3.9194	-3.9197	-3.9316	-3.9170
HOMO – LUMO gap (eV)	1.7484	1.7545	1.772	1.7220

Table 5.6: HOMO, LUMO and band gaps of isomers of $PC_{71}BM$.

SUMMARY

The three isomers of $PC_{71}BM$ have quite similar LUMO levels, -1.2784 eV for the MAJOR isomer, -1.2903 and -1.2907 meV for the two MINOR isomers. The MAJOR isomer has a slightly lower LUMO level around 12 meV, but better light absorption (Chapter 4) and ease of purification (Chapter 3) compared to the MINOR isomers. The slight difference of the LUMO level between the three isomers is lower than 26 eV, the threshold for the electron trap effect and can therefore be ignored. The interference from the MINOR isomers to the MAJOR ones for applications should be further investigated. OPV device production and characterisation are in progress with our collaborator in Groningen University.

5.7 Cyclic voltammetry for bis$PC_{62}BM$ isomers

The cyclic voltammetry tests of all 18 isomers were conducted using the same experimental conditions described above, while the scanning range was shortened from 0.8 to -1.3V with a 10 meV/s scanning rate. As the cyclic voltammograms of some bis$PC_{62}BM$ isomers show unclear oxidation peaks in the first round trial, a slower scanning rate from 50 meV/s to 10 meV/s was applied to obtain a better resolution of the tiny oxidation peaks. The reason for the shortening range is for the

ease of the over-reduced characters of some isomers, like F2.2 and F3.1, hence we kept the range not beyond the second reduction peak. Figure 5.16 shows the slightly over-reduced F3.1 with no clear oxidation peak and the typical reversible redox process of F5.1. The voltammogram of F3.1 has a total of three redox couples. Compared to the obvious reduction peaks in the lower half, the oxidation peaks in the upper half are asymmetric with tiny peaks. The straight down long tail after -2.5 V is likely due to solvent reduction to some extent. For further research, a solvent which is harder to reduce could be used.

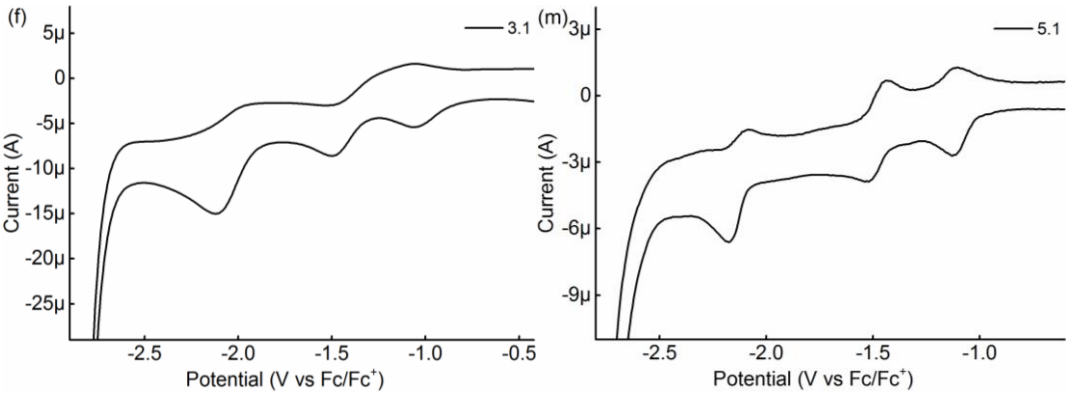

Figure 5.16: The cyclic voltammetry for F3.1 and F5.1 scanning from 1.0V to -2.5V with a scanning rate of 50 meV/s.

The cyclic voltammograms of all the isomers are given below. As a shorter scanning range from 0.8 to -1.3 V was used, all the isomers have only the reversible first redox peak couple appearing as in Figure 5.18. The cyclic voltammograms clearly demonstrate the positions of onset of the first reduction peak with a clear and flat baseline. The LUMO energy levels determined by the cyclic voltammetry of the 18 isomers by the onset of the first reduction peak are shown in Figure 5.17. The method of LUMO measurement and conversion follows Equation 2. [107] The LUMO level calculated from the equation is the energy level to the vacuum level. Here the

ferrocene with a LUMO of 4.8 eV to the vacuum level is treated as the zero point in the voltammograms. The LUMO level of an isomer defined by the onset of the first reduction peak is the point that the electrons of the working electrode are lifted up by more negative voltage to reach the level of the LUMO level of the isomer in the solution, hence the electron can be added into it. The onset of the reduction peak is defined by the intersection of two tangent lines drawn from the baseline and slope of the peak. The LUMOs of all the isomers were calculated by the method above and are presented in order of increasing HPLC retention time in Figure 5.17. For comparative purposes our measured LUMO levels of the mono-adduct $PC_{61}BM$ and the bis$PC_{62}BM$ isomer mixture, which are consistent with those presented in the literature review, are also given. The LUMO energy levels of the bis-$PC_{62}BM$ range between -3.901 eV and -3.729 eV. In comparison with the LUMO of the mono-adduct (-3.917 eV), the LUMOs of all 18 isomers of bis-$PC_{62}BM$ are higher. The increase in LUMO varies between 16 meV and 188 meV, with F2.1.1 being the lowest and F3.2.2 being the highest. This is consistent with the simulation results of all the isomers, via the time-dependent density functional theory (TD-DFT) from Jenny Nelson.[10] The simulation for all of the HOMOs was carried out by my colleague Tong Liu, which will be discussed in the next part. Furthermore, 12 of the 18 isomers have LUMO energy levels that are above the quasi-LUMO level (-3.823 eV) of the isomer mixture. F3 and F5 are the two most abundant fractions in the mixture, having higher LUMOs than other fractions. Five out of the six isomers from F3 have LUMOs higher than -3.794 eV. All the isomers of F5 are higher than the average with LUMOs from -3.803 to -3.782 eV. In addition, there is no clear relationship between the retention time and LUMO levels, however F1 and most of

F2 with short retention times have relatively lower LUMOs compared to the isomer with longer retention times.

$$E_{LUMO} = -[(E_{onset} - E_{1/2Fc}) + 4.8]\ eV$$ [7]

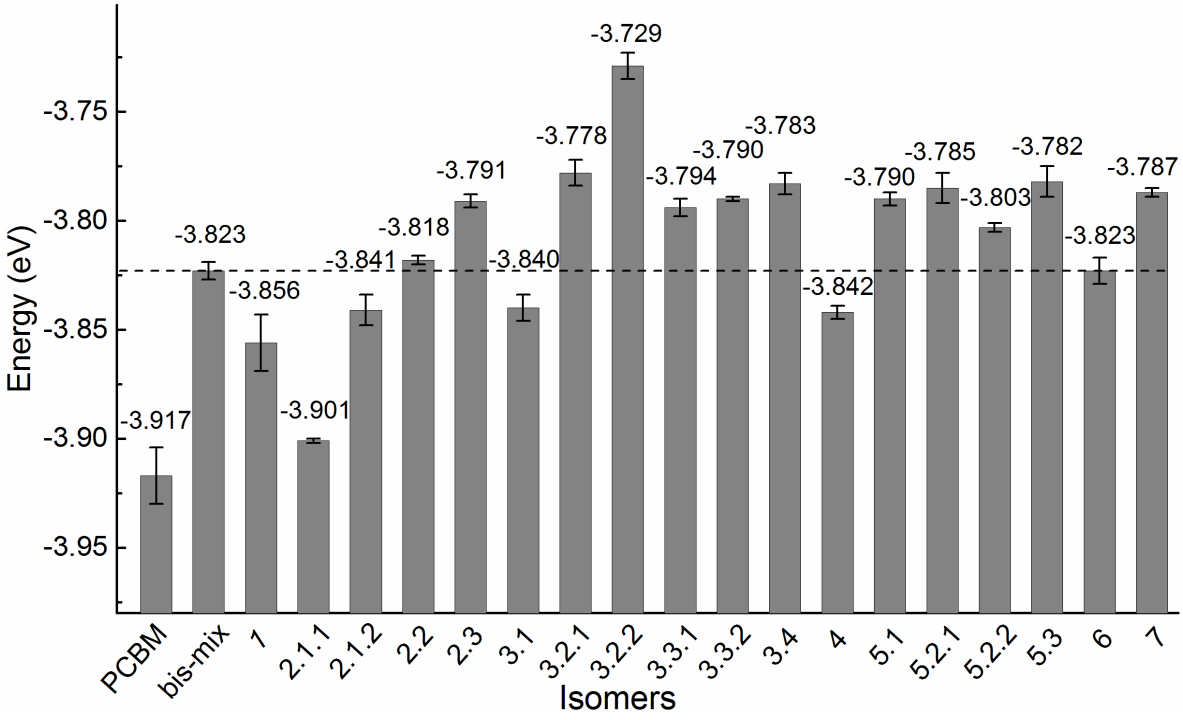

Figure 5.17: LUMOs of bis[60]PCBM

The near room temperature value of kT is about 26 meV. Hence, within the fullerene phase of a bulk-heterojunction OPV, if the LUMO levels of neighbouring bis-$PC_{62}BM$ isomers differ by more than 26 meV, there is the potential for the lower LUMO isomer to act as an electron trap. This is particular behaviour at low current densities. Of the 18 isomers the first two in order of HPLC retention time (F1 and F2.1.1) are of concern in relation to full mixture-based OPV devices. This is because they are the only isomers outside this range: at 33 meV and 78 meV below the average, respectively. Those isomers behaving like the electron traps not only

decrease the photocurrent but also suppress the Voc in the device. These two isomer fractions may be easily removed by a simple single pass HPLC treatment.

As a single pass HPLC is a necessary requirement to remove potential traps, it would be better to make OPV devices from the individual fractions for a balance of the cost and expecting properties. Individual F3.2.2 is the best, but the production cost is quite high, and likely to be impossible to commercialise, while the low cost of single pass purification can make F5 and F3 with promising properties highly viable to be applied for practical use. For example, an OPV device based on only F5, which represents 27% of the mixture, is likely to result in an increase in both voltage and current when compared to those made with the as-produced mixture. We say this for three reasons. Firstly, the average LUMO level of F5 is 33 meV above that of the mixture, which should result in a higher Voc. Secondly, the variation of the LUMOs of all four isomers of F5 is 21 meV, which is well below the 26 meV of thermal energy available to the system at room temperature, and hence should improve the current by reducing energetic disorder and potential traps. [108] Thirdly and finally, the reduction in the number of isomers (from 18 to 4) is likely to result in the improved morphology of the fullerene phase within the active layer, and thereby further improve the device current. That a reduction in the number of isomers results in improved morphology within the fullerene phase was demonstrated by Bouwer et al. [88] The same arguments can be made for F3 (at 33% of the mixture with an average LUMO 50 meV above that of the mixture), provided the low LUMO

initial sub-fraction F3.1 is dropped out before collection. This can be a useful guide for future purification and potential application.

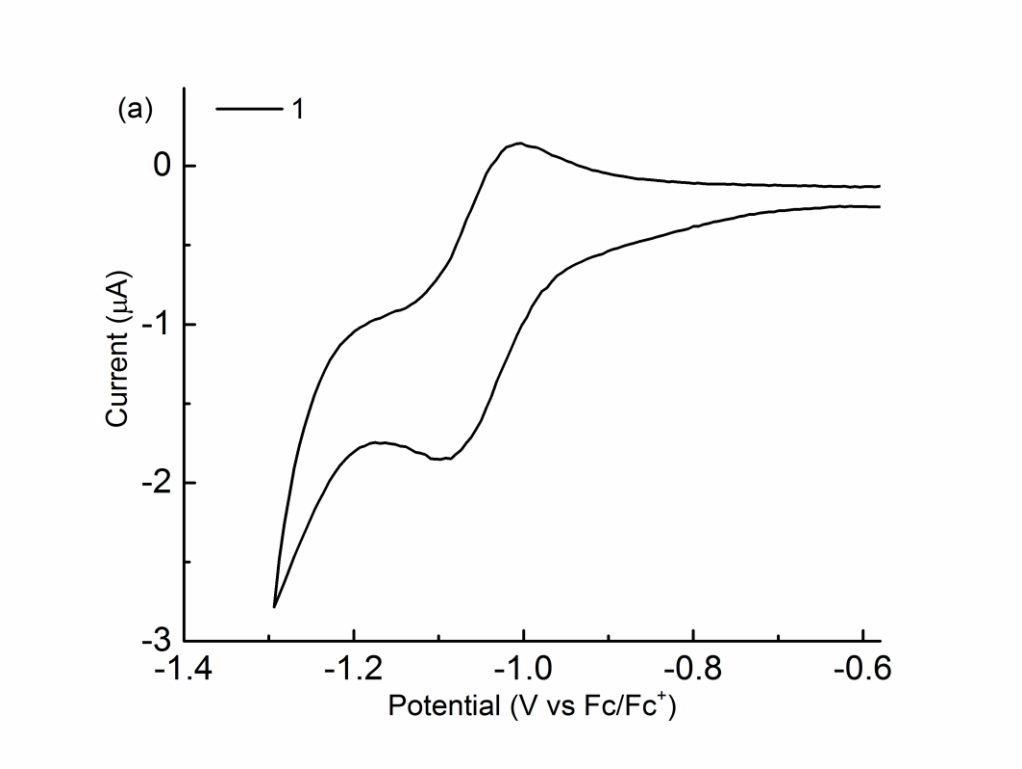

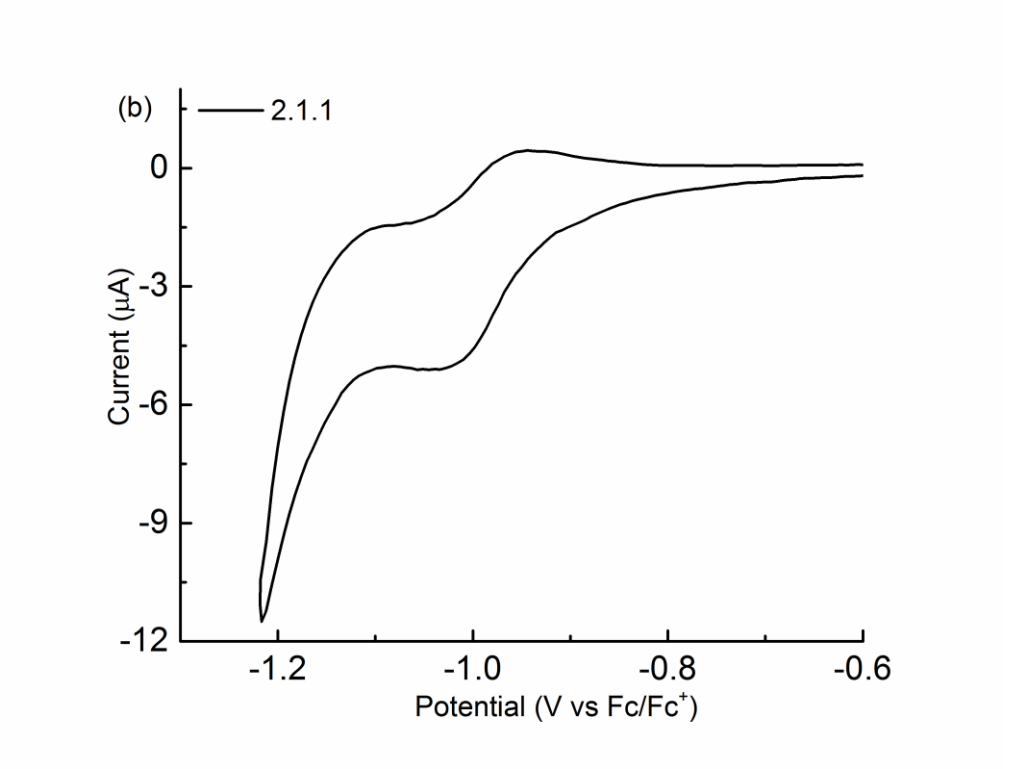

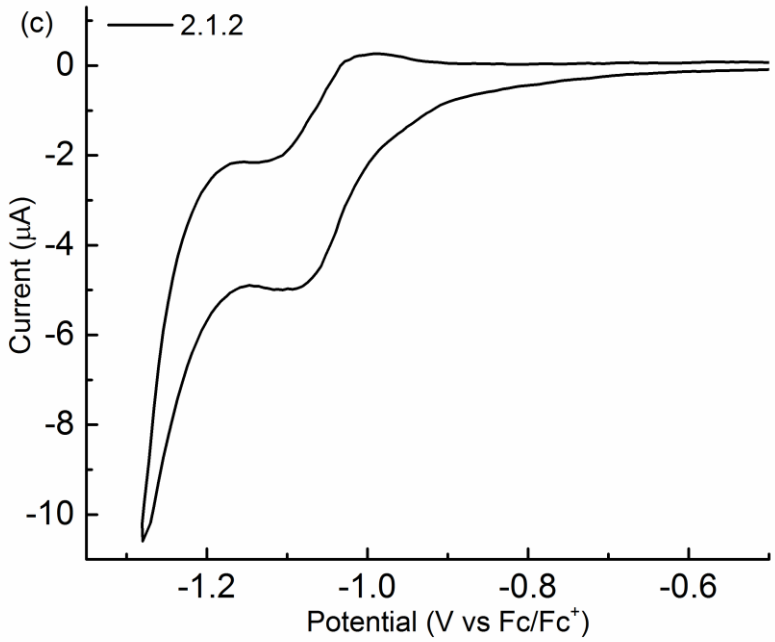
(c)
2.1.2
0
-2
-4
-6
-8
-10
Current (μA)
-1.2
-1.0
-0.8
-0.6
Potential (V vs Fc/Fc+)

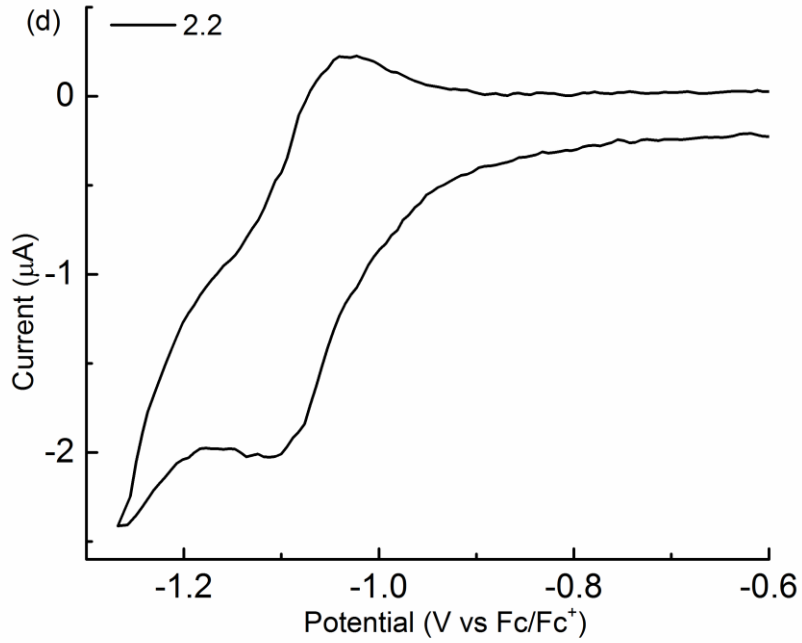
(d)
2.2
0
-1
-2
Current (μA)
-1.2
-1.0
-0.8
-0.6
Potential (V vs Fc/Fc+)

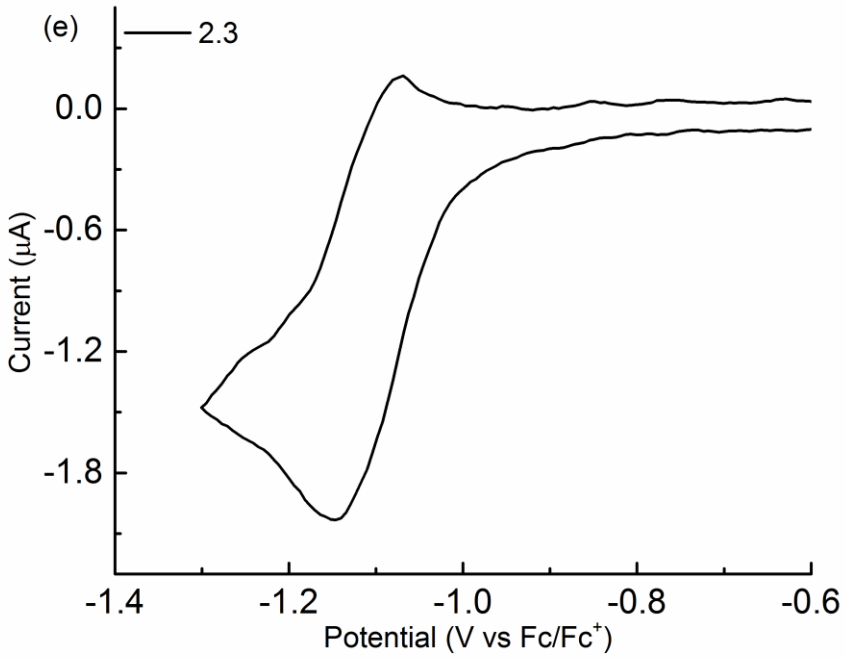
(e)
2.3
0.0
-0.6
-1.2
-1.8
Current (μA)
-1.4
-1.2
-1.0
-0.8
-0.6
Potential (V vs Fc/Fc+)

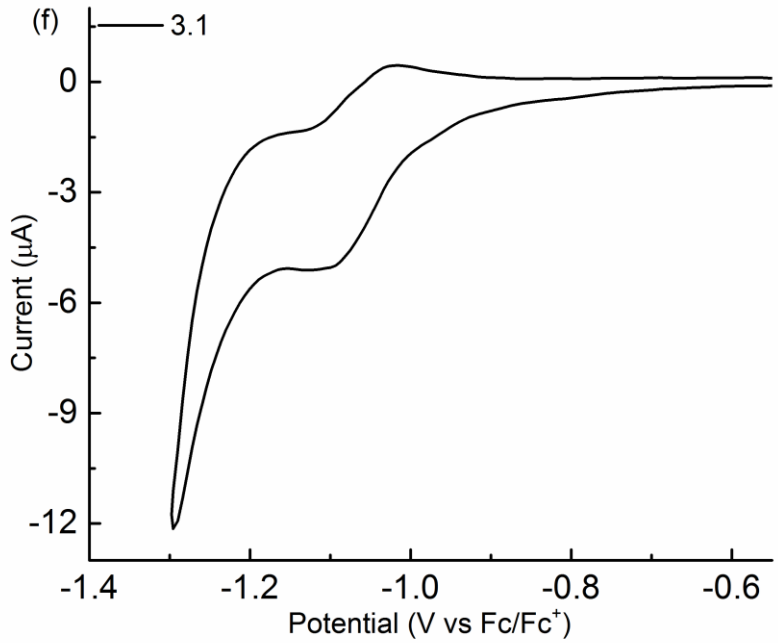
(f)
3.1
0
-3
-6
-9
-12
Current (μA)
-1.4
-1.2
-1.0
-0.8
-0.6
Potential (V vs Fc/Fc+)

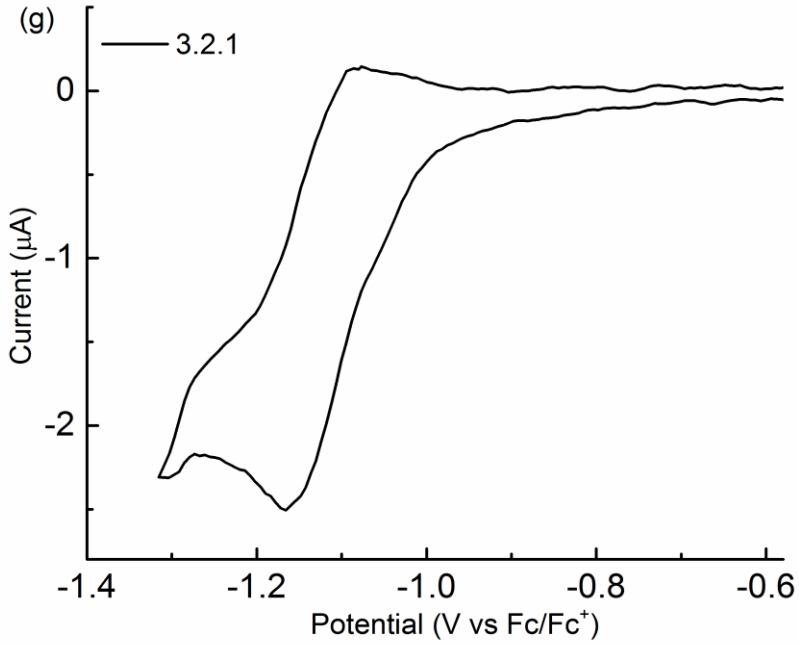
(g)
3.2.1
0
-1
-2
Current (μA)
-1.4
-1.2
-1.0
-0.8
-0.6
Potential (V vs Fc/Fc+)

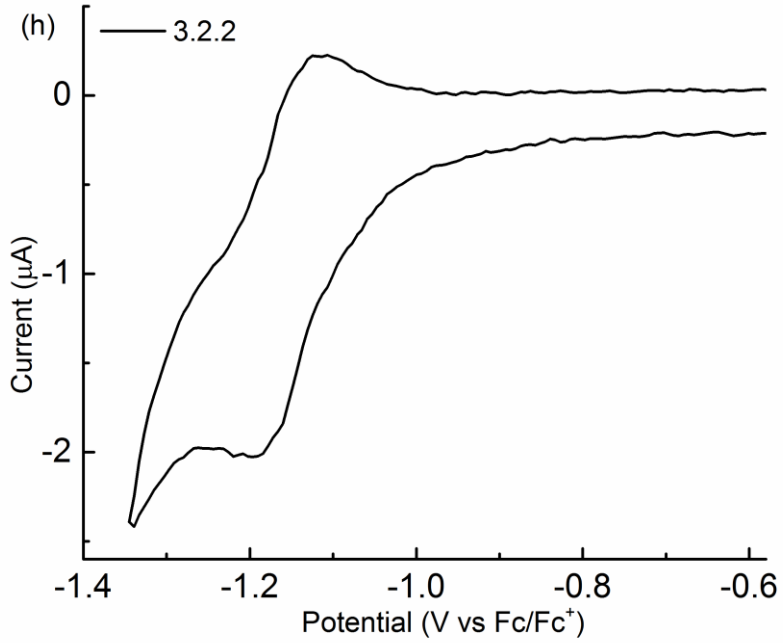
(h)
3.2.2
0
-1
-2
Current (μA)
-1.4
-1.2
-1.0
-0.8
-0.6
Potential (V vs Fc/Fc+)

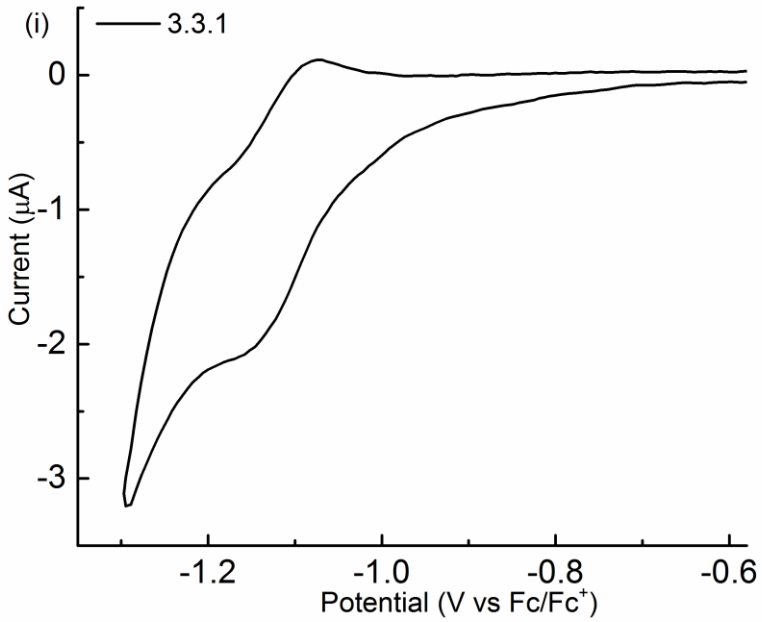
(i)
3.3.1
0
-1
-2
-3
Current (μA)
-1.2
-1.0
-0.8
-0.6
Potential (V vs Fc/Fc+)

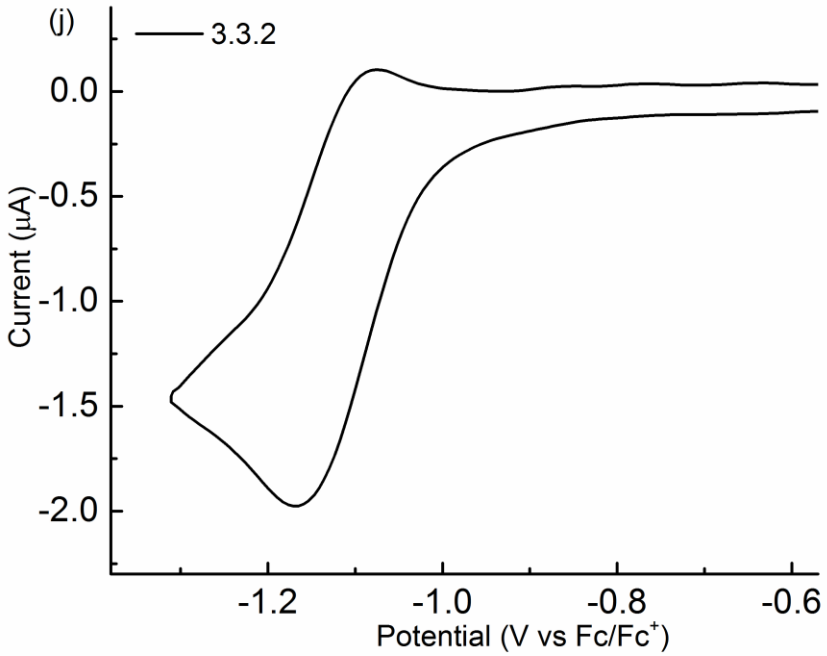
(j)
3.3.2
0.0
-0.5
-1.0
-1.5
-2.0
Current (μA)
-1.2
-1.0
-0.8
-0.6
Potential (V vs Fc/Fc+)

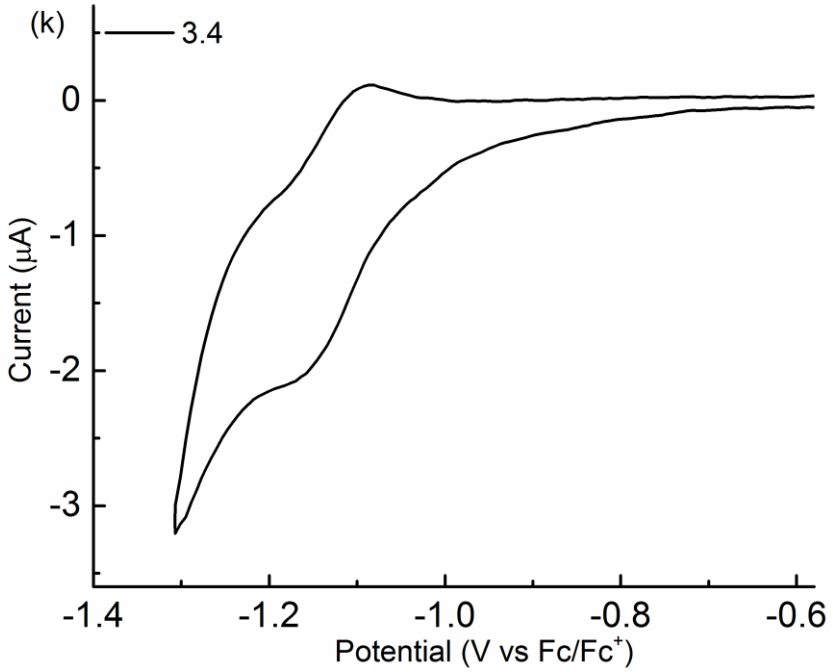
(k)
3.4
0
-1
-2
-3
Current (μA)
-1.4
-1.2
-1.0
-0.8
-0.6
Potential (V vs Fc/Fc+)

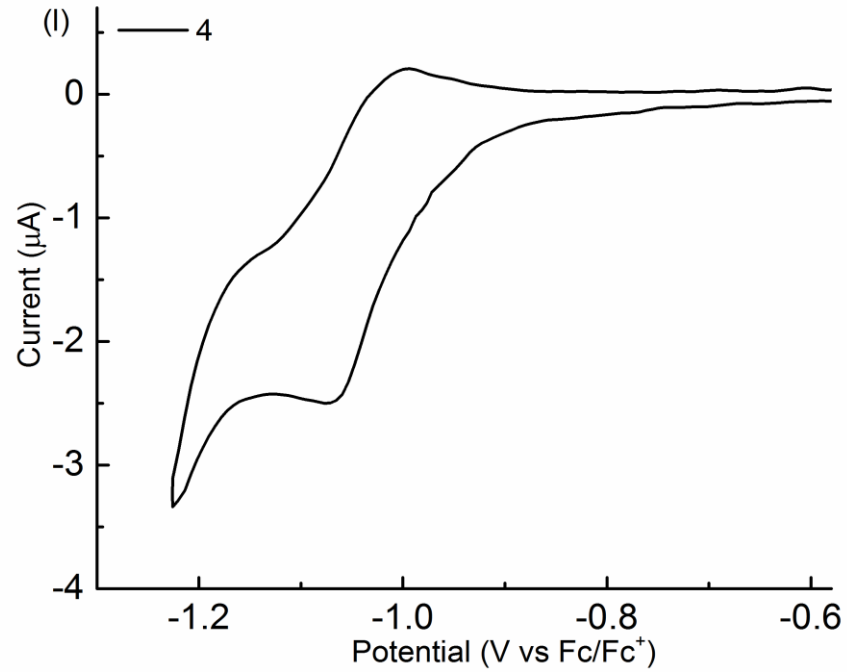
(l)
4
0
-1
-2
-3
-4
Current (μA)
-1.2
-1.0
-0.8
-0.6
Potential (V vs Fc/Fc+)

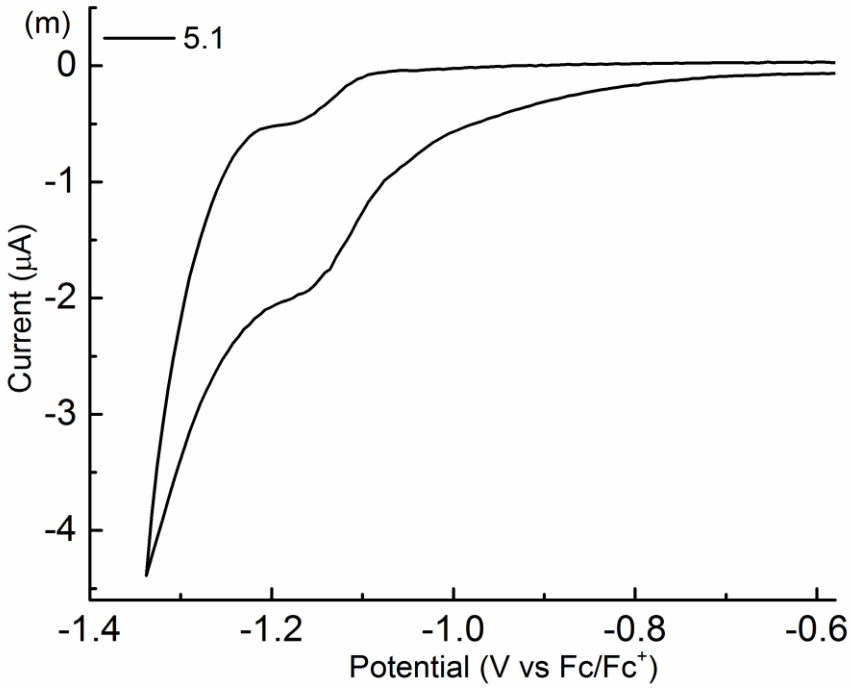
(m)
5.1
0
-1
-2
-3
-4
Current (μA)
-1.4
-1.2
-1.0
-0.8
-0.6
Potential (V vs Fc/Fc+)

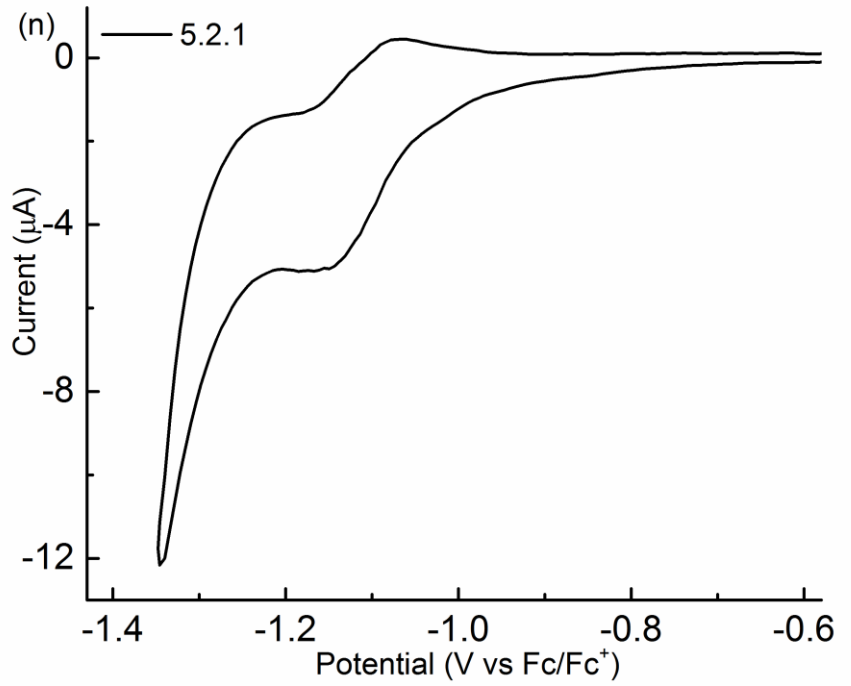
(n)
5.2.1
0
-4
-8
-12
Current (μA)
-1.4
-1.2
-1.0
-0.8
-0.6
Potential (V vs Fc/Fc+)

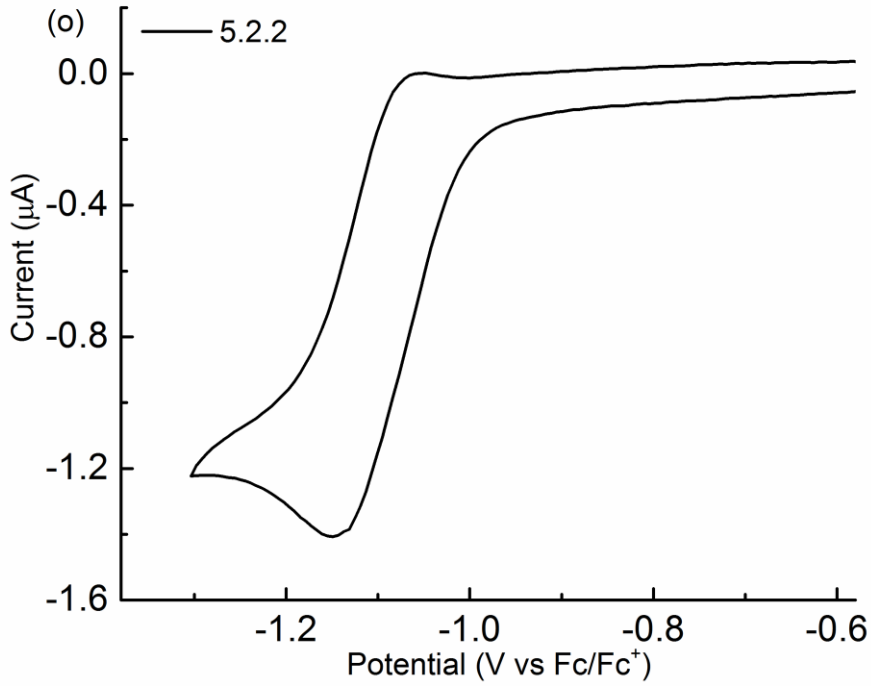
(o)
5.2.2
0.0
-0.4
-0.8
-1.2
-1.6
Current (μA)
-1.2
-1.0
-0.8
-0.6
Potential (V vs Fc/Fc+)

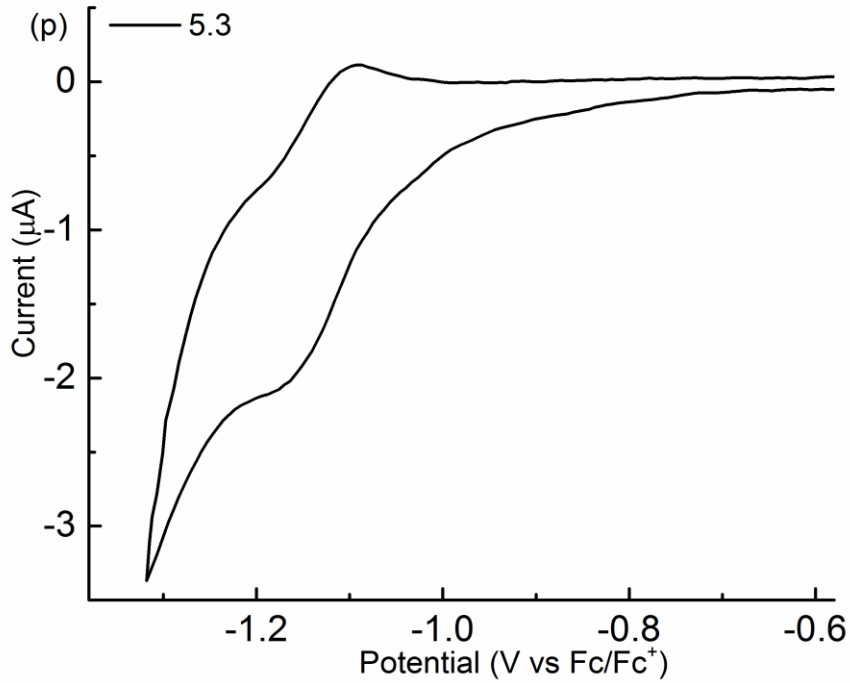
(p)
5.3
0
-1
-2
-3
Current (μA)
-1.2
-1.0
-0.8
-0.6
Potential (V vs Fc/Fc+)

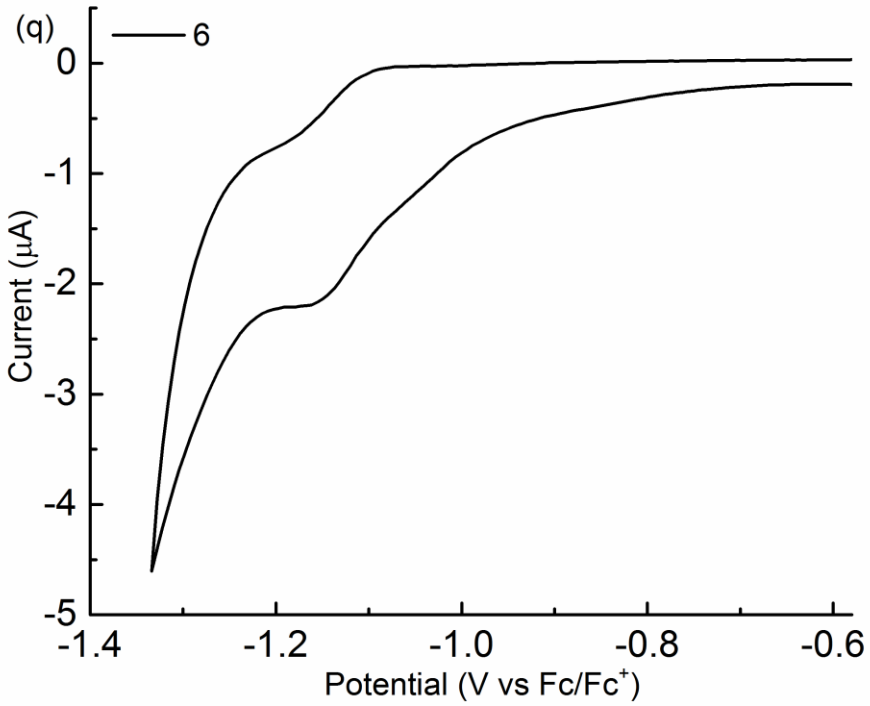
(q)
6
0
-1
-2
-3
-4
-5
Current (μA)
-1.4
-1.2
-1.0
-0.8
-0.6
Potential (V vs Fc/Fc+)

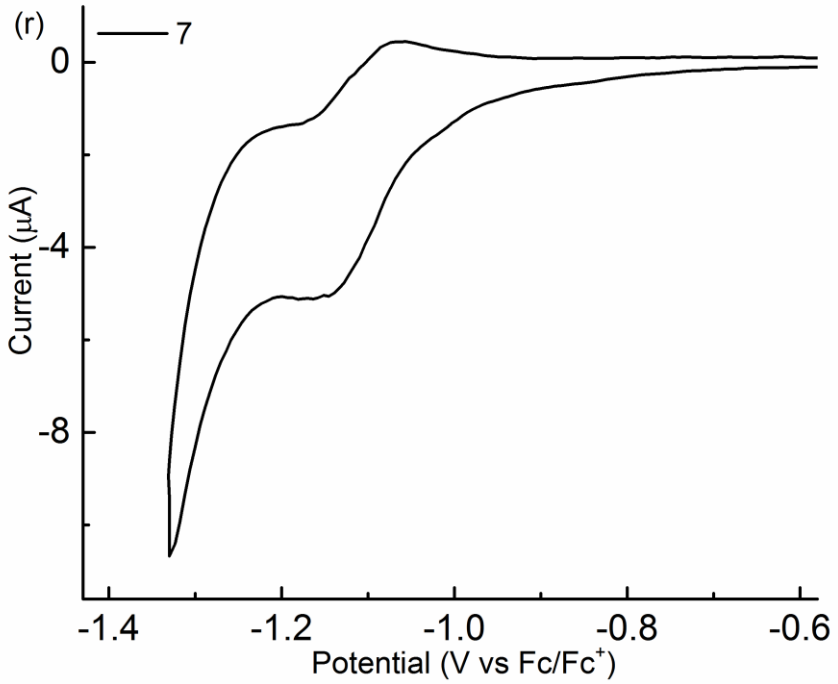
(r)
7
0
-4
-8
Current (μA)
-1.4
-1.2
-1.0
-0.8
-0.6
Potential (V vs Fc/Fc+)

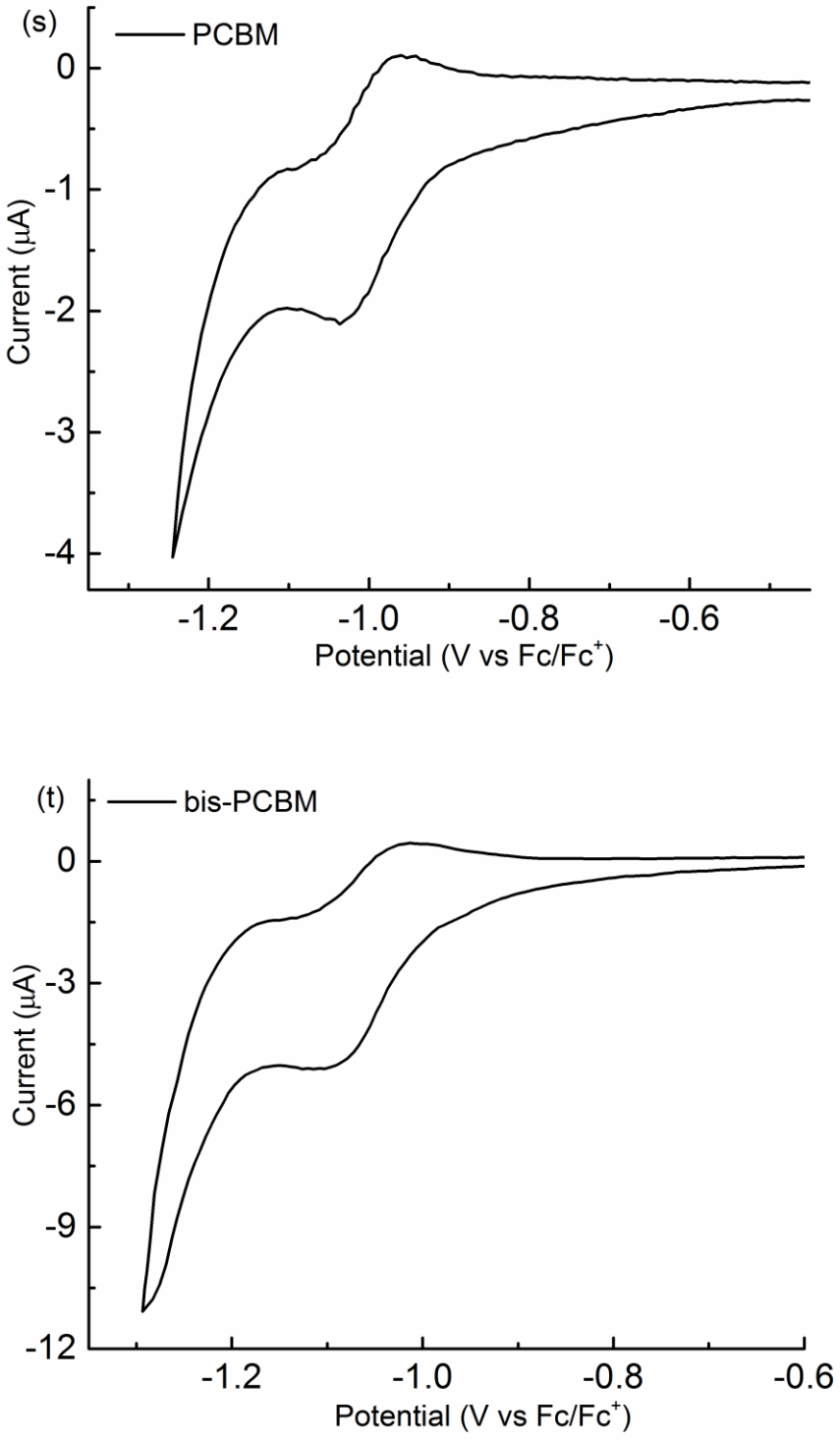

Figure 5.19: Cyclic volatmmagrams of the 18 isomers of bisPC62BM (a. F 1, b.F2.1.1, c. F2.1.2, d. F2.2, e. F2.3, f. F3.1, g. F3.2.1, h. F3.2.2, i. F3.3.1, j. F3.3.2, k. F3.4, l. F4, m. F5.1, n. F5.2.1, o. F5.2.2, p. F5.3, q. F6 and r.F7) BisPCBM mixture and PCBM

5.8 HOMOs of bisPC$_{62}$BM isomers

From the UV-Vis spectra the optical HOMO-LUMO gap (Eg) of each of the isomers has been determined. Eg varies between 1.664 eV and 1.883 eV with F3.4 being the smallest and F5.1 being the largest. The HOMO levels of the isomers, (determined via LUMO-Eg) range between -5.673 eV for F5.1 and -5.402 eV for F3.2.2. This range is reasonably consistent with the calculations of the HOMO energies. This is highly consistent with those obtained from DFT calculations [B3LYP/6-31(d,p)], which range from -5.56 to -5.36 eV by my college Tong Liu. It is also reasonably consistent with the results via the B3LYP/6-31G(d) level of theory for a representative subset of seven of the isomers by Frost et al., [109] which range from -5.612 to -5.432 eV. However, although the calculated HOMOs are within the range of the experimental values, the calculated range (180 meV) is somewhat narrower than the experimental range (271 meV). The F3.3.2 here is still the most promising isomer with the highest HOMO and highest LUMO within the isomers and the second smallest bond gap within the isomer. It could bring higher Voc of OPVs and the ease of electron promotion favourable for light absorption.

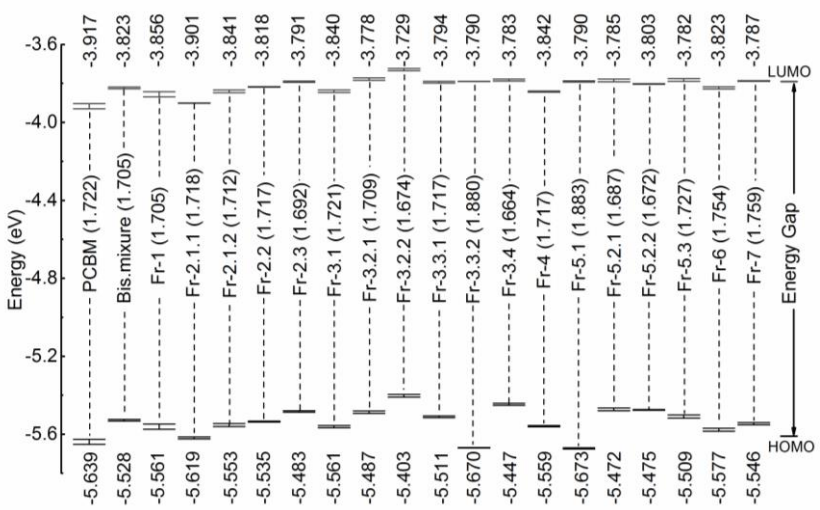

Figure 5.20: HOMO, LUOMO and Eg of all the 18 isomers, Bis-[60]PCBM and [60]PCBM

5.9 SUMMARY

The electronic characterisations of bis-$PC_{62}BM$ and $PC_{71}BM$ isomers have been conducted by UV-Vis spectroscopy and cyclic voltammetry. From the UV-Vis spectra, all the HOMO-LUMO gaps of bis-$PC_{62}BM$ and $PC_{71}BM$ isomers were obtained ranging from 1.664 to 1.883 eV and 1.748-1.772eV, respectively. Through the comparisons with the UV-Vis spectra of the different C_{60} bis-adducts from Hirsch, we found interesting similarities in our bis-$PC_{62}BM$ spectra and divided our 18 isomers into seven groups in terms of the second addition position from 'trans-1 to trans-4', 'cis-2 to cis-3' and e seven types of double bonds. The relationship between retention time and addition positions is that isomers with well separated addends isomers elute early, and vice versa, and this is due to the closer addends isomers having a higher polarity.

Cyclic voltammetry was applied to measure the LUMO levels of all the isomers. The LUMOs levels of bis-$PC_{62}BM$ isomers vary from -3.901 to -3.729 eV, higher than that of $PC_{61}BM$, which is consistent with the simulation results from literature. F3.2.2 has the highest LUMO -3.729 eV which is 94 meV higher than the average, while the lowest F2.1.1 plays the role of the energy traps in the mixture. The HOMOs of the bis-$PC_{62}BM$ isomers were determined by the difference between LUMOs and the Eg. Those range from -5.673 to -5.402 eV consistent with our recent simulation results. $PC_{71}BM$ isomers have similar LUMOs, -3.9316 eV for the MAJOR, -3.9194 and -3.9197 eV for the MINORs. The difference between the MINORs is negligible around 0.4 meV. The HOMOs of the isomers vary from -5.6678 to -5.7036. Due to the similar electronic structure of the isomers, the MAJOR would be suggested for

further application for its ease of purification and the optimisation of the morphology from the single isomer with a better assembling property and a higher crystallinity. All the results of the bis$PC_{62}BM$ isomers and $PC_{71}BM$ are listed in Table 5.7.

Isomer	**F1**	**F2.1.1**	**F2.1.2**	**F2.2**	**F2.3**	**F3.1**
HOMO (eV)	-5.56	-5.62	-5.55	-5.54	-5.48	-5.56
LUMO (eV)	-3.86	-3.90	-3.84	-3.82	-3.79	-3.84
*E*g (eV)	1.71	1.72	1.71	1.72	1.69	1.72
Abundance (%)	6.7	1.2	7.5	4.4	6.3	3.0
Assignment	*trans*-2	*trans*-1	*trans*-2	*trans*-4	*trans*-3	*trans*-2
Isomer	**F3.2.1**	**F3.2.2**	**F3.3.1**	**F3.3.2**	**F3.4**	**F4**
HOMO (eV)	-5.49	-5.40	-5.51	-5.67	-5.45	-5.56
LUMO (eV)	-3.78	-3.73	-3.79	-3.79	-3.78	-3.84
*E*g (eV)	1.71	1.67	1.72	1.88	1.66	1.72
Abundance (%)	7.0	7.5	3.4	10.4	1.8	6.2
Assignment	*trans*-3	*trans*-1	*trans*-3	*e*	*cis*-3	*trans*-4
Isomer	**F5.1**	**F5.2.1**	**F5.2.2**	**F5.3**	**F6**	**F7**
HOMO (eV)	-5.67	-5.47	-5.48	-5.50	-5.58	-5.55
LUMO (eV)	-3.79	-3.79	-3.80	-3.78	-3.82	-3.79
Eg (eV)	1.88	1.69	1.67	1.73	1.75	1.76
Abundance (%)	15.6	2.3	5.4	3.2	5.2	1.4
Assignment	*e*	*cis*-3	*cis*-3	*cis*-2	*cis*-2	*cis*-2
Isomer($PC_{71}BM$)	MINOR 1		MINOR 2		The MAJOR	
HOMO (eV)	-5.6678		-5.6742		-5.7036	
LUMO (eV)	-3.9194		-3.9197		-3.9316	
HOMO – LUMO gap (eV)	1.7484		1.7545		1.772	

Table 5.7: Energy levels in and isomer abundance of bis$PC_{62}BM$ and $PC_{71}BM$ isomers.

Conclusion and Outlook

The OPV acceptor bis$PC_{62}BM$ and $PC_{71}BM$ was purified into its 18 constituent isomers and three distinguishable isomers by the peak recycling HPLC method, each to a purity exceeding 99%. Three different columns, silica, 5PYE and 5PBB, were used and tried on each isomer to achieve the highest purification efficiency. For bis$PC_{62}BM$, F1, F4, F6 and F7 show one single peak after the first cycling in HPLC, indicating they can be easily separated from other isomers. However, F2, F3 and F5 appear with more peaks, which need four stages to purify all isomers in them. For $PC_{71}BM$, the MAJOR is easily purified in two stages, while the MINORs from the mixture require six to seven stages.

The UV-Vis spectra and cyclic voltammograms demonstrate that each of the isomers exhibit different electronic properties. The HOMO, LUMO and HOMO-LUMO gaps of BisPCBM isomers range from, -5.673 to -5.402 eV, from -3.901 to -3.729 eV, and from 1.664 to 1.883 eV, respectively. The LUMOs of the $PC_{71}BM$ isomers are similar, -3.9316 eV for the MAJOR, -3.9194 and -3.9197 for MINORs, which is close to the $PC_{61}BM$. The LUMO of the MAJOR isomer is higher and the light absorption is wider.

The LUMO levels of the majority of bis$PC_{62}BM$ isomers are above those of the isomer mixture, and hence, OPV devices based on each of those isomers are predicted to have a Voc higher than that of present devices based on the mixture (with F3.2.2 being the most promising at 94 meV above that of the mixture and 188

meV above that of $PC_{61}BM$). Furthermore, with the removal of the energetic and morphological disorder associated with the normal mixture of bis$PC_{62}BM$ isomers, it is also predicted that OPV devices based on all of the isomers will have better charge carrier transport properties, and thereby potentially higher currents, than those based on the mixture. F3 and F5 with higher LUMOs are suggested for potential applications and can be produced from a single HPLC pass. Based on comparisons with known UV-Vis absorption spectra of analogous materials purified and identified by others, we conclude that there is correlation between the HPLC retention time and the relative positions of the addends; in that generally the closer the addends are to each other the longer the retention time of the isomer, and vice versa. Experiments on optimising, characterising and comparing OPV devices based on each and every isomer are in progress within the collaborating groups.

All three isomers of $PC_{71}BM$ were characterised by ^{13}C NMR spectroscopy, UV-Vis absorption spectroscopy and cyclic voltammetry. These measurements were supported by B3LYP/6-31G(d,p) ab-initio calculations. All three isomers are methanofullerenes. The MAJOR isomer, comprising 85% of the mixture, exists as two enantiomers each involving a cyclo-addition to the 8-25 bond of C_{70}. Like the MAJOR isomer, the two MINOR isomers of $PC_{71}BM$ also both involve a cyclo-addition to the same bond of C_{70} (the 9-10 bond in this case) with opposing orientations of the addend. However, unlike the MAJOR isomer, these two isomers have separate r and s pseudo-symmetry about carbon atom 71. They comprise 9% and 6% of the mixture respectively. $PC_{71}BM$ isomers have similar LUMOs, -3.9316 eV for the MAJOR, -3.9194 and -3.9197 eV for the MINORs. The difference between

the MINORs is negligible at around 0.4 meV. The HOMOs of the isomers vary from -5.6678 to -5.7036. Due to the similar electronic structure of the isomers, the MAJOR would be suggested for further application for its ease of purification and the possible optimisation of the morphology from the single isomer with better assembly properties and a higher crystallinity.

We have recently collaborated with the Laboratory of Photonics and Interfaces of EPFL in Switzerland. As we have just discovered bisPCBM and its sub-fractions were found to increase the efficiency of the Perovskite solar cell up to 18% in June 2016 and the isomer-pure devices achieved a PCE >20% in August 2016. It also possibly improves the stability of the Perovskite solar cells. We plan to synthesis more materials and purify them into pure isomers for further investigation for the Perovskite solar cell for potential commercialisation.

RREFERENCES

[1] T. D. Nielsen, C. Cruickshank, S. Foged, J. Thorsen, F. C. Krebs, *Sol Energ Mat Sol C* **2010**, *94*, 1553-1571.

[2] P. M, *http://www.heliatek.com/en/press/press-releases/details/heliatek-sets-new-organic-photovoltaic-world-record-efficiency-of-13-2*, **2016**.

[3] F. W. Zhao, X. Y. Meng, Y. Q. Feng, Z. W. Jin, Q. Zhou, H. Li, L. Jiang, J. Z. Wang, Y. F. Li, C. R. Wang, *J Mater Chem A* **2015**, *3*, 14991-14995.

[4] A. Mohajeri, A. Omidvar, *Phys Chem Chem Phys* **2015**, *17*, 22367-22376.

[5] C. J. Brabec, A. Cravino, D. Meissner, N. S. Sariciftci, T. Fromherz, M. T. Rispens, L. Sanchez, J. C. Hummelen, *Adv Funct Mater* **2001**, *11*, 374-380.

[6] A. Gadisa, M. Svensson, M. R. Andersson, O. Inganas, *Appl Phys Lett* **2004**, *84*, 1609-1611.

[7] F. B. Kooistra, J. Knol, F. Kastenberg, L. M. Popescu, W. J. H. Verhees, J. M. Kroon, J. C. Hummelen, *Org Lett* **2007**, *9*, 551-554.

[8] K. L. Mutolo, E. I. Mayo, B. P. Rand, S. R. Forrest, M. E. Thompson, *J Am Chem Soc* **2006**, *128*, 8108-8109.

[9] K. Sarangerel, C. Ganzorig, M. Fujihira, M. Sakomura, K. Ueda, *Chem Lett* **2008**, *37*, 778-779.

[10] M. C. Scharber, D. Wuhlbacher, M. Koppe, P. Denk, C. Waldauf, A. J. Heeger, C. L. Brabec, *Adv Mater* **2006**, *18*, 789-+.

[11] K. Vandewal, A. Gadisa, W. D. Oosterbaan, S. Bertho, F. Banishoeib, I. Van Severen, L. Lutsen, T. J. Cleij, D. Vanderzande, J. V. Manca, *Adv Funct Mater* **2008**, *18*, 2064-2070.

[12] J. Nelson, *Mater Today* **2011**, *14*, 462-470.

[13] M. Lenes, S. W. Shelton, A. B. Sieval, D. F. Kronholm, J. C. Hummelen, P. W. M. Blom, *Adv Funct Mater* **2009**, *19*, 3002-3007.

[14] Y. Matsuo, *Chem Lett* **2012**, *41*, 754-759.

[15] R. K. M. Bouwer, G. J. A. H. Wetzelaer, P. W. M. Blom, J. C. Hummelen, *J Mater Chem* **2012**, *22*, 15412-15417.

[16] M. M. Wienk, J. M. Kroon, W. J. H. Verhees, J. Knol, J. C. Hummelen, P. A. van Hal, R. A. J. Janssen, *Angew Chem Int Edit* **2003**, *42*, 3371-3375.

[17] P. H. Wobkenberg, D. D. C. Bradley, D. Kronholm, J. C. Hummelen, D. M. de Leeuw, M. Colle, T. D. Anthopoulos, *Synthetic Met* **2008**, *158*, 468-472.

[18] H. P. Lang, V. Thommengeiser, C. Bolm, M. Felder, J. Frommer, R. Wiesendanger, H. Werner, R. Schlogl, A. Zahab, P. Bernier, G. Gerth, D. Anselmetti, H. J. Guntherodt, *Appl Phys a-Mater* **1993**, *56*, 197-205.

[19] P. A. Troshin, H. Hoppe, A. S. Peregudov, M. Egginger, S. Shokhovets, G. Gobsch, N. S. Sariciftci, V. F. Razumov, *Chemsuschem* **2011**, *4*, 119-124.

[20] F. P, *MIT Technology Review* **2016**.

[21] E. M. Perez, *Pure Appl Chem* **2011**, *83*, 201-211.

[22] A. Chodos, *APS News* **1954**.

[23] R. W. Miles, K. M. Hynes, I. Forbes, *Prog Cryst Growth Ch* **2005**, *51*, 1-42.

[24] S. S, *Transparency Market Research* **2015**.

[25] B. ltd, *http://www.belectric.co.uk/organic-pv-set-for-growth/, September, 2015*.

[26] T. M. Research, **2014**.

[27] G. Dennler, C. Lungenschmied, H. Neugebauer, N. S. Sariciftci, M. Latreche, G. Czeremuszkin, M. R. Wertheimer, *Thin Solid Films* **2006**, *511*, 349-353.

[28] C. W. Tang, *Appl Phys Lett* **1986**, *48*, 183-185.

[29] C. W. Tang, Google Patents, **1979**.

[30] I. Montanari, A. F. Nogueira, J. Nelson, J. R. Durrant, C. Winder, M. A. Loi, N. S. Sariciftci, C. Brabec, *Appl Phys Lett* **2002**, *81*, 3001-3003.
[31] N. S. Sariciftci, L. Smilowitz, A. J. Heeger, F. Wudl, *Science* **1992**, *258*, 1474-1476.
[32] N. S. Sariciftci, D. Braun, C. Zhang, V. I. Srdanov, A. J. Heeger, G. Stucky, F. Wudl, *Appl Phys Lett* **1993**, *62*, 585-587.
[33] G. Yu, J. Gao, J. C. Hummelen, F. Wudl, A. J. Heeger, *Science* **1995**, *270*, 1789-1791.
[34] V. I. Madogni, B. Kounouhewa, A. Akpo, M. Agbomahena, S. A. Hounkpatin, C. N. Awanou, *Chem Phys Lett* **2015**, *640*, 201-214.
[35] N. Grossiord, J. M. Kroon, R. Andriessen, P. W. M. Blom, *Org Electron* **2012**, *13*, 432-456.
[36] J. H. Wu, Z. Lan, J. M. Lin, M. L. Huang, Y. F. Huang, L. Q. Fan, G. G. Luo, *Chem Rev* **2015**, *115*, 2136-2173.
[37] I. H. Campbell, S. Rubin, T. A. Zawodzinski, J. D. Kress, R. L. Martin, D. L. Smith, N. N. Barashkov, J. P. Ferraris, *Phys Rev B* **1996**, *54*, 14321-14324.
[38] M. Hiramoto, K. Ihara, H. Fukusumi, M. Yokoyama, *J Appl Phys* **1995**, *78*, 7153-7157.
[39] M. Hiramoto, K. Ihara, M. Yokoyama, *Jpn J Appl Phys* **1995**, *34*, 3803.
[40] H. Hoppea, N. S. Sariciftci, *J. Mater. Res* **2004**, *19*, 1925.
[41] M. C. Scharber, N. S. Sariciftci, *Prog Polym Sci* **2013**, *38*, 1929-1940.
[42] G. Dennler, A. J. Mozer, G. Juska, A. Pivrikas, R. Osterbacka, A. Fuchsbauer, N. S. Sariciftci, *Org Electron* **2006**, *7*, 229-234.
[43] B. Fan, P. Wang, L. D. Wang, G. Q. Shi, *Sol Energ Mat Sol C* **2006**, *90*, 3547-3556.
[44] J.-F. Eckert, J.-F. Nicoud, J.-F. Nierengarten, S.-G. Liu, L. Echegoyen, F. Barigelletti, N. Armaroli, L. Ouali, V. Krasnikov, G. Hadziioannou, *J Am Chem Soc* **2000**, *122*, 7467-7479.
[45] S.-S. Sun, J. Brooks, T. Nguyen, A. Harding, D. Wang, T. David, *Energy Procedia* **2014**, *57*, 79-88.
[46] J. B. You, L. T. Dou, K. Yoshimura, T. Kato, K. Ohya, T. Moriarty, K. Emery, C. C. Chen, J. Gao, G. Li, Y. Yang, *Nat Commun* **2013**, *4*.
[47] W. J. da Silva, F. K. Schneider, A. B. Yusoff, J. Jang, *Sci Rep-Uk* **2015**, *5*.
[48] H. Kroto, *Lett. to Nature* **1985**, *318*.
[49] W. Kratschmer, L. D. Lamb, K. Fostiropoulos, D. R. Huffman, *Nature* **1990**, *347*, 354-358.
[50] G. Li, V. Shrotriya, J. S. Huang, Y. Yao, T. Moriarty, K. Emery, Y. Yang, *Nat Mater* **2005**, *4*, 864-868.
[51] Y. Kim, S. Cook, S. M. Tuladhar, S. A. Choulis, J. Nelson, J. R. Durrant, D. D. C. Bradley, M. Giles, I. Mcculloch, C. S. Ha, M. Ree, *Nat Mater* **2006**, *5*, 197-203.
[52] J. E. Anthony, A. Facchetti, M. Heeney, S. R. Marder, X. W. Zhan, *Adv Mater* **2010**, *22*, 3876-3892.
[53] M. Buhl, A. Hirsch, *Chem Rev* **2001**, *101*, 1153-1183.
[54] S. Saito, S. Okada, S. Sawada, N. Hamada, *Phys Rev Lett* **1995**, *75*, 685-688.
[55] J. Poater, M. Duran, M. Sola, *Int J Quantum Chem* **2004**, *98*, 361-366.
[56] C. J. Brabec, G. Zerza, G. Cerullo, S. De Silvestri, S. Luzzati, J. C. Hummelen, S. Sariciftci, *Chem Phys Lett* **2001**, *340*, 232-236.
[57] B. Bhushan, B. Gupta, G. W. Van Cleef, C. Capp, J. V. Coe, *Tribology transactions* **1993**, *36*, 573-580.
[58] A. F. Hebard, R. C. Haddon, R. M. Fleming, A. R. Kortan, *Appl Phys Lett* **1991**, *59*, 2109-2111.
[59] C. Brabec, U. Scherf, V. Dyakonov, *Organic photovoltaics: materials, device physics, and manufacturing technologies*, John Wiley & Sons, **2011**.
[60] J. W. Fergus, *Materials Science and Engineering: A* **2005**, *397*, 271-283.
[61] P. Peumans, A. Yakimov, S. R. Forrest, *J Appl Phys* **2004**, *95*, 2938-2938.

[62] F. C. Robles-Hernández, H. Calderon, in *MRS Proceedings, Vol. 1243*, Cambridge Univ Press, **2009**, p. 5.
[63] B. Oregan, M. Gratzel, *Nature* **1991**, *353*, 737-740.
[64] F. Langa, J.-F. Nierengarten, *Fullerenes: principles and applications*, Royal Society of Chemistry, **2007**.
[65] H. S. Nalwa, **1997**.
[66] S. Q. Xiao, A. C. Stuart, S. B. Liu, H. X. Zhou, W. You, *Adv Funct Mater* **2010**, *20*, 635-643.
[67] R. S. Ruoff, D. S. Tse, R. Malhotra, D. C. Lorents, *J Phys Chem-Us* **1993**, *97*, 3379-3383.
[68] T. Akasaka, A. Osuka, S. Fukuzumi, H. Kandori, Y. Aso, *Chemical Science of [pi]-Electron Systems*, Springer, **2015**.
[69] F. B. Kooistra, V. D. Mihailetchi, L. M. Popescu, D. Kronholm, P. W. M. Blom, J. C. Hummelen, *Chem Mater* **2006**, *18*, 3068-3073.
[70] R. B. Ross, C. M. Cardona, F. B. Swain, D. M. Guldi, S. G. Sankaranarayanan, E. Van Keuren, B. C. Holloway, M. Drees, *Adv Funct Mater* **2009**, *19*, 2332-2337.
[71] C. Yang, J. Y. Kim, S. Cho, J. K. Lee, A. J. Heeger, F. Wudl, *J Am Chem Soc* **2008**, *130*, 6444-6450.
[72] Y. Zhang, H. L. Yip, O. Acton, S. K. Hau, F. Huang, A. K. Y. Jen, *Chem Mater* **2009**, *21*, 2598-2600.
[73] L. P. Zheng, Q. M. Zhou, X. Y. Deng, M. Yuan, G. Yu, Y. Cao, *J Phys Chem B* **2004**, *108*, 11921-11926.
[74] P. A. Troshin, H. Hoppe, J. Renz, M. Egginger, J. Y. Mayorova, A. E. Goryochev, A. S. Peregudov, R. N. Lyubovskaya, G. Gobsch, N. S. Sariciftci, V. F. Razumov, *Adv Funct Mater* **2009**, *19*, 779-788.
[75] C. Liu, Y. J. Li, C. H. Li, W. W. Li, C. J. Zhou, H. B. Liu, Z. S. Bo, Y. L. Li, *J Phys Chem C* **2009**, *113*, 21970-21975.
[76] J. A. Mikroyannidis, A. N. Kabanakis, S. S. Sharma, G. D. Sharma, *Adv Funct Mater* **2011**, *21*, 746-755.
[77] I. Riedel, E. von Hauff, H. Parisi, N. Martin, F. Giacalone, V. Dyakonov, *Adv Funct Mater* **2005**, *15*, 1979-1987.
[78] A. Sánchez‐Díaz, M. Izquierdo, S. Filippone, N. Martin, E. Palomares, *Adv Funct Mater* **2010**, *20*, 2695-2700.
[79] Y. Matsuo, Y. Sato, T. Niinomi, I. Soga, H. Tanaka, E. Nakamura, *J Am Chem Soc* **2009**, *131*, 16048-+.
[80] Y. J. He, H. Y. Chen, J. H. Hou, Y. F. Li, *J Am Chem Soc* **2010**, *132*, 5532-5532.
[81] G. J. Zhao, Y. J. He, Y. F. Li, *Adv Mater* **2010**, *22*, 4355-+.
[82] Y. J. He, G. J. Zhao, B. Peng, Y. F. Li, *Adv Funct Mater* **2010**, *20*, 3383-3389.
[83] R. Mitsumoto, T. Araki, E. Ito, Y. Ouchi, K. Seki, K. Kikuchi, Y. Achiba, H. Kurosaki, T. Sonoda, H. Kobayashi, O. V. Boltalina, V. K. Pavlovich, L. N. Sidorov, Y. Hattori, N. Liu, S. Yajima, S. Kawasaki, F. Okino, H. Touhara, *J Phys Chem A* **1998**, *102*, 552-560.
[84] R. K. M. Bouwer, *Fullerene bisadducts for organic photovoltaics*, University Library Groningen][Host], **2012**.
[85] Y. J. He, H. Y. Chen, J. H. Hou, Y. F. Li, *J Am Chem Soc* **2010**, *132*, 1377-1382.
[86] R. Beal, *Morphology and Efficiency of Polymer: Fullerene Solar Cells*, Oxford University, **2010**.
[87] H. W. Liu, D. Y. Chang, W. Y. Chiu, S. P. Rwei, L. Wang, *J Mater Chem* **2012**, *22*, 15586-15591.
[88] R. K. M. Bouwer, J. C. Hummelen, *Chem-Eur J* **2010**, *16*, 11250-11253.
[89] M. Ozawa, E. Osawa, *Carbon* **1999**, *37*, 707-709.

[90] J. B. Howard, J. T. Mckinnon, Y. Makarovsky, A. L. Lafleur, M. E. Johnson, *Nature* **1991**, *352*, 139-141.
[91] M. S. Dresselhaus, G. Dresselhaus, P. C. Eklund, *Science of fullerenes and carbon nanotubes: their properties and applications*, Academic press, **1996**.
[92] A. Hirsch, *The chemistry of the fullerenes*, Wiley Online Library, **1994**.
[93] A. Hirsch, M. Brettreich, *Fullerenes: chemistry and reactions*, John Wiley & Sons, **2006**.
[94] H. Keypour, M. Noroozi, A. Rashidi, *Journal of Nanostructure in Chemistry* **2013**, *3*, 1-9.
[95] S. A. Korhammer, A. Bernreuther, *Fresen J Anal Chem* **1996**, *354*, 131-135.
[96] N. tesque, *http://www.nacalai.co.jp/global/cosmosil_cn/PBB_CN.html* **2016**.
[97] M. Hilton, D. W. Armstrong, *Journal of liquid chromatography* **1991**, *14*, 9-28.
[98] K. Ballschmiter, M. Wossner, *Fresen J Anal Chem* **1998**, *361*, 743-755.
[99] R. E. Majors, *Anal Chem* **1972**, *44*, 1722-&.
[100] D. R. Mckenzie, C. A. Davis, D. J. H. Cockayne, D. A. Muller, A. M. Vassallo, *Nature* **1992**, *355*, 622-624.
[101] P. J. Mohr, B. N. Taylor, D. B. Newell, *Journal of Physical and Chemical Reference Data* **2012**, *41*, 043109.
[102] A. V. Nikolaev, T. J. S. Dennis, K. Prassides, A. K. Soper, *Chem Phys Lett* **1994**, *223*, 143-148.
[103] S. Vansmaalen, V. Petricek, J. L. Deboer, M. Dusek, M. A. Verheijen, G. Meijer, *Chem Phys Lett* **1994**, *223*, 323-328.
[104] H. Ajie, M. M. Alvarez, S. J. Anz, R. D. Beck, F. Diederich, K. Fostiropoulos, D. R. Huffman, W. Kratschmer, Y. Rubin, K. E. Schriver, D. Sensharma, R. L. Whetten, *J Phys Chem-Us* **1990**, *94*, 8630-8633.
[105] J. P. Hare, H. W. Kroto, R. Taylor, *Chem Phys Lett* **1991**, *177*, 394-398.
[106] K. Akhtari, K. Hassanzadeh, B. Fakhraei, H. Hassanzadeh, G. Akhtari, S. A. Zarei, *Comput Theor Chem* **2014**, *1038*, 1-5.
[107] A. Shafiee, M. M. Salleh, M. Yahaya, *Sains Malays* **2011**, *40*, 173-176.
[108] C. Leach, K. D. Vernon-Parry, N. K. Ali, *J Electroceram* **2010**, *25*, 188-197.
[109] J. M. Frost, M. A. Faist, J. Nelson, *Adv Mater* **2010**, *22*, 4881-+.

List of Publications

1. Purification and electronic characterisation of 18 isomers of the OPV acceptor material bis-[60]PCBM.
Shi W, Hou X, Liu T et al. ***Chem Commun (Camb),*** Volume 53, issue 5, page 975, 10th January 2017. DOI: 10.1039/c6cc07820f

2. Isomer-Pure Bis-PCBM-Assisted Crystal Engineering of Perovskite Solar Cells Showing Excellent Efficiency and Stability

Fei Zhang, Wenda Shi et al. **Advanced Materials**, DOI: 10.1002/adma.201606806. First published: 27 February 2017